

AN ABSTRACT OF THE DISSERTATION OF

Omar Guillermo Chiriboga Novillo for the degree of Doctor of Philosophy in Chemical Engineering presented on May 18, 2018.

Title: Nutrient Addition Strategies for the Marine Diatom *Cyclotella* sp to Control Cell, Lipid, and Chitin Formation.

Abstract approved: _____

Gregory L. Rorrer

Marine diatoms are unicellular photosynthetic organisms that produce unique nanomaterials, energy dense lipid-molecules, and specialty carbohydrate molecules that can be all extracted from a single microorganism. The centric marine diatom *Cyclotella* sp. was used as a model organism for cultivation in a biorefinery system, where multiple co-products can be harvested simultaneously. *Cyclotella* was phototrophically cultivated in an engineered 5-liter bubble column photobioreactor system. The effects of silicon, nitrogen, and phosphorus macro-nutrient delivery was evaluated under different nutrient addition strategies. The nutrient addition strategies were used to control cell, lipid, and *N*-Acetyl glucosamine (chitin) production under nutrient starvation conditions. Cell division of *Cyclotella* can be controlled through the rate of silicon addition. *Cyclotella* extrudes extracellular chitin nanofibers through its specialized ports that are located in the rims of the valves. Chitin production can be controlled by cell division. Lipid production is photosynthetically driven, and the phosphorus available per cell determines the lipid class production. In a phosphorus-starved cell, neutral lipid production is favored, whereas in a phosphorus replete cell, phospholipid production is favored. Maximum volumetric productivities were determined to be $5.23 \times 10^{-2} \pm 1.67 \times 10^{-3}$ cells $\times 10^9$ /L-hr, 1.64 ± 0.07 mg lipid/L-hr, and 0.82 ± 0.10 mg chitin/L-hr for cells, lipid, and chitin respectively. With this nutrient addition strategies, we have come to a fundamental

understanding of the nutrient needs of the model diatom *Cyclotella*, and have established nutrient bioprocess parameters that can be used in scalable cultivation systems.

©Copyright by Omar Guillermo Chiriboga Novillo
May 18, 2018
All Rights Reserved

Nutrient Addition Strategies for the Marine Diatom *Cyclotella* sp to Control Cell,
Lipid, and Chitin Formation

By

Omar Guillermo Chiriboga Novillo

A DISSERTATION

submitted to

Oregon State University

in partial fulfillment of
the requirements for the
degree of

Doctor of Philosophy

Presented May 18, 2018
Commencement June 2018

Doctor of Philosophy dissertation of Omar Guillermo Chiriboga Novillo presented on May 18, 2018.

APPROVED:

Major Professor, representing Chemical Engineering

Head of the School of Chemical, Biological, and Environmental Engineering

Dean of the Graduate School

I understand that my dissertation will become part of the permanent collection of Oregon State University libraries. My signature below authorizes release of my dissertation to any reader upon request.

Omar Guillermo Chiriboga Novillo, Author

ACKNOWLEDGEMENTS

I would like to acknowledge the support of this research by the National Science Foundation (NSF), and Emerging Frontiers for Research and Innovation program (EFRI) under award number 1240488.

I want to express my sincere appreciation to my advisor, Gregory L. Rorrer, for his mentoring, and Altan Ozkan and Paul LeDuff for their help in developing my research skills and keeping a great work environment at the Rorrer Lab.

I want to thank my wife Kali Chiriboga for all her love and support, which always helped me envision the brighter side of everything, and I also want to thank my family members; Zoila, Emma, Ricardo, Randy, Myra, Veronica, Andres, Hernan, and Jason for all their support along this fruitful tenure at Oregon State University (I hope they understand why I missed their birthday parties).

Last but not least, I want to thank Luna the Great Dane and Lobo the Irish Wolfhound for keeping my feet warm while writing this dissertation.

CONTRIBUTION OF AUTHORS

Paul LeDuff from the Rorrer Lab is the microscope imaging expert, and thanks to his great effort, he contributed with the light microscope and SEM images shown in Chapters 2, 3, and 5.

Bob Durst from the Linus Pauling Science Center was in charge of analyzing the chitin derivatized samples and thanks to his contribution I was able to present the chitin data in Chapters 3-5.

TABLE OF CONTENTS

	<u>Page</u>
Chapter 1- General Introduction	1
Research motivation.....	2
Diatoms	2
Macronutrients	3
Chitin.....	4
Nutrient addition	4
Photosynthesis.....	5
Research goals	6
Chapter 2 – Extracellular chitin nanofibers from marine diatoms.....	11
Summary	12
Introduction.....	12
Historical perspective.....	13
Current understanding.....	13
Biosynthesis	14
Fiber structure	15
Crystalline structure	16
Future applications.....	16
References.....	18
Chapter 3 - Control of chitin nanofiber production by the lipid-producing diatom <i>Cyclotella sp.</i> through fed-batch addition of dissolved silicon and nitrate in a bubble- column photobioreactor	27
Abstract	28
Introduction.....	28
Experimental section.....	30
Diatom cell culture.....	30
Photobioreactor design and operation.....	30
Light delivery to photobioreactor	32
Fed-batch delivery to photobioreactor	32

TABLE OF CONTENTS (Continued)

Analytical methods	33
SEM	34
Results.....	34
Batch photobioreactor cultivation.....	34
Fed-batch photobioreactor cultivation	35
Discussion	37
Conclusions.....	40
References.....	42
Chapter 4 - Effects of nitrogen delivery on chitin nanofiber production during batch cultivation of the diatom <i>Cyclotella</i> sp. in a bubble-column photobioreactor.....	56
Abstract.....	57
Introduction.....	57
Materials and methods	59
Results.....	60
Discussion.....	63
References.....	66
Chapter 5 - Effects of phosphate concentration on lipid class and chitin nanofiber production during a two stage cultivation of the diatom <i>Cyclotella</i> sp. in a bubble-column photobioreactor	75
Abstract.....	76
Introduction.....	76
Materials and methods	78
Statistical analysis of data.....	81
Results.....	82
Discussion.....	86
Conclusions.....	89
References.....	91
Chapter 6 - Conclusions.....	104
Appendices.....	108

LIST OF FIGURES

<u>Figure</u>	<u>Page</u>
2.1	Light microscope images of the marine diatom <i>Cyclotella</i> sp. with chitin nanofibers emanating from the cell. The color images are also presented in black and white create a better contrast to visualize the chitin nanofiber. (a,b) Color image of <i>Cyclotella</i> with irradiating chitin nanofibers under 40X magnification with its complimentary black and white image; (c,d) Color image of <i>Cyclotella</i> with irradiating chitin nanofibers under 63X magnification with its complimentary black and white image21
2.2	Molecular structure of homopolymer chitin with repeating N-acetyl glucosamine units.....22
2.3	Proposed biosynthetic pathway for chitin in marine diatom, starting with glucose-6-phosphate23
2.4	Schematics of diatom cell. (a) Cylindrical diatom cell with extracellular chitin nanofibers extruded from the symmetrically arranged fultoportulae; (b) cross section of cell; (c) fultoportulae structure with chitin pocket and chitin nanofiber formation process24
2.5	SEM images of marine diatoms of genus <i>Thalassiosira</i> (a) and <i>Cyclotella</i> (b,c) shown with extracellular chitin nanofibers surrounding the cell25
2.6	β Chitin paracrystalline structure. (a) X-Ray diffraction (XRD) patterns of isolated extracellular chitin nanofibers from marine diatoms of genus <i>Cyclotella</i> and <i>Thalassiosira</i> . Distinctive peaks for β -chitin occur at 10° and 20°; (b) schematic of the molecular structure of β -chitin nanofibers with hydrogen bonds, obtained from: Pillai, C.K.S. Paul, Willi; Sharma, Chandra P. Chitin and chitosan polymers: Chemistry, solubility and nanofiber formation. Progress in Polymer Science. 2009, Vol. 34 Issue 7, pages 641-67826
3.1	Two-stage photobioreactor cultivation of <i>Cyclotella</i> diatom cells with pulse addition of nutrients at the beginning of Stage II. (a) Cell number density, dissolved silicon concentration, and nitrate concentration vs. cultivation time; (b) volumetric chitin production, lipid production vs. cultivation time. Error bars are 1.0 S.D. from triplicate assays.....47
3.2	Two-stage photobioreactor cultivation of <i>Cyclotella</i> diatom cells with a Stage II fed-batch nutrient medium addition time of 4 days. (a) Cell number density, dissolved silicon concentration, and nitrate concentration vs. cultivation time; (b) volumetric chitin production, lipid production vs. cultivation time. Error bars are 1.0 S.D. from triplicate assays48

LIST OF FIGURES (Continued)

- 3.3 Two-stage photobioreactor cultivation of *Cyclotella* diatom cells with a Stage II fed-batch nutrient medium addition time of 14 days. (a) Cell number density, dissolved silicon concentration, and nitrate concentration vs. cultivation time; (b) volumetric chitin production, lipid production vs. cultivation time49
- 3.4 Linear profiles for nutrient consumption and product formation during Stage II fed batch operation at nutrient medium addition times of 4 and 14 days. (a) Silicon and nitrate delivery and consumption profiles; (b) total cell and chitin production50
- 3.5 Rates of linear cell production and specific chitin production vs. silicon delivery rate in Stage II. Error bars for each were generally within the size of the symbol. For cell production (open triangle symbol), the least squares slope was $3.87 \cdot 10^9 \pm 6.9 \cdot 10^8$ cells / mmol Si ($r^2= 0.913$, $n = 5$, 1.0 S.E.). For chitin production (open diamond symbol), the least-squares slope was 16.63 ± 1.86 mg chitin / mmol Si / 10^9 cells ($r^2= 0.964$, $n = 5$, 1.0 S.E.)51
- 3.6 Final yields of lipid and chitin (mg / 10^9 cells) vs. Stage II nutrient delivery time at fixed total nutrient loading. The cumulative yields averaged over the three conditions were 13 ± 1 mg chitin/ 10^9 cells and 33 ± 3 mg lipid/ 10^9 cells. All errors were determined from propagated 1.0 S.E. errors.....52
- 3.7 Comparison of chlorophyll a formation during Stage II nutrient addition times of 0 days (pulse addition), 4 days continuous fed-batch operation, (96 hr) and 14 days continuous fed-batch operation (336 hr)53
- 3.8 SEM image of whole *Cyclotella* diatom cell after critical point drying. (a) Typical diatom cell at beginning of cultivation, Stage I; (b) typical diatom cell at end of cultivation, Stage II. Chitin fibers are shown emanating from pores lining frustule valve rim.....54
- 3.9 A simplified depiction of dissolved silicon, nitrate, and CO₂ uptake into the diatom cell, and the direction of these inputs to cellular products.....55
- 4.1 Comparison of the batch cultivation of the diatom *Cyclotella* sp. in a bubble-column photobioreactor at two initial N/Si molar ratios. (a) Cell number density, medium silicon concentration, and medium nitrate concentration vs. time; (b) chitin concentration in cell suspension vs. time; (c) chlorophyll *a* concentration in cell suspension vs. time. The smooth solid lines are the fit of the data to the logistic model for cell number density (Equation. 4.1) and chitin concentration (Equation. 4.2).....70

LIST OF FIGURES (Continued)

4.2	Effects of initial N/Si molar ratio on cell number yield based on silicon consumption ($Y_{X/Si}$) and specific growth rate (μ). Solid line is the fit of $Y_{X/Si}$ to Equation. 4.4	71
4.3	Effects of initial N/Si molar ratio on chitin yield per cell ($Y_{X/p}$) and the fraction of nitrate delivered incorporated into the chitin product (mol chitin-N mol ⁻¹ N consumed). Solid line is the fit of $Y_{X/Si}$ to Equation. 4.6.....	72
4.4	Effect of initial N/Si molar ratio on peak rate of chitin production (R_p). Dotted line is best fit from linear regression ($r^2 = 0.89$).....	73
4.5	Conceptual model of substrate flows into cellular materials at low and high molar N/Si ratios. Not drawn to scale	74
5.1	Two Stage photobioreactor cultivation of <i>Cyclotella</i> diatom cells under Type-A nutrient conditions, with variable phosphorus concentration at the beginning of Stage I. (a) Cell number density, dissolved silicon concentration, nitrate concentration, and phosphate concentration vs. cultivation time; (b) Silicon, nitrate and phosphate concentration delivered to the cell suspension vs. cultivation time	96
5.2	Two stage photobioreactor cultivation of <i>Cyclotella</i> diatom cells under Type-B nutrient conditions, with fixed phosphorus concentration on Stage I and variable phosphorus addition on Stage II. (a) Cell number density, dissolved silicon concentration, nitrate concentration, and phosphate concentration vs. cultivation time; (b) Silicon, nitrate and phosphate concentration delivered to the cell suspension vs. cultivation time.....	97
5.3	Comparison of the biomass, total lipid, and chitin concentration vs. cultivation time profiles at two different type of experiments corresponding to a different phosphate concentration (a) Type-A experiment with phosphate concentration 0.03 mM; (b) Type-A experiment with phosphate concentration 0.37 mM....	98
5.4	Comparison of the biomass concentration, $F'v/F'm$ vs. cultivation time profiles at two different type of experiments corresponding to a different phosphate concentration (a) Type-A experiment with phosphate concentration 0.03 mM; (b) Type-A experiment with phosphate concentration 0.37 mM....	99
5.5	Comparison of biomass, lipid, and chitin yield per 10 ⁹ cells vs. overall phosphate concentration (mM) in the cell suspension, (a-b) Type-A experiment with phosphate concentration window between 0 – 0.05 mM; (c-d) Type-B experiment with phosphate concentration window between 0 – 0.5 mM.....	100

LIST OF FIGURES (Continued)

- 5.6 Comparison of cell, lipid, and chitin productivity vs. overall phosphate concentration (mM) in the cell suspension, (a-b) Type-A experiment with phosphate concentration window between 0 – 0.05 mM; (c-d) Type-B experiment with phosphate concentration window between 0 – 0.5 mM.....101
- 5.7 Comparison of lipid class abundance compared by area count divided by lipid amount in milligrams of lipidomic data at time point of 9 days after the beginning of Stage II for a representative sample of Type-A (a) and Type-B (b) experiments (0.03 and 0.37 mM phosphate respectively). Triacylglycerides (TAG), diacylglycerides (DG), free fatty acids (FFA), lysophosphatidylcholine (LPC), phosphatidylcholine (PC), phosphatidylglycerol (PG), and lysophosphatidylglycerol (LPG)102
- 5.8 SEM image of *Cyclotella* sp. diatom cell showing native chitin nanofibers surrounding the cell (a) girdle band view, (b) valve view103

LIST OF TABLES

<u>Table</u>	<u>Page</u>
3.1 Dissolved silicon (Si) and nitrate (N) delivery for two-stage batch/fed-batch photobioreactor cultivation experiments. In all photobioreactor cultivation experiments, the intended total nutrient delivery was 0.8 mM Si and 1.2 mM nitrate for each stage, with Stage I + II cumulative delivery of 1.6 mM Si and 2.4 mM nitrate. Average final cell number densities after each stage are also presented	46
4.1 Yield parameters for the diatom <i>Cyclotella</i> sp	69
5.1 Nutrient process parameters for the cultivation of the diatom <i>Cyclotella</i> sp ..	94
5.2 Lipid class molecules found in samples, categorized as neutral lipids and phospholipids. Symbol represents the area response range of the extracted ion chromatogram. (- : no response; + : $1 \leq x < 5 \times 10^4$; ++ : $5 \times 10^4 \leq x < 5 \times 10^5$; +++ : $5 \times 10^5 \leq x < 5 \times 10^6$; ++++ : $5 \times 10^6 \geq x$)	95

Chapter 1: General Introduction

Introduction

The energy sustainability of the future will depend on the renewable energy sources that are developed today. Microalgae have shown to be excellent candidates to become renewable energy platforms, however, the current economics of biofuels derived from algae are not promising with costs of biodiesel ranging from 0.82 to 75.77 \$/L in the year 2012 (1). With such a variability in prices of biodiesel, the field needs a new way to approach this problem.

If the focus of microalgae production is based not solely on biofuels, but it is based on highly valued bioproducts, there are better chances that we can address the problem of long term sustainable energy sources. A diatom based photosynthetic biorefinery puts together these problems into a new perspective, where the economics of microalgae is not solely based on biofuels. The aforementioned biorefinery seeks to harness the photosynthetic capabilities of diatoms into producing valued bioproducts with different streams, all coming from a single microorganism (2). In order to achieve this, there is a need to understand the biochemistry of the microorganism and how it is affected by the deliberate addition of nutrients under special nutrient induced conditions. Acquiring the fundamental understanding of diatoms will enable the controlled production of high value bioproducts that will be economically and environmentally sustainable.

The next section is an overview of diatoms, their nutrient requirements, and their products.

Diatoms are aquatic photosynthetic organisms. They are accounted for 39% of the organic matter production of the oceans (3). The capability of diatoms to metabolically produce antibiotics, antioxidants, toxins, and bioactive compounds is supported by a vast amount research, and it makes them very attractive for novel applications (4). Another reason why diatoms are unique is that they utilize silicon as a substrate to build their intricate nano-patterned structured cell wall (5). The nano-patterned cell walls of diatoms are called frustules, and they are made of silicon oxide (6). The way diatoms utilize this substrate for their benefit is what makes them very successful and robust organisms that have colonized vast surfaces of water in the

world. The silicon metabolism of diatoms has evolved to require low amounts of energy for silicon uptake, deposition, and cell wall formation (7).

Nutrients consumed by diatoms can be categorized as macronutrients and micronutrients. Macronutrients are present in higher concentrations relative to micronutrients and diatoms have evolved to be able to utilize substrates under low concentrations. Soluble silicon is found in seawater at concentrations below 2 mM (8), and diatoms are able to uptake it either by diffusion or active transport of the substrate through the membrane via specialized substrate specific transporters (9). Nitrogen and phosphorus are other macronutrients that are of importance for cells. Nitrogen and phosphorus are usually present in seawater as soluble inorganic salts, and they are assimilated to produce amino acids, proteins, nucleic acids, phospholipids and chemical energy carrier molecules (10).

Micronutrients are utilized by diatoms as cofactors for enzymatic processes. Despite the fact that they are present in the media in trace concentrations, they play important roles in the biochemistry of the microorganism. Inorganic micronutrients include iron, cobalt, copper, boron, manganese, molybdenum and zinc (10).

Silicon is used to build the frustule of the cell, therefore silicon controls the division of diatoms. The amount of silicon that is available for a cell is directly correlated to the progeny that the cells can create (8). This is an advantage when working with diatoms, since the coupling of cell division to a unique substrate makes them easily controllable organisms. When silicon is depleted from the media, cell division is arrested and other cellular processes are triggered, specifically lipid accumulation (11).

Diatoms are known to concentrate lipids as a response to starvation of nutrients. There is a significant body of literature that has studied this phenomena (12 -14). The underlying significance of nutrient deprivation in diatoms is to force the cells to reallocate their nitrogen and phosphorus sources that are within the cell into alternate metabolic pathways. The shift of pathways results in lipid production, which is a desired response for lipid accumulation(12). There can also be other shifts in the metabolic pathways that result in carbohydrate accumulation, which is discussed next.

Chitin is the second most abundant biopolymer on earth after cellulose (15). Despite its abundance, chitin is very hard to find in a pure form, since it is associated with proteins and other fine structures (16). There are two diatom species that produce chitin, *T. Pseudonana* and *Cyclotella* sp, with the latter extruding pure chitin fibers out of special pores located in the perimeter of the valve face (2). Chitin fibrils are used in biomedical applications such as in wound dressings, bone substitutes, tissue engineering, and drug delivery (16). Chitin fibers have also been used to create templates of nitrogen-doped carbon materials in supercapacitor electrodes, and nanostructured organic-inorganic silica hybrid materials (5).

The phototrophic cultivation of diatoms requires specialized platforms that are generically labelled as photobioreactors. There are many types of photobioreactors that can be used to culture diatoms; commonly used are the bubble column and airlift photobioreactors. The photobioreactor platform should be capable of delivering light, carbon dioxide (air), and have an adequate mixing system that will homogenize the culture medium without disrupting the cells (10). The platform for cultivation of *Cyclotella* sp. is a bubble column photobioreactor, and the design can be found in (17) with the modifications described in (18).

By strategic feeding of nutrients in batch and fed-batch cultivations of the marine diatom *Cyclotella* sp., we intend to control cell production, and the formation of lipid and chitin.

Phosphorus is a key nutrient in microalgae, since it is part of proteins, nucleic acids, and phospholipids (membrane lipids). P also plays a significant role in the energy transport mechanism of photosynthesis with the molecule adenosine triphosphate (ATP) (19). The results from Objectives 1-2 and previous literature suggest that P may play a significant role in the stimulation of lipid production in the cell.

Photosynthesis requires phosphorus for photosynthetic carbon assimilation. ATP is used in the photosynthetic carbon reduction (PCR) cycle, where CO₂ is fixed into a C₃ moiety (triose-P) (20). The energy required to carry out this reaction comes from the light that PSII converts into chemical energy. Phosphorus limitation inhibits the overall photosynthetic capability of diatoms. The photosynthesis rate depends on the

equilibrium between ATP and the following strong reducing molecules; nicotinamide adenine dinucleotide phosphate (NADPH), nicotinamide adenine dinucleotide (NADH), and ferredoxin. Any alteration in this balance due to phosphorus limitation, will inhibit photosynthesis (20). In the onset of P limitation, cells can downregulate their metabolism to 50% of their original phosphorus demand by relocating intracellular phosphorus (21- 22), which helps them undergo cell division and perform other cellular processes (23). P limitation causes damage in the photosystem of the cell (23), and it is expressed as a decline of the photosynthetic quantum efficiency (24-25).

Carbon assimilation and carbon partitioning is correlated to the photosynthetic activity (20). Experiments carried out with microalgae in replete phosphorus conditions showed the highest expression of central enzymes for carbon fixation during cultivation. It was also found that nine fatty acid genes were upregulated during the light period of cultivation, eight of them reached maximum expression (26). This suggests that phosphorus is important for microalgae photosynthetic production and carbon partitioning into energy dense molecules.

Replenishing P to P-limited cultures restores the overall photosynthetic capabilities of the cell. Studies have demonstrated that adding P to P-deficient cultures stimulates growth rates (27) and allows for the recovery of the photosystems, evidenced by the increase of photosynthetic quantum yields (24).

The overall goal of this dissertation is to create a deep understanding of the key metabolic pathways of the marine diatom *Cyclotella* that can be controlled to product formation through bioprocess engineering techniques, namely, through the controlled delivery of soluble nutrients.

The objectives of this dissertation are the following:

- Highlight the current understanding of chitin production in marine diatoms.
- Assess how nitrogen availability affects chitin production during batch cultivation of the marine diatom *Cyclotella* sp.

- Develop a nutrient feeding strategy to control the production of the valued coproduct chitin from the lipid-producing diatom *Cyclotella* sp.
- Assess how phosphate concentration affects cells, lipid, and chitin formation during a two stage cultivation of the diatom *Cyclotella* sp.

References

1. Nagarajan S, Chou SK, Cao S, Wu C, Zhou Z. An updated comprehensive techno-economic analysis of algae biodiesel. *Bioresour Technol.* 2013;145:150–6.
2. Rorrer GL, Antonio J, Durst R, Kelly C, Gale D, Maddux B, et al. The Potential of a Diatom-Based Photosynthetic Biorefinery for Biofuels and Valued Co-Products chitin. *Curr Biotechnol.* 2016;5:237–48.
3. Obata T, Fernie AR, Nunes-Nesi A. The central carbon and energy metabolism of marine diatoms. *Metabolites* [Internet]. 2013 May 7 [cited 2016 Oct 25];3(2):325–46. Available from: <http://www.ncbi.nlm.nih.gov/pubmed/24957995>
4. Kannan DC, Pattarkine VM. Algal Biorefineries. Vol. 1, Algal Biorefineries. 2014. 297-310 p.
5. Jeffryes C, Agathos SN, Rorrer G. Biogenic nanomaterials from photosynthetic microorganisms. Vol. 33, *Current Opinion in Biotechnology.* 2015. p. 23–31.
6. Coombs J, Darley WM, Volcani BE. Studies on the Biochemistry and Fine Structure of Silica Shell Formation in Diatoms. Chemical Composition of *Navicula pelliculosa* during Silicon-Starvation Synchronyl. *Plant Physiol.* 1967;42:1601–6.
7. Martin-Jezequel V, Hildebrand M, Brzezinski MA. SILICON METABOLISM IN DIATOMS: IMPLICATIONS FOR GROWTH. *J Phycol* [Internet]. 2000 Oct [cited 2016 Oct 26];36(5):821–40. Available from: <http://doi.wiley.com/10.1046/j.1529-8817.2000.00019.x>
8. Hildebrand M, Davis AK, Smith SR, Traller JC, Abbriano R. The place of diatoms in the biofuels industry. *Biofuels.* 2012;3(2):221–40.
9. Thamatrakoln K, Hildebrand M. Silicon uptake in diatoms revisited: a model for saturable and nonsaturable uptake kinetics and the role of silicon transporters. *Plant Physiol* [Internet]. 2008 Mar [cited 2016 Oct

26];146(3):1397–407. Available from:
<http://www.ncbi.nlm.nih.gov/pubmed/18162598>

10. Rorrer GL. Bioprocess Engineering of Phototrophic Marine Organisms. In: Kim S-K, editor. Springer Handbook of Marine Biotechnology [Internet]. Berlin, Heidelberg: Springer Berlin Heidelberg; 2015. p. 257–94. Available from: http://dx.doi.org/10.1007/978-3-642-53971-8_9
11. Zhao P, Gu W, Wu S, Huang A, He L, Xie X, et al. Silicon enhances the growth of *Phaeodactylum tricornutum* Bohlin under green light and low temperature. *Sci Rep* [Internet]. 2014 Feb 4 [cited 2016 Sep 10];4:237–40. Available from: <http://www.nature.com/articles/srep03958>
12. Fields MW, Hise A, Lohman EJ, Bell T, Gardner RD, Corredor L, et al. Sources and resources: importance of nutrients, resource allocation, and ecology in microalgal cultivation for lipid accumulation. *Appl Microbiol Biotechnol* [Internet]. 2014 Jun [cited 2016 Oct 26];98(11):4805–16. Available from: <http://www.ncbi.nlm.nih.gov/pubmed/24695829>
13. Adams C, Godfrey V, Wahlen B, Seefeldt L, Bugbee B. Understanding precision nitrogen stress to optimize the growth and lipid content tradeoff in oleaginous green microalgae. *Bioresour Technol*. 2013;131:188–94.
14. d’Ippolito G, Sardo A, Paris D, Vella F, Adelfi M, Botte P, et al. Potential of lipid metabolism in marine diatoms for biofuel production. *Biotechnol Biofuels*. 2015;8(1):28.
15. Durkin CA, Mock T, Armbrust EV. Chitin in diatoms and its association with the cell wall. *Eukaryot Cell* [Internet]. 2009 Jul [cited 2016 Sep 13];8(7):1038–50. Available from: <http://www.ncbi.nlm.nih.gov/pubmed/19429777>
16. Khor E. Chitin: Fulfilling a Biomaterials Promise. 1st ed. Amsterdam: Elsevier; 2001. 1-136 p.
17. Jeffryes C, Gutu T, Jiao J, Rorrer GL. Two-stage photobioreactor process for the metabolic insertion of nanostructured germanium into the silica

- microstructure of the diatom *Pinnularia* sp. *Mater Sci Eng C* [Internet]. 2008 Jan [cited 2016 Jul 26];28(1):107–18. Available from:
<http://linkinghub.elsevier.com/retrieve/pii/S0928493107000045>
18. Chiriboga N. OG, Rorrer GL. Control of Chitin Production by the Lipid-Producing Diatom *Cyclotella* sp. through Fed-Batch Addition of Dissolved Silicon and Nitrate in a Bubble-Column Photobioreactor. *Biotechnol Prog*. 2017;33(2):407–15.
 19. Tantanasarit C, Englande AJ, Babel S, Meksumpun S. Nitrogen, phosphorus and silicon uptake kinetics by marine diatom *Chaetoceros calcitrans* under high nutrient concentrations. *J Exp Mar Bio Ecol* [Internet]. 2013 Aug [cited 2016 Oct 5];446:67–75. Available from:
<http://linkinghub.elsevier.com/retrieve/pii/S0022098113001792>
 20. Rychter AM, Rao IM. Role of phosphorus in photosynthetic carbon metabolism. In: *Handbook of photosynthesis*. Taylor and Francis Group LLC; 2005. p. 123–48.
 21. Van Mooy BAS, Fredricks HF, Pedler BE, Dyhrman ST, Karl DM, Koblížek M, et al. Phytoplankton in the ocean use non-phosphorus lipids in response to phosphorus scarcity. *Nature* [Internet]. 2009 Mar 5 [cited 2016 Oct 4];458(7234):69–72. Available from:
<http://www.nature.com/doi/10.1038/nature07659>
 22. Martin P, Van Mooy BA, Heithoff A, Dyhrman ST. Phosphorus supply drives rapid turnover of membrane phospholipids in the diatom *Thalassiosira pseudonana*. *ISME J* [Internet]. 2011 Jun 16 [cited 2016 Oct 4];5(6):1057–60. Available from: <http://www.nature.com/doi/10.1038/ismej.2010.192>
 23. Feng T-Y, Yang Z-K, Zheng J-W, Xie Y, Li D-W, Murugan SB, et al. Examination of metabolic responses to phosphorus limitation via proteomic analyses in the marine diatom *Phaeodactylum tricornutum*. *Sci Rep* [Internet]. 2015 May 28 [cited 2016 Aug 8];5:10373. Available from:
<http://www.nature.com/articles/srep10373>

24. Qi H, Wang J, Wang Z. A comparative study of maximal quantum yield of photosystem II to determine nitrogen and phosphorus limitation on two marine algae. *J Sea Res.* 2013;80:1–11.
25. Napoléon C, Raimbault V, Claquin P. Influence of Nutrient Stress on the Relationships between PAM Measurements and Carbon Incorporation in Four Phytoplankton Species. *PLoS One* [Internet]. 2013 [cited 2016 Oct 4];8(6):e66423. Available from: <http://www.ncbi.nlm.nih.gov/pubmed/23805221>
26. Chauton MS, Winge P, Brembu T, Vadstein O, Bones AM. Gene regulation of carbon fixation, storage, and utilization in the diatom *Phaeodactylum tricornutum* acclimated to light/dark cycles. *Plant Physiol* [Internet]. 2013 Feb [cited 2016 Oct 12];161(2):1034–48. Available from: <http://www.ncbi.nlm.nih.gov/pubmed/23209127>
27. Litchman E, Steiner D, Bossard P. Photosynthetic and growth responses of three freshwater algae to phosphorus limitation and daylength. *Freshw Biol* [Internet]. 2003 Dec [cited 2016 Oct 12];48(12):2141–8. Available from: <http://doi.wiley.com/10.1046/j.1365-2427.2003.01157.x>

Chapter 2: Extracellular chitin nanofibers from marine diatoms

Omar G. Chiriboga N., Paul LeDuff, Gregory L. Rorrer

Submitted as a book chapter for the Encyclopedia of Marine Biotechnology – Se-Kwon Kim, editor. Wiley publishers.

Summary

Diatom algae are diverse platform for sustainable production of advanced nanomaterials. In addition to nanostructured biosilica, some diatoms also produce nanofibers of the N-acetyl glucosamine biopolymer commonly known as called chitin. Many marine organisms also make shells of chitin that are intercalated with minerals, proteins, and other carbohydrates. However, a few species of diatoms extrude pure, paracrystalline β -chitin nanofibers of 50 nm diameter through specialized pores ringing the perimeter of the diatom cell wall. This chapter will describe the cellular mechanisms of chitin nanofiber formation by centric marine diatoms, their structural properties, and their biomedical and biotechnology applications.

Introduction

Marine diatoms are photosynthetic microalgae that make a unique biosilica cell wall called the frustule that possesses intricate pore arrays ordered at the submicron and nanoscale. The frustules of diatoms have evolved to help them collect photons from sunlight needed for photosynthesis (1-2). Diatom are responsible for a nearly 40% of carbon fixation in the ocean. There are a broad spectrum of carbon compounds produced by marine diatoms, such as proteins, lipids, and carbohydrates (3-4).

Light microscopy images of the centric marine diatom *Cyclotella* sp. taken in our laboratory are presented in Figure 2.1. The whiskers shown emanating from the living cells are chitin nanofibers. Chitin is the second most abundant biopolymer on Earth (5). Chitin is a homopolymeric chain comprised of N-acetyl-glucosamine with subunits linked through a glycosidic bond in the β -1,4 conformation.

Figure 2.2 shows the molecular structure of the chitin homopolymer. Chitin exists in three polymorph structures named α , β , and γ . The difference between the polymorphs is the hydration degree, and the orientation of its chains, which determines the crystalline structure (6). Despite the vast presence of chitin in Nature, only a few centric marine diatoms are known to produce these unique extracellular β -chitin nanofibers, which are the focus of this chapter.

Historical perspective

Extracellular chitin nanofibers from marine diatoms were first described as “diatom silk” in 1899 by the German Botanist Franz Schütt (7). Schütt was part of an expedition that took place around the North Atlantic Ocean to study the behavior of phytoplankton. Schütt observed that the fibers that emanated from the valves affected the settling time of the diatom in the water column, but did not connect this diatom silk to “fungine” and “chitine” described by his contemporaries in other organisms, materials we know today as chitin (9-10). Later studies noted that the mucilages or spines that irradiated from the centric diatoms had some particularly interesting chemical properties (11). In 1965, McLachlan et al. were the first investigators to cultivate the marine diatom *Thalassiosira fluviatilis* and isolate the chitin fibers (12); however they named the fibers “chitan”. The authors used this term because chitin fibers known at that time were associated with proteins, carbohydrates and other organic materials, while the nanofibers from *T. fluviatilis* had none of these constituents (13). By 1967, the different naming system for the fibers extruded from the marine diatoms *Thalassiosira fluviatilis* and *Cyclotella cryptica* was resolved by Blackwell et al., who named them as β -chitin. However, some studies use the terms chitin and chitan interchangeably (14 -15).

Current understanding

It is now known today that chitin produced by marine diatoms consists of nanoscale fibers of β -chitin. Some marine diatoms possess an intracellular mesh of chitin

nanofibers imbedded within the biosilica frustule. The function of this intracellular chitin meshwork is to provide additional support structure to the biosilica (16-18).

Extracellular chitin nanofibers are found in centric diatoms of the genera *Cyclotella* and *Thalassiosira* (19). The chitin nanofibers are extruded from a special cylindrical port located at the rim of the frustule theca called a fultoportulae. The average number of fultoportulae on *Cyclotella* and *Thalassiosira* are 20 and 12 per theca respectively, which are symmetrically spaced along the theca rim. The reason why these diatoms produce extracellular chitin nanofibers is not fully understood. The idea of buoyancy control that Schütt proposed from his observations is still accepted today, as studies have shown that extracellular chitin nanofibers are produced during late exponential growth to promote the formation of multicellular flocs needed to mediate buoyancy in the water column (20-21).

Biosynthesis

Chitin biosynthesis has been extensively studied in insects (22). However, it is not fully understood in marine diatoms. A proposed chitin biosynthesis pathway in marine diatoms is presented in Figure 2.3. The proposed pathway is based on the assumption that chitin biosynthesis in marine diatoms is similar to chitin biosynthesis in insects. There are six key biochemical reactions, starting with glucose-6-phosphate, and ending with the homopolymer chitin. Marine diatoms fix inorganic carbon by photosynthesis and make glucose-6-phosphate through carbohydrate metabolism (23). In Reaction 1, glucose-6-phosphate is isomerized to fructose-6-phosphate by glucose-6-P isomerase. Reaction 2 is the amination process, where fructose-6-phosphate gains an amine group by transforming glutamine to glutamic acid, producing glucosamine-6-phosphate catalyzed by glutamine-fructose-6-P aminotransferase. Reaction 3 is the acetylation of glucosamine-6-phosphate by transformation of acetyl coenzyme A to coenzyme A, producing N-acetyl glucosamine-6-phosphate catalyzed by glucosamine-6-P N-acetyltransferase. In Reaction 4, the phosphate group of N-acetyl glucosamine-6-phosphate is relocated

from carbon 6 to carbon 1, producing N-acetyl glucosamine-1-phosphate catalyzed by phosphor-N-acetyl glucosamine mutase. In Reaction 5, N-acetyl glucosamine-1-phosphate gains the uridine diphosphate (UDP) by converting uridine triphosphate (UTP) to phosphate, producing UDP-N-acetylglucosamine catalyzed by UDP-N-acetylglucosamine pyrophosphorylase. Finally, Reaction 6 occurs by formation of glycosidic bond in the β -1,4 configuration between the chitin polymer and UDP-N-acetylglucosamine, which is catalyzed by chitin synthase.

Fiber structure

Figure 2.4 is a conceptual schematic describing how the centric marine diatom produces chitin nanofibers. Chitin nanofiber formation occurs in three steps: polymerization, crystallization and extrusion. The polymerization step occurs in the chitin pockets that are located below each fulcportulae. The polymerization is a transmembrane process where the membrane bound chitin synthase utilizes UDP-N-acetylglucosamine and links it to the growing chitin chain with a glycosidic bond. The chitin chain is released to the chitin pocket. The crystallization process occurs in the chitin pocket between different chitin chains that interact with each other, creating inter- and intra- chain hydrogen bonds. The chains crystallize in a parallel structure, where reducing ends are pushed away from the site of biosynthesis, whereas the non-reducing ends are closer to the site of biosynthesis (24), creating the β -Poly-N-Acetyl glucosamine nanofiber. Diatom-derived chitin has a nominal molecular weight of 2.8×10^6 Da (25). Once the β -chitin nanofiber has crystallized, it is extruded outside of the fulcportulae into the surrounding liquid medium, but is still attached to the cell.

Scanning electron microscopy (SEM) images of centric marine diatoms of within genus *Thalassiosira* and *Cyclotella* taken by our laboratory are presented in Figure 2.5. Figure 2.5a shows a single cell extruding β -chitin nanofibers. Figure 2.5b shows two cells that are in the process of division. The cells are still attached to each other at the valve face, but as the frustules detach from each other, β -chitin nanofibers will be produced. Figure 2.5c shows two separate cells that have β -chitin nanofibers attached to their fulcportulae. The images also show β -chitin nanofibers that are not attached

to a particular cell, indicating that the nanofibers can be dislodged from the cell. The extracellular chitin nanofibers appear as stiff rods with average diameter of 50 nm and several microns in length.

Crystalline Structure

X-ray diffraction (XRD) spectra of chitin nanofibers from marine diatoms cultured in our laboratory is presented in Figure 2.6a. A schematic of the molecular β -structure of the chitin taken from the literature is presented in Figure 2.6b. The XRD spectrum of the chitin nanofibers from the diatoms *Thalassiosira* and *Cyclotella* both show distinctive peaks at 10 and 20°, which are characteristic of β -chitin. These peaks are a consequence of the three dimensional, parallel arrangement of the individual chitin biopolymer chains. The XRD spectrum also shows the purity of the nanofibers, which are not attached to other carbohydrate, proteins, or structural material.

Future applications

The uses and applications of chitin and chitosan are extensively studied (26). Below we highlight promising future applications of pure β -chitin nanofibers.

A key feature of β -chitin in comparison to α -chitin is that the β -polymorph has lower degree of hydrogen bonding than the α -polymorph. This makes the fiber easier to dissolve and more amenable to chemical modification and functionalization (27). In this context, β -chitin nanofibers are an exceptional biomaterials for biomedical and bionanotechnology fields such as tissue engineering, stem cell technology, and neural networks, as described by several studies (5) (26)(28- 29). Chitin nanofibers can also be used in bioelectronics applications (30-32).

To advance the applications of β -chitin nanofibers, a reliable, consistent, and sustainable source of β -chitin nanofibers is needed. Marine diatoms are source of β -chitin nanofibers. The nanofibers extruded from centric marine diatom *Cyclotella* sp. are pure and paracrystalline, and are not attached to proteins or other structural

polysaccharide material. Controlled production of β -chitin nanofibers in a bioprocessing environment through diatom cultivation enables traceability of materials and recovery of the bio-product. Marine diatoms require macronutrients, micronutrients, carbon dioxide, and a light source to divide and produce the chitin nanofibers. Achieving high cell number density and targeting nutrient addition to maximize chitin nanofiber production by the marine diatom *Cyclotella* will enable the expansion of the β -chitin nanofiber applications research, and is a current focus of our laboratory (20) (33- 34).

Acknowledgements

This work was supported by the US National Science Foundation (NSF), Emerging Frontiers for Research and Innovation program (EFRI), under award number 1240488.

References

1. De Tommasi, E., Rea, I., Mocella, V., et al. (2010) Multi-wavelength study of light transmitted through a single marine centric diatom. *Optics Express*, **18** (12), 12203.
2. Ferrara, M.A., Dardano, P., De Stefano, L., et al. (2014) Optical Properties of Diatom Nanostructured Biosilica in *Arachnoidiscus* sp: Micro-Optics from Mother Nature. *PLoS One*, **9** (7), e103750.
3. Svetličić, V., Žutić, V., Pletikapić, G., and Radić, T. (2013) Marine Polysaccharide Networks and Diatoms at the Nanometric Scale. *International Journal of Molecular Sciences.*, **14** (10), 20064–20078.
4. Yi, Z., Xu, M., Di, X., et al. (2017) Exploring Valuable Lipids in Diatoms. *Frontiers in Marine Science*, **4**.
5. Elieh-Ali-Komi, D., and Hamblin, M.R. (2016) Chitin and Chitosan: Production and Application of Versatile Biomedical Nanomaterials. *International Journal of Advanced Research*, **4** (3), 411–427.
6. Khoushab, F., and Yamabhai, M. (2010) Chitin research revisited. *Marine Drugs*, **8** (7), 1988–2012.
7. Schütt, F. (1899) Ein neues Mittel der Koloniebildung bei Diatomeen und seine systematische Bedeutung. *Bericht der deutschen botanischen Gessellschaft*, **17**, 215–221.
8. Damkaer, D.M., and Mrozek-Dahl, T. (1980) The Plankton-Expedition and the Copepod Studies of Friedrich and Maria Dahl, in *Oceanography: The Past*, Springer New York, New York, NY, pp. 462–473.
9. Braconnot, H. (1811) Sur la nature des champignons. *Ann. Chim Phys*, **79**, 265–304.
10. Odier, A. (1823) Mémoire sur la composition chimique des parties cornées des insectes. *Memoire la Societe d’Histoire Natural Paris*, **1**, 29–42.
11. Guillard, R.R.L., and Ryther, J.H. (1962) Studies of marine planktonic diatoms: I. *Cyclotella* Nana Hustedt, and *Detonula* Cnfervacea (cleve) gran. *Canadian Journal of Microbiology*, **8** (2), 229–239.
12. McLachlan, J., Mcinnes, A.G., and Falk, M. (1965) Studies of the chitan (chitin: Poly-N-Acetylglucosamine) fibers of the diatom *Thalassiosira fluviatilis* hustedt I. Production and Isolation of chitan fibers. *Canadian Journal of Botany*, **43** (6), 707–713.
13. Hoagland, K.D., Rosowski, J.R., Gretz, M.R., and Roemer, S.C. (1993) Diatom extracellular polymeric substances: function, fine structure, chemistry, and physiology. *Journal of Phycology.*, **29** (5), 537–566.
14. Blackwell, J., Parker, K.D., and Rudall, K.M. (1967) Chitin fibres of the

- diatoms *Thalassiosira fluviatilis* and *Cyclotella cryptica*. *Journal of Molecular Biology*, **28** (2), 383–385.
15. Khor, E. (2001) *Chitin: Fulfilling a Biomaterials Promise*, Elsevier, Amsterdam.
 16. Durkin, C.A., Mock, T., and Armbrust, E.V. (2009) Chitin in diatoms and its association with the cell wall. *Eukaryotic Cell*, **8** (7), 1038–50.
 17. Kotzsch, A., Pawolski, D., Milentyev, A., et al. (2016) Biochemical Composition and Assembly of Biosilica-associated Insoluble Organic Matrices from the Diatom *Thalassiosira pseudonana*. *Journal of Biological Chemistry*, **10** (291), 4982–4997.
 18. Brunner, E., Richthammer, P., Ehrlich, H., et al. (2009) Chitin-Based Organic Networks: An Integral Part of Cell Wall Biosilica in the Diatom *Thalassiosira pseudonana*. *Angewandte Chemie International Edition*, **48** (51), 9724–9727.
 19. Jeffryes, C., Agathos, S.N., and Rorrer, G. (2015) Biogenic nanomaterials from photosynthetic microorganisms. *Current Opinion on Biotechnology*, **33**, 23–31.
 20. Ozkan, A., and Rorrer, G.L. (2017) Lipid and chitin nanofiber production during cultivation of the marine diatom *Cyclotella* sp. to high cell density with multistage addition of silicon and nitrate. *Journal of Applied Phycoogy*, 1–8.
 21. Chiriboga, O., and Rorrer, G.L. (2017) Control of Chitin Nanofiber Production by the Lipid-Producing Diatom *Cyclotella* sp. through Fed-Batch Addition of Dissolved Silicon and Nitrate in a Bubble-Column Photobioreactor. *Biotechnology Progress*, **33** (2), 407–415.
 22. Muthukrishnan, S., Merzendorfer, H., Arakane, Y., and Kramer, K.J. (2012) 7 – Chitin Metabolism in Insects, in *Insect Molecular Biology and Biochemistry*, pp. 193–235.
 23. Kroth, P.G., Chiovitti, A., Gruber, A., et al. (2008) A Model for Carbohydrate Metabolism in the Diatom *Phaeodactylum tricornutum* Deduced from Comparative Whole Genome Analysis. *PLoS One*, **3** (1).
 24. Sugiyama, J., Boisset, C., Hashimoto, M., and Watanabe, T. (1999) Molecular directionality of β -chitin biosynthesis. *Journal Molecular Biology*, **286** (1), 247–255.
 25. Vournakis, J.N., Demcheva, M., Whitson, A., et al. (2004) Isolation, purification, and characterization of poly-N-acetyl glucosamine use as a hemostatic agent. *Journal of Trauma*, **57** (1 Suppl), S2-6.
 26. Ogawa, Y., Kimura, S., and Wada, M. (2011) Electron diffraction and high-resolution imaging on highly-crystalline β -chitin microfibril. *Journal of Structural Biology*, **176** (1), 83–90.
 27. Muzzarelli, R., Mehtedi, M., and Mattioli-Belmonte, M. (2014) Emerging Biomedical Applications of Nano-Chitins and Nano-Chitosans Obtained via

- Advanced Eco-Friendly Technologies from Marine Resources. *Marine Drugs*, **12** (11), 5468–5502.
28. Jin, J., Lee, D., Im, H.-G., et al. (2016) Chitin Nanofiber Transparent Paper for Flexible Green Electronics. *Advanced Materials*, **28** (26), 5169–5175.
 29. Wan, A.C.A., and Tai, B.C.U. (2013) CHITIN — A promising biomaterial for tissue engineering and stem cell technologies. *Biotechnology Advances*, **31** (8), 1776–1785.
 30. Cooper, A., Zhong, C., Kinoshita, Y., et al. (2012) Self-assembled chitin nanofiber templates for artificial neural networks. *Journal of Material Chemistry*, **22** (3105).
 31. Zhong, C., Deng, Y., Roudsari, A.F., et al. (2011) A polysaccharide bioprotonic field-effect transistor. *Nature Communications*, **2**, 476.
 32. Deng, Y., Josberger, E., Jin, J., et al. (2013) H⁺-type and OH⁻-type biological protonic semiconductors and complementary devices. *Scientific Reports.*, **3** (1), 2481.
 33. Gordonov, T., Liba, B., Terrell, J.L., et al. (2012) Bridging the Bio-Electronic Interface with Biofabrication. *J. Vis. Exp.*, (64), e4231.
 34. Rorrer, G.L., Antonio, J., Durst, R., et al. (2016) The Potential of a Diatom-Based Photosynthetic Biorefinery for Biofuels and Valued Co-Products chitin. *Curr. Biotechnol.*, **5**, 237–248.

Figure 2.1. Light microscope images of the marine diatom *Cyclotella* sp. with chitin nanofibers emanating from the cell. The color images are also presented in black and white create a better contrast to visualize the chitin nanofiber. (a,b) Color image of *Cyclotella* with irradiating chitin nanofibers under 40X magnification with its complimentary black and white image; (c,d) Color image of *Cyclotella* with irradiating chitin nanofibers under 63X magnification with its complimentary black and white image.

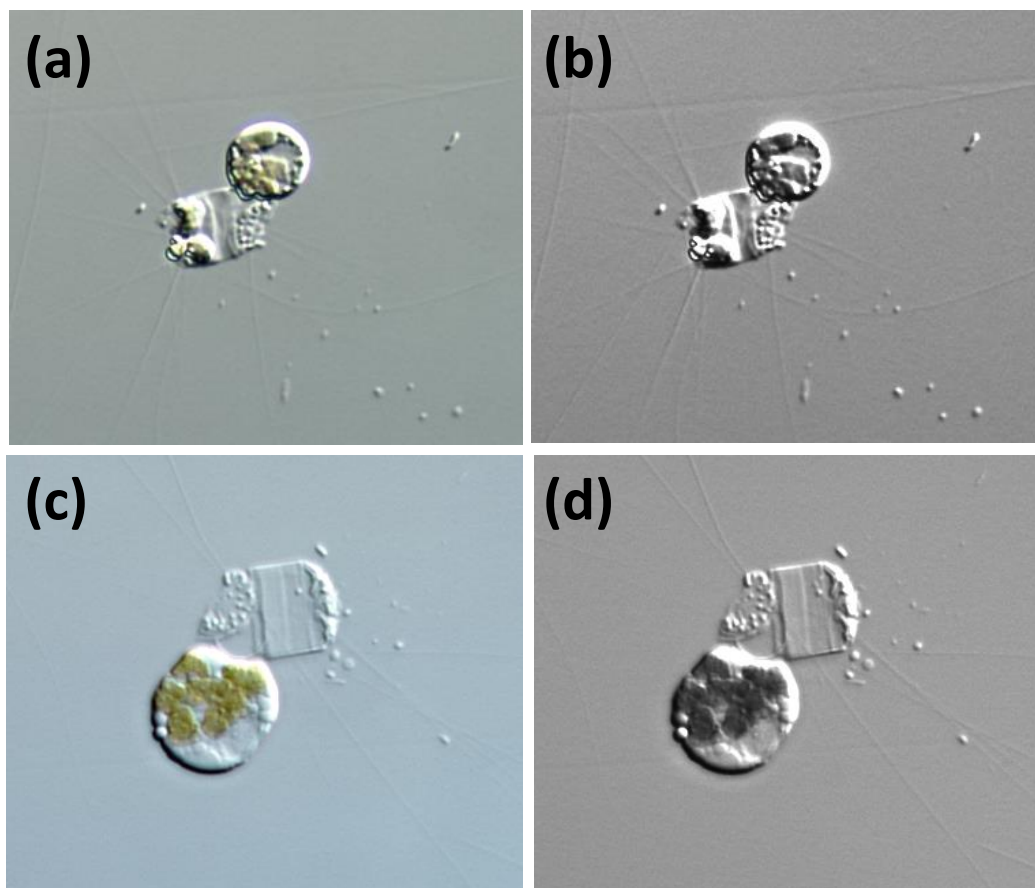


Figure 2.2. Molecular structure of homopolymer chitin with repeating *N*-acetyl glucosamine units.

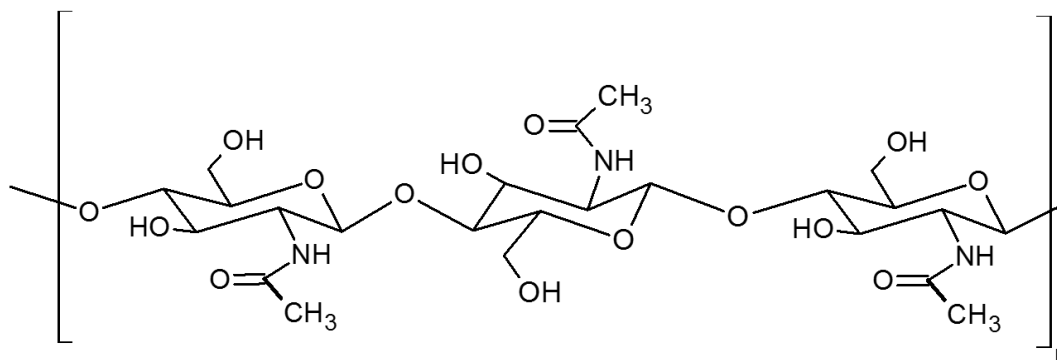


Figure 2.3. Proposed biosynthetic pathway for chitin in marine diatom, starting with glucose-6-phosphate.

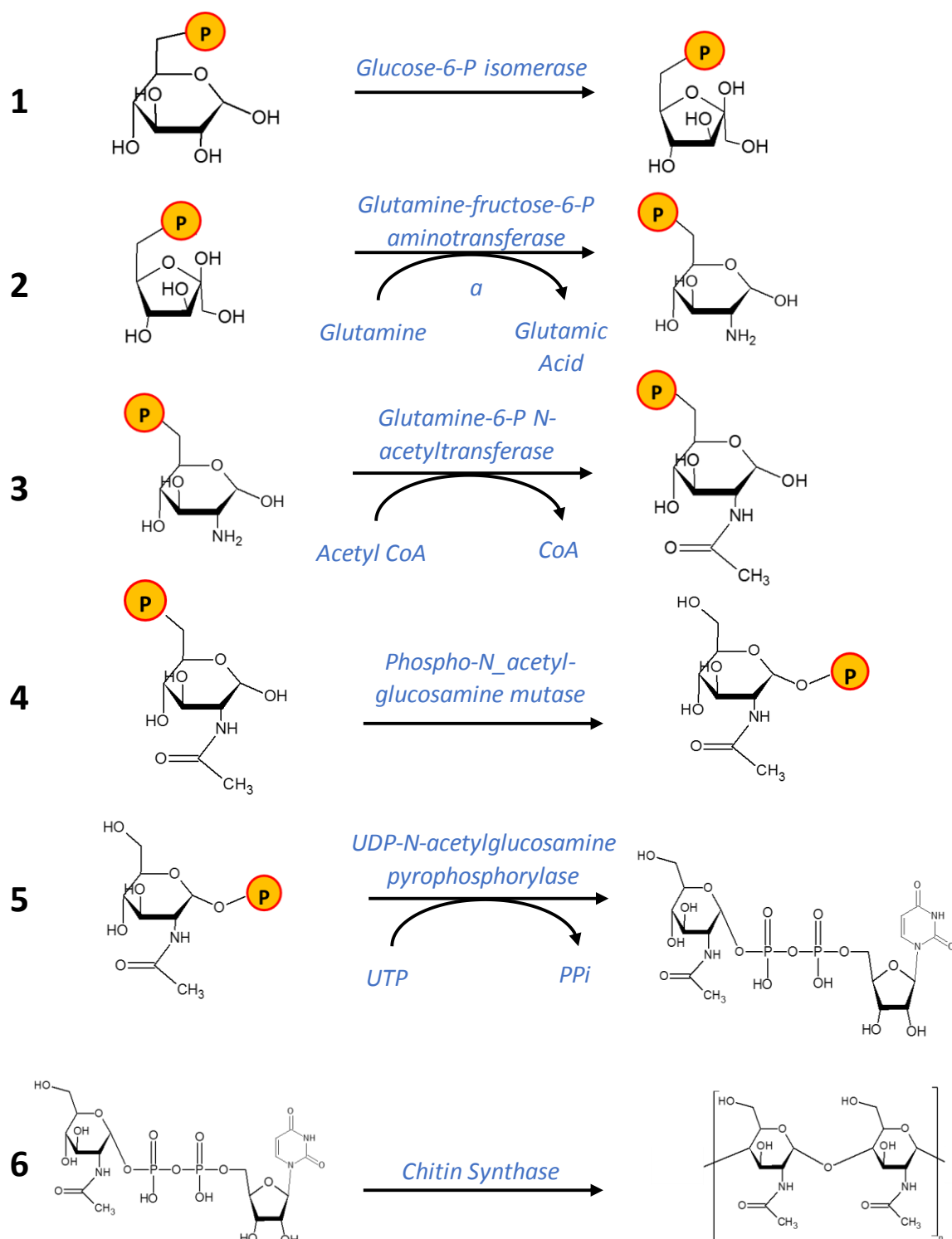


Figure 2.4. Schematics of diatom cell. (a) Cylindrical diatom cell with extracellular chitin nanofibers extruded from the symmetrically arranged fuloportulae; (b) cross section of cell; (c) fuloportulae structure with chitin pocket and chitin nanofiber formation process.

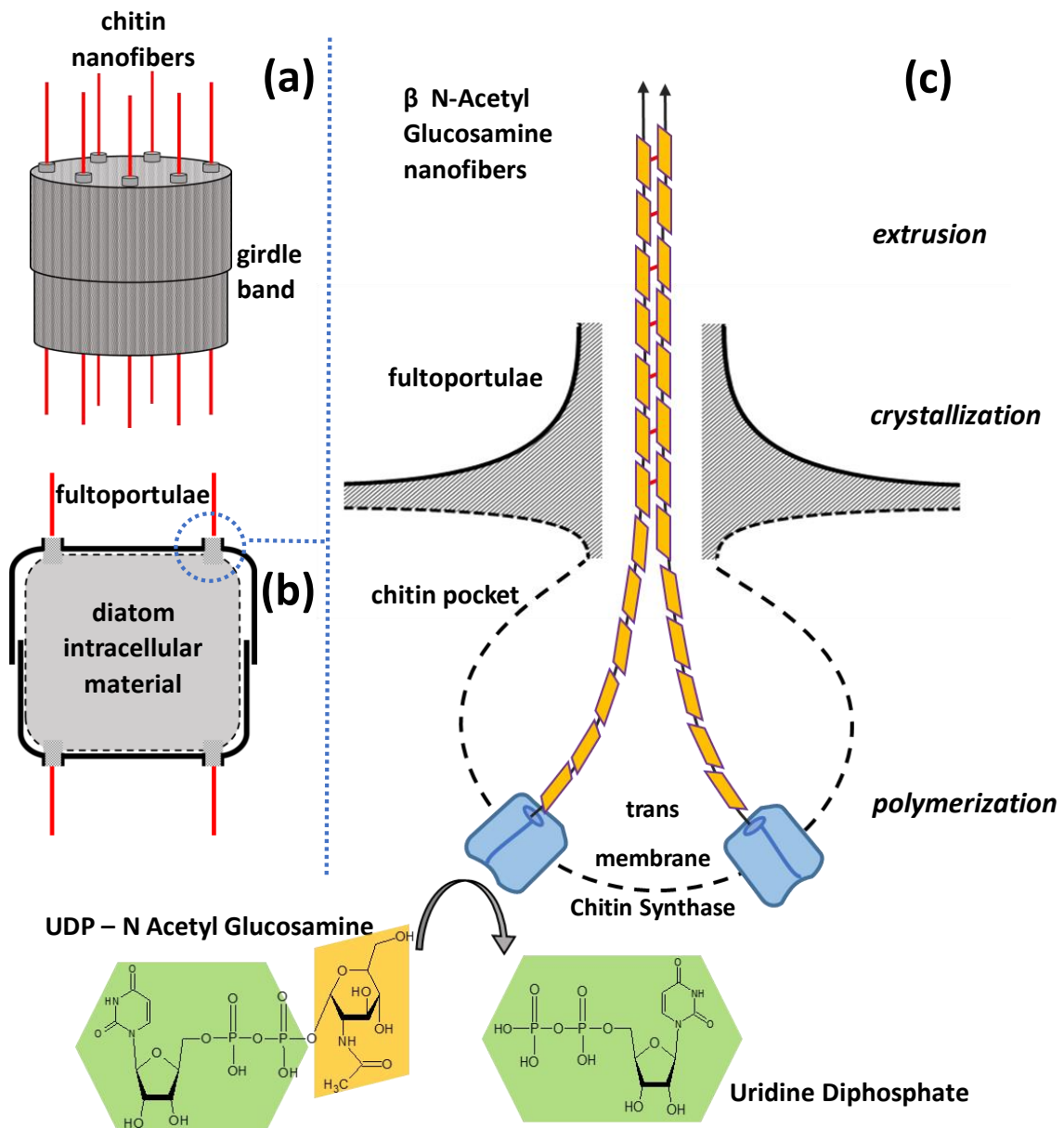


Figure 2.5. SEM images of marine diatoms of genus *Thalassiosira* (a) and *Cyclotella* (b,c) shown with extracellular chitin nanofibers surrounding the cell.

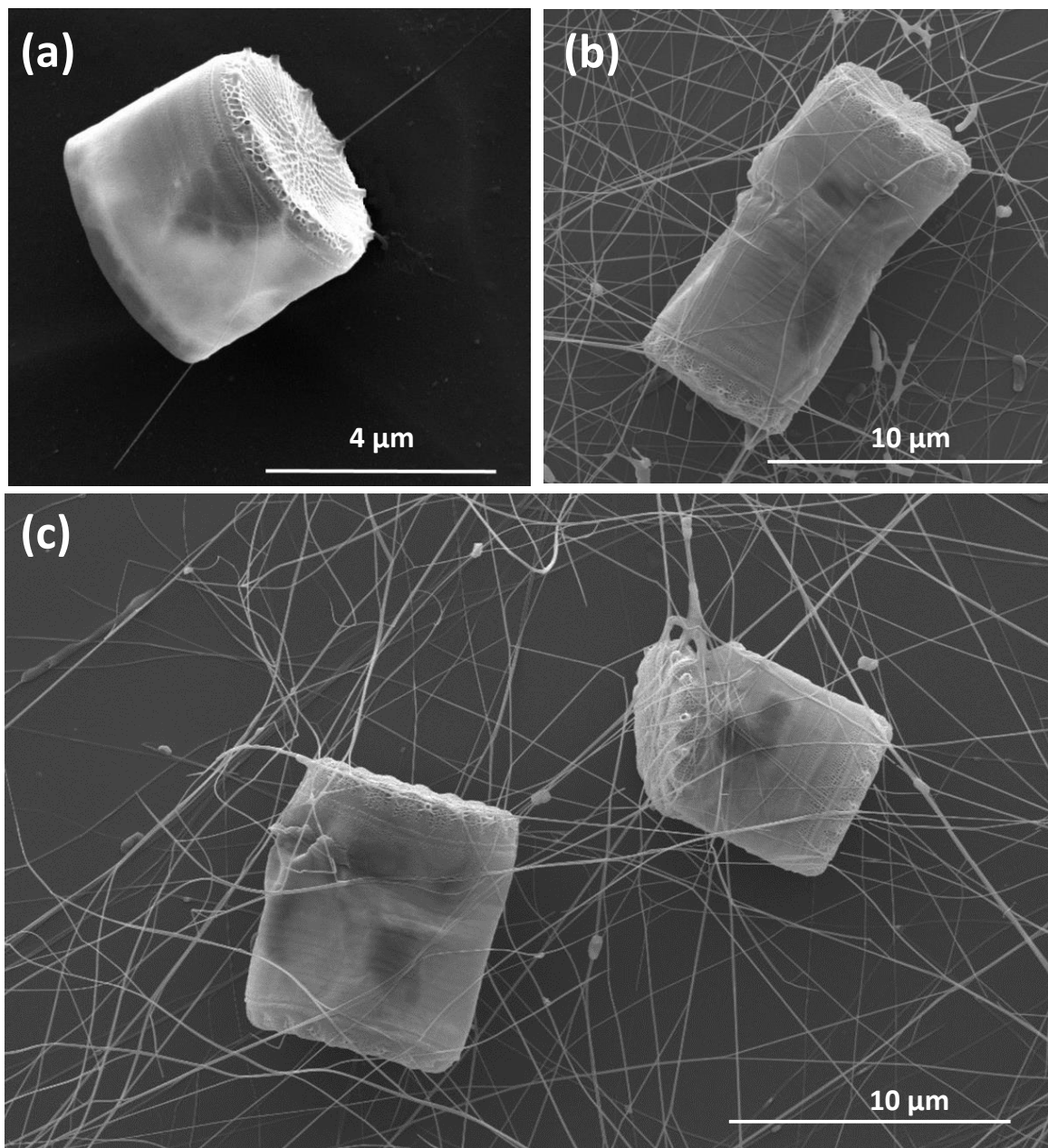
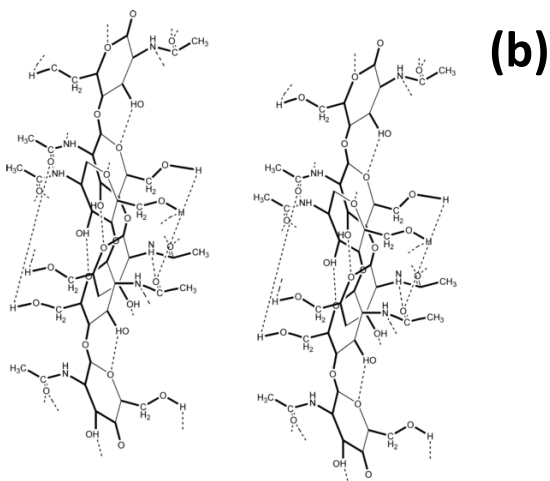
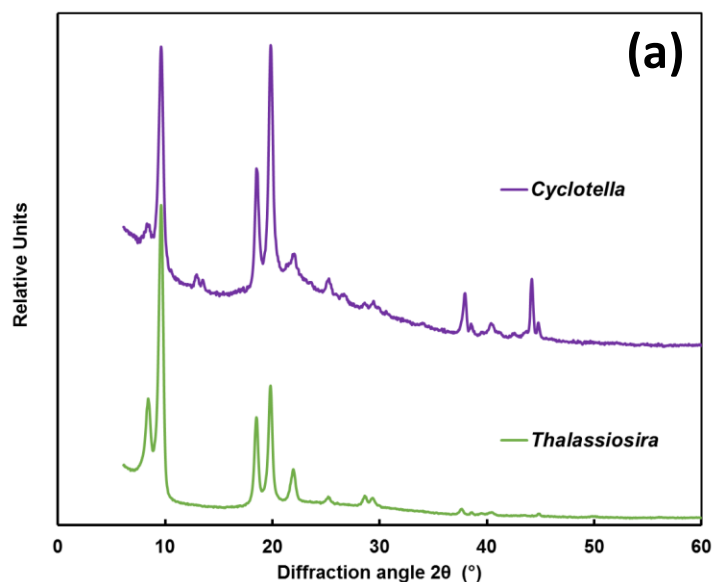


Figure 2.6. β -Chitin paracrystalline structure. (a) X-Ray diffraction (XRD) patterns of isolated extracellular chitin nanofibers from marine diatoms of genus *Cyclotella* and *Thalassiosira*. Distinctive peaks for β -chitin occur at 10° and 20° ; (b) schematic of the molecular structure of β -chitin nanofibers with hydrogen bonds, obtained from: Pillai, C.K.S. Paul, Willi; Sharma, Chandra P. Chitin and chitosan polymers: Chemistry, solubility and nanofiber formation. Progress in Polymer Science. 2009, Vol. 34 Issue 7, pages 641-678.



Chapter 3: Control of chitin nanofiber production by the lipid-producing diatom *Cyclotella sp.* through fed-batch addition of dissolved silicon and nitrate in a bubble-column photobioreactor.

Omar G. Chiriboga N., Gregory L. Rorrer

Biotechnology Progress, 2017 Mar;33(2):407-415. doi: 10.1002/btpr.2445. E-pub
2017 Mar 23

Abstract

Diatoms are single-celled algae that make cell walls of nanopatterned biogenic silica called frustules through metabolic uptake of dissolved silicon and its templated condensation into biosilica. The centric marine diatom *Cyclotella sp.* also produces intracellular lipids and the valued coproduct chitin, an N-acetyl glucosamine biopolymer that is extruded from selected frustule pores as pure nanofibers. The goal of this study was to develop a nutrient feeding strategy to control the production of chitin nanofibers from *Cyclotella* with the coproduction of biofuel lipids. A two-stage phototrophic cultivation process was developed where Stage I set the cell suspension to a silicon-starved state under batch operation, and the Stage II continuously added silicon and nitrate to the silicon-starved cells to enable once more cell doubling to 4×10^6 cells mL⁻¹. The silicon delivery rate was set to enable a silicon-limited cell division rate under cumulative delivery of 0.8 mM Si and 1.2 mM nitrate (1.5:1 mol N/mol Si) over a 4- to 14-day addition period. In Stage II, both cell number and chitin production were linear with time. Cell number and the specific chitin production yields of 13 ± 1 mg chitin / 10^9 cells and 33 ± 3 mg lipid / 10^9 cells. Therefore, chitin production is controlled through cell division, which is externally controlled through silicon delivery. Lipid production was not linearly correlated to silicon delivery and occurred primarily during Stage I, just after the complete co-consumption of both dissolved silicon and nitrate.

Introduction

Diatoms are single-celled algae that make cell walls of biogenic silica called frustules that are patterned at the submicron and nanoscale. This unique attribute of the diatom cell wall has been harnessed for many potential applications in nanomaterials and nanotechnology (1-2). Diatoms within genera *Cyclotella* and *Thalassiosira* also produce biofuel lipids approaching 40-42 wt% in the biomass (3). Consequently, given their high lipid yield and productivity under diverse environmental conditions, diatoms have recently garnered considerable interest as a platform organism for biofuel production in algal biorefineries (4-5). In addition to silicon metabolism, diatoms possess unique carbon partitioning pathways, (6-8) and make a variety of

unique and valuable coproducts. (8-10) A particular unique bioproduct known to only two species of diatoms with genera *Cyclotella* and *Thalassiosira* is the *N*-acetyl glucosamine biopolymer called chitin, which is extruded from the diatom cell as rigid microfibrils of 50 nm diameter (11-14) with high purity in β -crystalline form (15). As a potential algal biorefinery product, chitin is also of particular commercial interest, given its high value, biomedical properties, and its hydrolysis to glucosamine, a widely used nutraceutical (16).

In diatoms, biosilica cell wall biosynthesis occurs just prior to cell division through the uptake of dissolved silicon as silicic acid, and its subsequent peptide-mediated, condensation into biosilica within a deposition vesicle formed at the plane of cell division. This process is templated to self-assemble the nanostructured silica precursors into frustules with intricate pore arrays (17-19). Thus, the requirement of dissolved silicon as a substrate, and its unique role in controlling the diatom cell division cycle, (20-21) provides an opportunity to develop bioprocessing strategies for directing the production of metabolites. In previous work, we described how silicon starvation was harnessed to stimulate the accumulation of lipids in diatoms cells (22), a process which was later investigated at the cellular and molecular level (23-24). In this previous work, we showed that sequential batch cultivation of the photosynthetic marine diatoms *Cyclotella* to silicon limitation allowed for the coproduction of cell biomass with intracellular lipids and chitin to yield of 35 and 15 wt%, respectively (16).

The goal of this study is to develop a nutrient feeding strategy to control the production of the valued coproduct chitin from the lipid-producing diatom *Cyclotella*. In this article, the strategy will focus in a two-stage cultivation process where Stage I brings the diatom cell suspension to a silicon-starved state, and Stage II continuously adds silicon and nitrate to the silicon-starved cells in fed-batch operation. Because silicon is required for cell division, and nitrate provides soluble nitrogen for chitin production, if silicon and nitrate are added to the silicon-starved diatom cell suspension at a rate where both are immediately consumed, then the rate of silicon and nitrate addition may control both cell number production and product formation.

Furthermore, if the cells are kept in the Si-starved state while continually adding these key nutrients that maintain cell division and product formation, then controlled and co-current production of cell biomass and metabolites may be possible based on the rate of silicon delivery.

Toward this end, continuous feeding of dissolved silicon and nitrate during Stage II of the cultivation process enabled the controlled, linear production of both diatom cells, and chitin over time, with final yields determined by the cumulative amount of silicon and nitrate delivered. Biofuel lipids were also co-produced through this process. This cultivation strategy was carried out within a bubble-column photobioreactor to provide sufficient and uniform CO₂ and light delivery to the well-mixed diatom cell suspension. The performance of the fed-batch cultivation strategy for Stage II was also compared with a two-stage batch cultivation process where silicon and nitrate were added only at the beginning of Stage II.

Experimental Section

Diatom cell culture

The marine centric diatom *Cyclotella sp.* Was obtained from UTEX Culture Collection of Algae (UTEX #1269) and cultivated un 100 mL of autoclaved Harrison's artificial seawater medium (25) enriched with 0.50 mM Na₂SiO₃ (sodium metasilicate), 5.0 mM NaNO₃ (sodium nitrate) and 0.20 mM NaH₂PO₄·H₂O (sodium phosphate monobasic) in 500 mL foam-stoppered glass flasks. Cultures were incubated in 22°C at 100 μE/m²-s incident light intensity on a 14h/10h light/dark cycle, and subcultured at 10% v/v every 28 days. To facilitate gas exchange, each flask was swirled for 10 s once per day.

Photobioreactor design and operation

Cyclotella diatom cell suspension were cultivated in the bubble-column photobioreactors described previously (26), with modification described below. The photobioreactor was equipped with temperature control, external illumination, medium delivery, and aeration gas delivery. The bioreactor vessel was a Pyrex glass tube of 10.5-cm inner diameter, 69-cm length, and 4.8-mm wall thickness mounted on

stainless-steel bottom and headplates with sealing gaskets. The working liquid volume was 5.0 L. Temperature control at 22°C was provided by a stainless steel U tube (3/8 in. outer diameter, 0.305-in wall thickness, 1.5 m working length) connected to a chilling circulator. When required, supplemental medium was continuously added to the cell suspension by an Aladdin 8000 syringe pump through a port in the vessel head plate.

The baseplate assembly housed a stainless steel sparger plate consisting of four 1.0 mm diameter holes on a 3.6 cm square pitch. Pressurized house air with CO₂ concentration of 380 ppm was particulate filtered, metered through a flow meter, and introduced to the baseplate of the bioreactor at a flowrate of 1000 mL min⁻¹ (0.2 mL air/mL-culture-min). The rising air bubbles were the sole source of agitation for the cell suspension. Other process conditions for the photobioreactor cultivation experiments are summarized below. At the aeration conditions described above, the volumetric mass transfer coefficient (k_La) was 13 h⁻¹, determined using dynamic gassing-out method using a dissolved oxygen electrode. The CO₂ transfer rate (CO₂-TR) was determined by two methods. The first was based on the aeration gas flow rate and flow rate and CO₂ concentration, and the second one was based on interphase mass transfer with $CO_2\text{-TR} = P_{CO_2} k_La / H$, where H is the Henry's law constant for CO₂ in seawater (). By the first method, CO₂-TR was 0.3 mmol CO₂-L-hr, and by the second method, CO₂-TR was 0.150 mmol CO₂/L-hr. The lowest value of CO₂-TR was taken as the limiting CO₂ delivery rate. Sodium bicarbonate was added to the medium concentration (3.9 mM) needed to provide a setpoint pH value of 8.5 as described previously (27).

Details on bioreactor setup and inoculation are described previously (16). The nutrient medium was filter sterilized (thermos Scientific Rapid-Flow polyethersulfone filter, pore size 0.2 μm) and loaded into the autoclaved vessel prior to inoculation. During cultivation, the cell suspension was harvested periodically by pressurizing the gas headspace with nitrogen gas to enable liquid flow to a 500-mL flask equipped with a sterile air filter to prevent backflow contamination.

Light delivery to photobioreactor

Light to the cylindrical vessel was delivered by three banks of vertically mounted 20 W fluorescent lamps (2700°K/PL9, 2 lamps per bank, 56 cm length) positioned around the vessel surface. The illumination photoperiod was set to 14 h on / 10 h off. The incident light intensity to the cylindrical vessel (I_o) was determined by the average of photosynthetically active radiation (PAR) measurements (LI-COR SA190) at 2.5 cm intervals along the circumference and vertical position along the inner surface (420 measurements). Under this configuration, the average I_o was 95 $\mu\text{E}/\text{m}^2\text{-s}$. For a cylindrical vessel, the mean light intensity (I_m) at a given cell number density (X_N) was determined by

$$I_m(X_N) = \frac{4I_o e^{-k_c X_N R} \sinh(k_c X_N R)}{k_c X_N R} \quad \text{Equation 3.1}$$

With light attenuation constant of $k_c = 2.4 \times 10^{-7}$ mL/cells-cm, using methods described previously (27). At the target cell number densities of 2×10^6 cells/mL for Stage I, and 5×10^6 cells/mL for Stage II, the values for I_m were 76 and 30 $\mu\text{E}/\text{m}^2\text{-s}$, respectively. In previous work (16), we determined the photosynthetic-irradiance curve of *Cyclotella* diatom cells followed the exponential model with I_k of 59 ± 2 $\mu\text{E}/\text{m}^2\text{-s}$ (1.0 S.E.). Therefore, at the target cell number densities of 2×10^6 cells/mL and $4\text{-}5 \times 10^6$ cells/mL for Stages I and II, the cultivations were conducted at 72% of light saturation by the end of Stage I and 40% of light saturation by the end of Stage II, based on an average incident light intensity of 95 $\mu\text{E}/\text{m}^2\text{-s}$.

Fed-batch nutrient delivery to photobioreactor

In the fed-batch nutrient delivery experiments, a concentrated mixture of sodium nitrate (NaNO_3) and sodium metasilicate (Na_2SiO_3) solution in water without phosphate was continuously pumped into the silicon-starved diatom suspension at a fixed volumetric flowrate of 1.26 mL h^{-1} for times 4, 7, 10, and 14 days. The total amount of fluid delivered ranged from 121 to 436 mL, and so culture dilution due to nutrient medium addition was <15% based on a 5 L nominal culture volume. In all

cultivation experiments, the total nutrient loading at the end of Stage II was targeted at 0.80 mM Si and 1.2 mM nitrate. Because the flowrate was fixed, the required dissolved silicon concentration in the nutrient delivery medium ($C_{Si,o}$) was determined by material balance, given by

$$C_{Si,o} = \frac{C_{Si,f}}{1 - V_{i,II}/v_o / (V_{i,II}/v_o + t_f)} \quad \text{Equation 3.2}$$

Where $C_{Si,f}$ is the final nutrient delivery concentrations, $V_{i,II}$ is culture volume at the beginning of Stage II, and v_o is the volumetric flowrate of the nutrient delivery medium, and t_f is the total nutrient delivery time. The required nitrate concentration ($C_{N,o}$) was determined similarly. Target nutrient delivery rates are presented in Table 3.1.

Analytical methods

Diatom cell suspension samples pulled from the photobioreactor cultivation experiment were assayed for cell number density, dissolved silicon concentration, dissolved nitrate concentration, total lipid and chitin, as described previously (16). Cell number density was determined by a Beckman Z2 Coulter Counter at minimum threshold of 6 μm . Dissolved nitrate and silicon concentration in the culture medium were determined by spectrophotometric assay. Total lipid in the cell mas was assayed spectrophotometrically following centrifugation of 50 mL cell suspension (1000 g \times 10 min) drying of the centrifuged pellet (80C, 24 h), and solvent extraction pf the dried pellet with 5 mL of 2:1 (v/v) chloroform/methanol for 12 h at room temperature under continuous shaking. The chitin content in the biomass was determined by acid hydrolysis of the pellet from a centrifuged (16000g, 15 min) and washed diatom cell suspension sample (10 mL) in 8 M HCl at 90°C for 3 h to convert chitin to glucosamine. Glucosamine was quantified by high-performance liquid chromatograph (HPLC) of the NaOH-neutralized and filtered samples using a Dionex MA-1 strong anion-exchange column at 30°C, 0.4 mL min⁻¹ 0.75M NaOH isocratic mobile phase eluent, and pulsed amperometric mode detection of the column effluent with a

Dionex ED-40 electrochemical detector. Chlorophyll-a was determined spectrophotometrically at 632, 649, 665, 696 nm following extraction of the centrifuged biomass pellet in ethanol for 2 min at room temperature under vortexing.

All values were reported as the average of triplicate measurements, taken from the starting point of the assay, with errors reported as ± 1.0 standard deviation (1.0 S.D.). Errors from linear regression were reported as ± 1.0 S.E.

SEM

Whole diatom cells settled on a glass slide were prepared for scanning electron microscopy (SEM) by fixation with 2.5 wt% glutaraldehyde (in 1 wt% paraform and 0.1 M sodium cacodylate buffer for 30 min, 20°C), rinsing with 0.1 M sodium cacodylate buffer, ethanol dehydration, (20% to 100% EtOH in steps), and critical point drying. Samples were sputtered with gold and then imaged on a FEI Quanta 600 FEG SEM.

Results

Batch photobioreactor cultivation

Cell number density, soluble nutrient concentration (Si and N) and product concentration (lipid, chitin, chl-a) vs. time profiles for the two-stage batch photobioreactor cultivation of *Cyclotella* diatom cells are presented in Figure 3.1. Nutrient loadings of 0.8 mM Si and 1.2 mM nitrate were added to the cell suspension at both the beginning of both Stages I and II, with a cumulative nutrient loading ratio of 1.5 mol N/mol Si. Phosphate was only added to Stage I was designed to allow for 4 cell doublings, from an initial cell density of nominally 1.25×10^5 cells mL⁻¹, to a final cell number density of 2.0×10^6 cells mL⁻¹. Stage I was allowed to proceed until all of the dissolved silicon was consumed from the medium to achieve a silicon-starved culture condition. Stage II was initiated after at least 48 h of silicon starvation in Stage I. The amount of silicon added to Stage II was intended to enable one additional cell doubling to ~ 4 to 5×10^6 cells mL⁻¹. At the end of Stage I, all of the silicon and nitrate were consumed as long as they were added together, and the increase in cell number density was commensurate with the silicon added (Figure

3.1a). At the end of Stage II, some efflux of silicon was observed, although the cell number density still doubled (Figure 3.1b). Lipid production occurred primarily during Stage I. When 0.8 mM Si and 1.2 mM nitrate were added to Stage II, the final lipid accumulation modestly increased from about 100-130 mg L⁻¹. However, chitin production approximately doubled from 27 to 58 mg L⁻¹ from Stages I to II, consistent with the doubling in cell number density (Figure 3.1b).

Fed-batch photobioreactor cultivation

Fed-batch photobioreactor cultivation of *Cyclotella* diatom cells at Stage II nutrient addition times of 4 and 14 days are compared in Figures 3.2 and 3.3 respectively. Details of the nutrient loading are presented in Table 1. Stage II was initiated by delivering a concentrated nutrient solution containing dissolved silicon and nitrate to nutrient-starved cells from Stage I. The cumulative nutrient loading remained fixed at the end of Stage II for all batch and fed-batch photobioreactor cultivation experiments, and so only the rate of delivery to this final nutrient loading was varied. At both nutrient addition rates, the dissolved silicon and nitrate concentrations within the cell suspension were zero during the entire duration of Stage II. The total amount of silicon added to Stage II was designed to enable at least one cell doubling, from $\sim 2 \times 10^6$ cells mL⁻¹ at the end of Stage I to 5×10^6 cell mL⁻¹ at the end of Stage II (Table 1).

The nutrient delivery and consumption profiles at Stage II nutrient addition times of 4 and 14 days are presented in Figure 3.4. In Stage II, the nutrient delivery vs. time profile was linear and matched the nutrient consumption vs. time profile for both Si and nitrate. In the regime where the silicon consumption vs. time profile was linear, the total cell number and chitin production profiles were also linear with time, as also shown in Figure 3.4. From Figure 3.4, the cumulative amount of production of both cells and chitin after 4 days (96 h) and 14 days (336 h) were the same. The cells production rate (R_{cell}) and chitin production rate (R_{chit}) were determined by the least-squares slope of the cell and chitin production vs. time data respectively, and then scaled to the volumetric cell production rate (\hat{R}_{cell} , 10⁶ cells/L-hr) and the specific chitin production rate (\hat{R}_{chit} , mg chitin/10⁶ cells-hr) by the following relationships:

$$\hat{R}_{\text{cell}} = \frac{R_{\text{cell}}}{\bar{V}_L} \quad \text{Equation 3.3}$$

$$\hat{R}_{\text{chit}} = \frac{R_{\text{chitin}}}{[X_{n,f} - X_{n,i}] \cdot \bar{V}_L} \quad \text{Equation 3.4}$$

Where \bar{V}_L is the average volume of the cell suspension in the bioreactor (mL) without sampling, and $[X_{n,f} - X_{n,i}]$ is the generation of cells during the nutrient medium addition (cells/mL). The silicon delivery rate during Stage II was defined by

$$R_{\text{Si}} = C_{\text{Si},o} \cdot \frac{v_o}{\bar{V}_L} \quad \text{Equation 3.5}$$

Where $C_{\text{Si},o}$ is the silicon concentration in the nutrient addition medium and v_o is the volumetric medium addition rate (mL/hr).

The effect of Stage II silicon delivery rate (R_{Si}) on the volumetric cell production rate and the specific chitin production rate is presented in Figure 3.5. When the silicon delivery rate was increased from 0.05 to 0.2 mmol Si/L-day, corresponding to nutrient delivery times of 4-14 days, the rates of cell production rate and specific chitin production linearly increased. In this silicon delivery-limited cultivation mode, cell number and chitin production rates increased linearly with the increasing rate of dissolved silicon delivery. Because diatom cell division is controlled by silicon availability, this result suggested that chitin production was tied to cell number production as long as nitrogen delivery was sufficient. At the end of Stage II nutrient delivery, cell number and chitin production ceased. The final cell number density ($\sim 4 \times 10^6$ cell mL⁻¹) did not change in response to increasing the Stage II nutrient delivery. However, this result was by the experimental design, since the cumulative loading of Si and N were not changed.

Volumetric lipid production increased with time during nutrient delivery, but the profile was not linear, although the lipid accumulation ceased after nutrient delivery ended. Lipid production occurred primarily during Stage I, similar to the two-stage batch cultivation. The final yields of chitin and lipid for each stage of the two-stage batch and fed-batch photobioreactor cultivation experiments are compared in Figure 3.6. Again, the final yields of chitin were consistent with cell number production, whereas lipid production was not. From these observations, although chitin production was tightly tied to cell division controlled through silicon delivery, lipid production was more generally correlated to its accumulation within cells maintained in a viable state through continuous nutrient addition.

Both chitin and chlorophyll-a (chl-a) contain nitrogen bearing moieties. The chl-a concentration vs. time profile was flat during the entire 14-day nutrient medium addition time, but increased during shorter 4-day nutrient delivery time (Figure 3.7). The 4-day nutrient delivery time corresponded to a faster nutrient delivery rate. Therefore, chl-a production appeared to be tied to cell growth and photosynthetic rate, whereas chitin production was tied to cell division.

The nitrogen consumption to chl-a never exceeded 2% of the nitrogen delivered. Furthermore, these two processes did not appear to compete with one another, as the sum total of N contribution to chl-a and chitin was generally 15% the cumulative nitrogen fed during Stages I and II.

Representative SEM images of the chitin fibers during Stage II of cultivation are presented in Figure 3.8. A single continuous chitin fiber was extruded from each pore lining the rim of the top valve face of the frustule (biosilica cell wall).

Discussion

A simplified depiction of dissolved silicon (as silicic acid), nitrate, and CO₂ uptake into the diatom cell, and the direction of these inputs to cellular products, is presented in Figure 3.9. Dissolved silicon is a required substrate for cell division. In the silicon-starved cell, chitin and lipid are accumulated.

This study developed a two-stage nutrient feeding strategy to selectively control the phototrophic production of chitin, a linear polymer of N-acetyl glucosamine, by the centric marine diatom *Cyclotella* through continuous feeding of dissolved silicon and nitrate to a silicon and nitrate-starved cell suspension. The silicon delivery rate was set to enable a silicon-limited cell rate. Both cell and chitin production were linear with time, and all of the silicon and nitrate delivered were consumed (Figure 3.4). Furthermore, the cell production rate and the specific chitin production rate per cell increased linearly with increasing silicon delivery rate, as long as the dissolved silicon delivery limited cell production (Figure 3.5). This result suggests that chitin production is controlled through cell division, which is externally controlled through silicon delivery. This observation is supported by molecular studies, which revealed that the transcript abundance for the gene encoding of one of the six chitin synthase types in *Thalassiosira pseudonana* increased when cells resumed division after short-term silicic acid starvation (28).

Lipid was also produced during photobioreactor cultivation of the diatom *Cyclotella* but was not linearly correlated to silicon delivery. Lipid production occurred primarily during the batch cultivation phase in Stage I, particularly just after the complete co-consumption of both dissolved silicon and nitrate (Figures 3.1-3.3). The continuous feeding of Si and nitrate to the cell suspension during Stage II did not result in significantly greater lipid accumulation, even though the feeding rate was designed to stimulate a Si and N-starved condition with essentially zero concentrations of dissolved silicon and nitrate in the culture suspension. Chitin was also produced following co-consumption of both Si and nitrate in Stage I, but was maintained during Si and nitrate addition in Stage II. Consequently, chitin production was only favored over lipid production during Stage II (Figure 3.6).

Previous studies on lipid metabolism following true nitrogen starvation in the model diatom *Phaeodactylum tricornutum* generally concurred that redirection of the metabolic energy for nitrate reduction to fatty acid biosynthesis was ultimately responsible for lipid accumulation, but photosynthetic activity was compromised (29) (30) (31). In this present study, the results suggest that this N-starvation condition was

active during Stage I but not Stage II. Furthermore, nitrate reduction for chitin production in Stage II could compete with the metabolic energy requirements for lipid biosynthesis.

The results of this study also suggest that chitin and lipid production are directed by separate processes within the *Cyclotella* diatom cell. Although the energetics of lipid vs. carbohydrate metabolism are not known in diatoms, in green microalgae, lipid biosynthesis has a higher metabolic energy requirements than carbohydrate biosynthesis (32-33). Therefore, chitin, as an *N*-acetyl glucosamine biopolymer, would presumably have a lower metabolic energy requirements for biosynthesis relative to lipid biosynthesis in the diatom *Cyclotella*. Furthermore, as noted earlier, chitin production is tied to cell division, and cell division is controlled by silicon metabolism, which is downstream of photosynthetic processes in the diatom cell (21). Both of these factors suggest that chitin production was favored during Stage II of the cultivation because the processing environment did not provide the metabolic energy for sustained lipid production. In the green alga *Neochloris oleabundans*, simultaneous growth and lipid accumulation under nutrient stress was enabled by controlling the light energy uptake through chemostat operation (34). This observation suggest that increasing the light delivery to Stage II combined with fed-batch addition of all nutrients (particularly phosphate) to boost photosynthesis, but still at a rate where these processes are limited by the rate of nutrient delivery, could stimulate lipid production. However, consideration of this strategy in the experimental design was beyond the scope of this present study.

In *Cyclotella*, the chitin is extruded as nanofibers outside of the cell through pores lining the valve rim (Figure 3.8), whereas lipids were retained within the cell as lipid bodies (16-22). From an ecological perspective, the reason for extrusion of chitin nanofibers from the *Cyclotella* frustule surface is unknown, although it is speculated that the fibers may enable buoyancy control in the water column (35). In *Thalassiosira*, chitin is involved in cell wall biosynthesis, and chitin fiber networks imbedded with the cell wall biosilica is proposed as a template for silica deposition (36). But in the case of *Cyclotella*, it appears that extrusion of rigid linear fibers from

cell, as opposed to their integration into the biosilica cell wall, provides the best morphology for enabling high rates of chitin production. The extrusion of pure nanofibers from the cell is also of key benefit from a bioprocessing perspective, as it could facilitate harvest of the chitin product from the cell in a pure form. In contrast, chitin produced in cultured fungal cells is imbedded within the cell wall matrix (37), which complicates its isolation. Thus, the ability to extrude pure chitin fibers would have advantages over other processes for chitin production by isolation from shellfish waste or by microbial fermentation.

In this study, the photobioreactor cultivation experiments were framed to intensify strategies for chitin and lipid production at fixed cumulative silicon and nitrate nutrient delivery, as well as fixed light and CO₂ delivery. The process conditions and cultivation strategy were not designed for intensification of lipid production. Based on our new understanding of chitin production from the diatom *Cyclotella*, future studies will consider process intensifications through controlled feeding at higher nutrient loadings to increase chitin and cell number concentration, as well as studies at higher light intensity with continuous feeding of all nutrients, but at rates designed to stimulate nutrient stress, to enhance photosynthesis and increase lipid accumulation.

Conclusions

The photosynthetic marine diatom *Cyclotella* requires dissolved silicon as required substrate for cell wall biosynthesis and cell division, produces intracellular lipids, and also extrudes chitin nanofibers from its biosilica cell wall. A two-stage, fed-batch photobioreactor cultivation process was developed to control the production of chitin from lipid-producing *Cyclotella* cells through controlled feeding of silicon and nitrate. When dissolved silicon was continuously fed to the cell suspension at rate which limited cell division, both cell division and chitin production were linear with time. Increasing the rate of silicon delivery linearly increased the rate of cell number division and chitin production. Therefore, silicon delivery controls chitin production through control of the cell division rate. Lipid production was not correlated to silicon delivery. As a potential algal biorefinery product, chitin is of particular commercial

interest, given its high value, biomedical properties, and its hydrolysis to glucosamine, a widely used nutraceutical.

Acknowledgements

This work was supported by the US National Science Foundation (NSF), Emerging Frontiers for research and innovation program (EFRI), under award number 1240488.

References

1. Jeffryes C, Campbell J, Li H, Jiao J, Rorrer, G. The potential of diatom nanobiotechnology for applications in solar cells, batteries, and electroluminescent devices. *Energy Environ.* 2011; 4: 3930-3941.
2. Jeffryes C, Agathos SN, Rorrer G. Biogenic nanomaterials from photosynthetic microorganisms. *Curr Opin Biotechnol.* 2015; 33:23–31.
3. d'Ippolito G, Sardo A, Paris D, Vella FM, Adelfi MG, Botte P, Gallo C, Fontana A. Potential of lipid metabolism in marine diatoms for biofuel production. *Biotechnol Biofuels* 2015; 8:28.
4. Hildebrand M, Davis AK, Smith SR, Trailer JC, Abbriano R. The place of diatoms in the biofuel industry. *Biofuels* 2012; 3: 221-240.
5. Levitan O, Dinamarca J, Hochman G, Falkowski PG. Diatoms: A fossil fuel of the future. *Trends Biotechnol.* 2014; 32:117–124.
6. Smith SR, Abbriano RM, Hildebrand M. Comparative analysis of diatom genomes reveals substantial differences in the organization of carbon partitioning pathways. *Algal Res.* 2012; 1:2–16.
7. Obata T, Fernie AR, Nunes-Nesi A. The central carbon and energy metabolism of marine diatoms. *Metabolites* 2013; 3:325–46.
8. Gügi B, Costaouec T Le, Burel C, Lerouge P, Helbert W, Bardor M. Diatom-specific oligosaccharide and polysaccharide structures help to unravel biosynthetic capabilities in diatoms. *Mar Drugs* 2015; 13:5993–6018.
9. Lebeau T, Robert J-M. Diatom cultivation and biotechnologically relevant products. Part II: Current and putative products. *Appl Microbiol Biotechnol.* 2003; 60:624–632.
10. Fu W, Wichuk K, Brynjólfsson S. Developing diatoms for value-added products: Challenges and opportunities. *N Biotechnol.* 2015; 32:547–551.
11. McLachlan J, Mcinnes AG And Michael Falk, M. Studies on the chitan (chitin: poly-nacetylglucosamine) fibers of the diatom *Thalassiosira fluviatilis* Hustedt. I. Production and isolation of chitan fibers. *Can J Bot.* 1965; 43:707-712.

12. Herth W, Zugenmaier P. Ultrastructure of the chitin fibrils of the centric diatom *Cyclotella cryptica*. *J Ultrastuct Res.* 1977; 61:230-239.
13. Herth W. The site of β -chitin fibril formation in centric diatoms. II. The chitin-forming cytoplasmic structures. *J Ultrastuct Res.* 1979; 68: 16-27.
14. Herth W, Barthlott W. The site of β -chitin fibril formation in centric diatoms. I. Pores and fibril formation, *J Ultrastuct Res.* 1979; 68: 6-15.
15. Ogawa Y, Kimura S, Wada M. Electron diffraction and high-resolution imaging on highly-crystalline β -chitin microfibril. *J Struct Biol.* 2011; 176:83–90.
16. Rorrer GL, Torres JA, Durst R, Kelly C, Gale D, Maddux B, Ozkan A. The potential of a diatom-based photosynthetic biorefinery for biofuels and valued co-products. *Current Biotechnol.* 2016; 5: 237-248.
17. Sumper M, Brunner E. Learning from diatoms: Nature's tools for the production of nanostructured silica. *Adv Funct Mater.* 2006; 16:17–26.
18. Davis, AK, Hildebrand M. Molecular processes of biosilicification in diatoms. In: Sigel A, Sigel H, Sigel RKO. *Biomineralization: from nature to application.* Chichester: John Wiley & Sons Ltd 2008: 255-294.
19. Tesson B, Hildebrand M. Dynamics of silica cell wall morphogenesis in the diatom *Cyclotella cryptica*: Substructure formation and the role of microfilaments. *J Struct Biol.* 2010;169:62-74.
20. Martin-Jézéquel V, Hildebrand M, Brzezinski MA. Silicon metabolism in diatoms: Implications for growth. *J. Phycol.* 2000; 36:821–840.
21. Huysman MJJ, Vyverman W, De Veylder L. Molecular regulation of the diatom cell cycle. *J. Exp. Bot.* 2014; 65:2573–2584.
22. Jeffryes C, Rosenberger J, Rorrer GL. Fed-batch cultivation and bioprocess modeling of *Cyclotella sp.* for enhanced fatty acid production by controlled silicon limitation. *Algal Res.* 2013; 2:16–27.
23. Shrestha RP, Hildebrand M. Evidence for a regulatory role of diatom silicon transporters in cellular silicon responses. *Eukaryot Cell* 2015; 14:29-40.
24. Smith SR, Glé C, Abbriano RM, Traller JC, Davis A, Trentacoste E, Vernet M, Allen AE, Hildebrand M. Transcript level coordination of carbon pathways

- during silicon starvation-induced lipid accumulation in the diatom *Thalassiosira pseudonana*. *New Phytol.* 2016; 210:890–904.
25. Berges JA, Franklin DJ, Harrison PJ. Evolution of an artificial seawater medium: Improvements in enriched seawater, artificial water over the last two decades. *J. Phycol.* 2001; 37:1138–1145.
 26. Jeffryes C, Gutu T, Jiao J, Rorrer GL. Two-stage photobioreactor process for the metabolic insertion of nanostructured germanium into the silica microstructure of the diatom *Pinnularia sp.* *Mater Sci Eng. C* 2008; 28:107–118.
 27. Rorrer GL. Bioprocess engineering of phototrophic marine organisms. In: Kim SK. Springer Handbook of Marine Biotechnology. Heidelberg: Springer Publishing, 2015: 385-422.
 28. Durkin CA, Mock T, Armbrust EV. Chitin in diatoms and its association with the cell wall. *Eukaryot Cell* 2009; 8:1038–1050.
 29. Frada MJ, Burrows EH, Wyman KD, Falkowski PG. Quantum requirements for growth and fatty acid biosynthesis in the marine diatom *Phaeodactylum tricorutum* (Bacillariophyceae) in nitrogen replete and limited conditions. *J Phycol.* 2013; 49:381–388.
 30. Yang Z-K, Niu Y-F, Ma Y-H, Xue J, Zhang M-H, Yang W-D, Liu J-S, Lu S-H, Guan Y, Li H-Y. Molecular and cellular mechanisms of neutral lipid accumulation in diatom following nitrogen deprivation. *Biotechnol Biofuels* 2013; 6:67.
 31. Levitan O, Dinamarca J, Zelzion E, Lun DS, Guerra LT, Kim MK, Kim J, Van Mooy BAS, Bhattacharya D, Falkowski PG. Remodeling of intermediate metabolism in the diatom *Phaeodactylum tricorutum* under nitrogen stress. *Proc Natl Acad Sci.* 2015; 112:412–417.
 32. Chen CY, Zhao XQ, Yen HW, Ho SH, Cheng CL, Lee DJ, Bai FW, Chang JS. 2013. Microalgae-based carbohydrates for biofuel production. *Biochem. Eng. J.* 78:1–10.
 33. Subramanian S, Barry AN, Pieris S, Sayre RT. Comparative energetics and kinetics of autotrophic lipid and starch metabolism in chlorophytic microalgae:

- implications for biomass and biofuel production. *Biotechnol Biofuels* 2013; 6:150.
34. Klok AJ, Martens DE, Wijffels RH, Lamers PP. Simultaneous growth and neutral lipid accumulation in microalgae. *Bioresour Technol.* 2013; 134:233–243.
 35. Morin LG, Smucker RA, Herth W. Effects of two chitin synthesis inhibitors on *Thalassiosira fluviatilis* and *Cyclotella cryptica*. *FEMS Microbiol Lett.* 1986; 37:263-268.
 36. Brunner E, Richthammer P, Ehrlich H, Paasch S, Simon P, Ueberlein S, van Pée K-H. Chitin-based organic networks: an integral part of cell wall biosilica in the diatom *Thalassiosira pseudonana*. *Angew Chemie In. Ed.* 2009; 48:9724–9727.
 37. Bowman SM, Free SJ. The structure and synthesis of the fungal cell wall. *BioEssays* 2006; 28:799–808.

Table 3.1. Dissolved silicon (Si) and nitrate (N) delivery for two-stage batch/fed-batch photobioreactor cultivation experiments. In all photobioreactor cultivation experiments, the intended total nutrient delivery was 0.8 mM Si and 1.2 mM nitrate for each stage, with Stage I + II cumulative delivery of 1.6 mM Si and 2.4 mM nitrate. Average final cell number densities after each stage are also presented.

Process Parameter	Stage I	Stage II	Fed-Batch Delivery Time				
	Batch	Batch	0 day	4 day	7 day	10 day	14 day
Initial Si (mmol Si/L)	0.8	0.8	0	0	0	0	0
Initial nitrate (mmol N/L)	1.2	1.2	0	0	0	0	0
Calculated $C_{Si,o}$			18.6	11.7	9.8	6.3	
Calculated $C_{N,o}$			27.8	17.6	14.8	9.4	
Calculated Delivery Rate							
Si (mmol Si/L-day)			0.20	0.11	0.080	0.057	
Nitrate (mmol N/L-day)			0.30	0.17	0.120	0.086	
Actual Delivery Rate							
Si (mmol Si/L-day)		-	0.20	0.12	0.093	0.049	
Nitrate (mmol N/L-day)		-	0.42	0.17	0.103	0.085	
Final Cell Number Density (± 1.0 S.E.)	$2.4 \cdot 10^6$ $2.0 \cdot 10^5$	$4.5 \cdot 10^6$ $1.2 \cdot 10^5$	$5.3 \cdot 10^6$ $1.6 \cdot 10^5$	$5.5 \cdot 10^6$ $8.6 \cdot 10^4$	$4.2 \cdot 10^6$ $5.3 \cdot 10^4$	$5.1 \cdot 10^6$ $8.1 \cdot 10^4$	

Figure 3.1. Two-stage photobioreactor cultivation of *Cyclotella* diatom cells with pulse addition of nutrients at the beginning of Stage II. (a) Cell number density, dissolved silicon concentration, and nitrate concentration vs. cultivation time; (b) volumetric chitin production, lipid production vs. cultivation time. Error bars are 1.0 S.D. from triplicate assays.

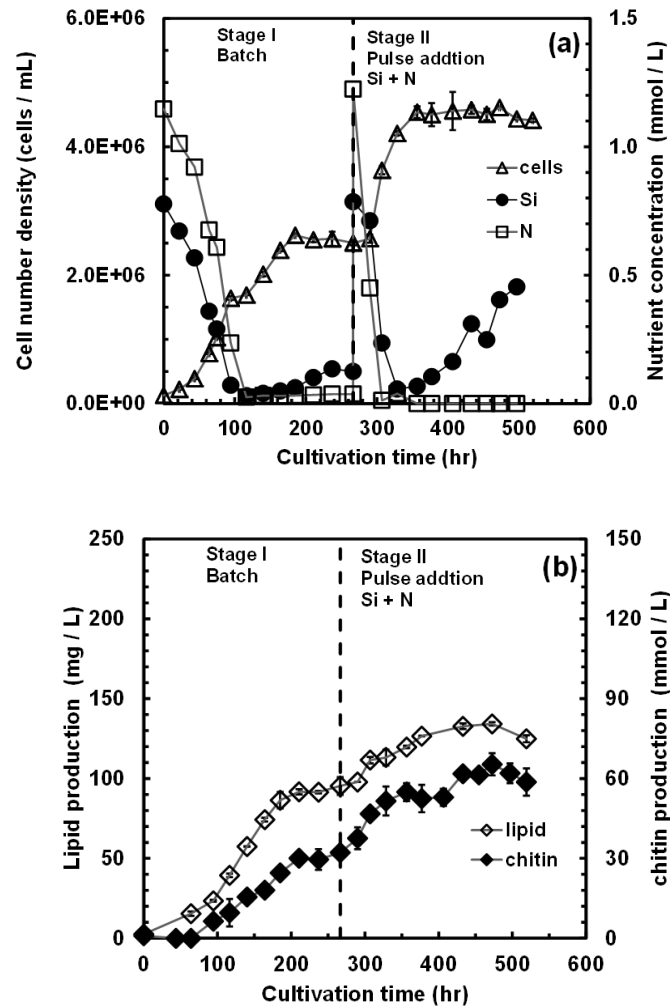


Figure 3.2. Two-stage photobioreactor cultivation of *Cyclotella* diatom cells with a Stage II fed-batch nutrient medium addition time of 4 days. (a) Cell number density, dissolved silicon concentration, and nitrate concentration vs. cultivation time; (b) volumetric chitin production, lipid production vs. cultivation time. Error bars are 1.0 S.D. from triplicate assays.

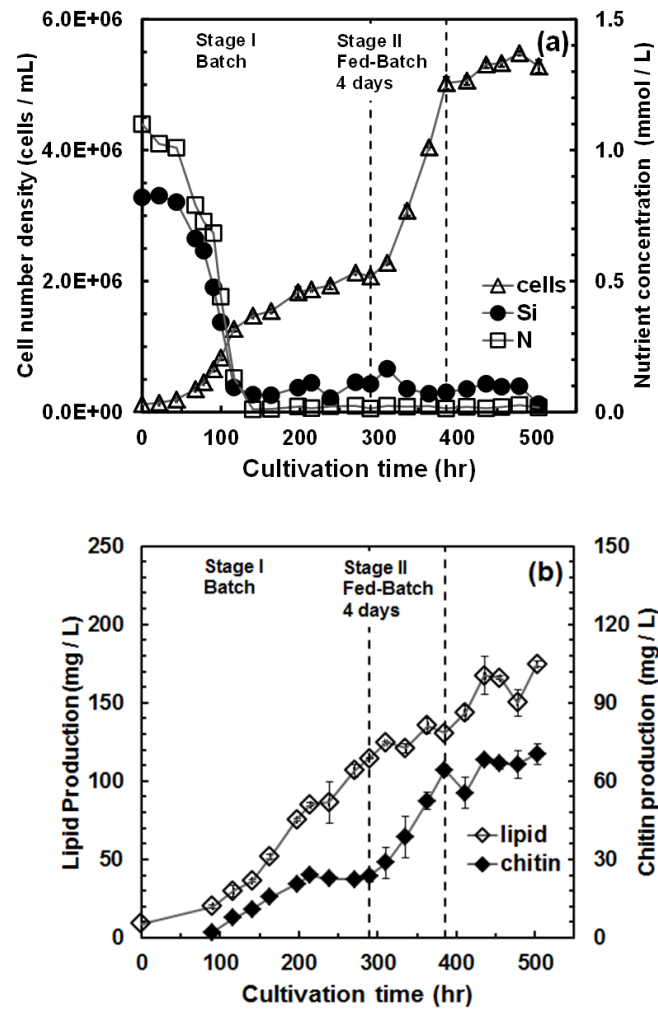


Figure 3.3. Two-stage photobioreactor cultivation of *Cyclotella* diatom cells with a Stage II fed-batch nutrient medium addition time of 14 days. (a) Cell number density, dissolved silicon concentration, and nitrate concentration vs. cultivation time; (b) volumetric chitin production, lipid production vs. cultivation time.

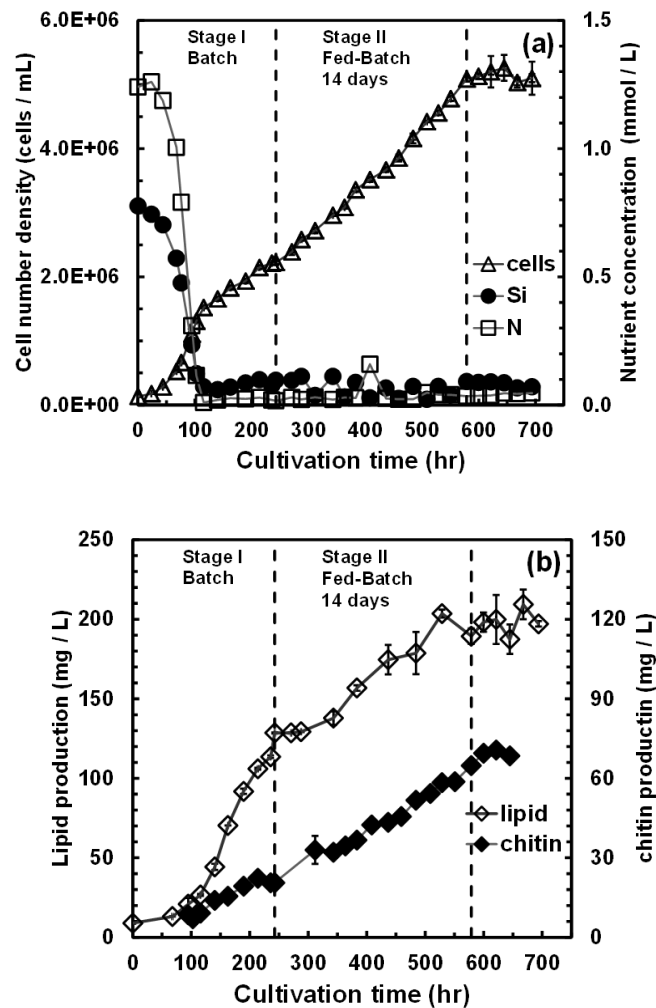


Figure 3.4. Linear profiles for nutrient consumption and product formation during Stage II fed batch operation at nutrient medium addition times of 4 and 14 days. (a) Silicon and nitrate delivery and consumption profiles; (b) total cell and chitin production.

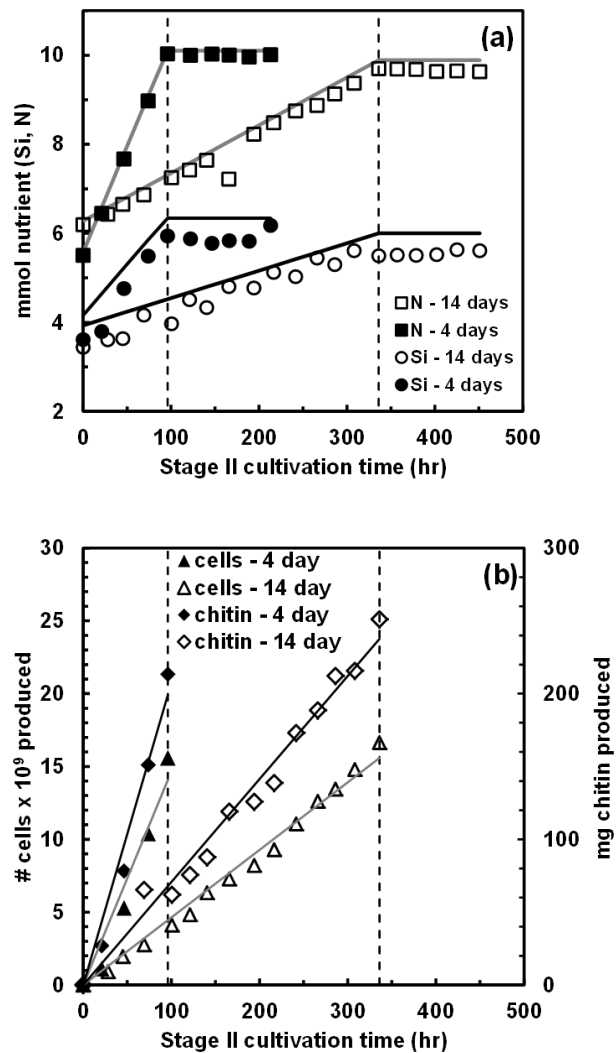


Figure 3.5. Rates of linear cell production and specific chitin production vs. silicon delivery rate in Stage II. Error bars for each were generally within the size of the symbol. For cell production (open triangle symbol), the least squares slope was $3.87 \cdot 10^9 \pm 6.9 \cdot 10^8$ cells / mmol Si ($r^2 = 0.913$, $n = 5$, 1.0 S.E.). For chitin production (open diamond symbol), the least-squares slope was 16.63 ± 1.86 mg chitin / mmol Si / 10^9 cells ($r^2 = 0.964$, $n = 5$, 1.0 S.E.).

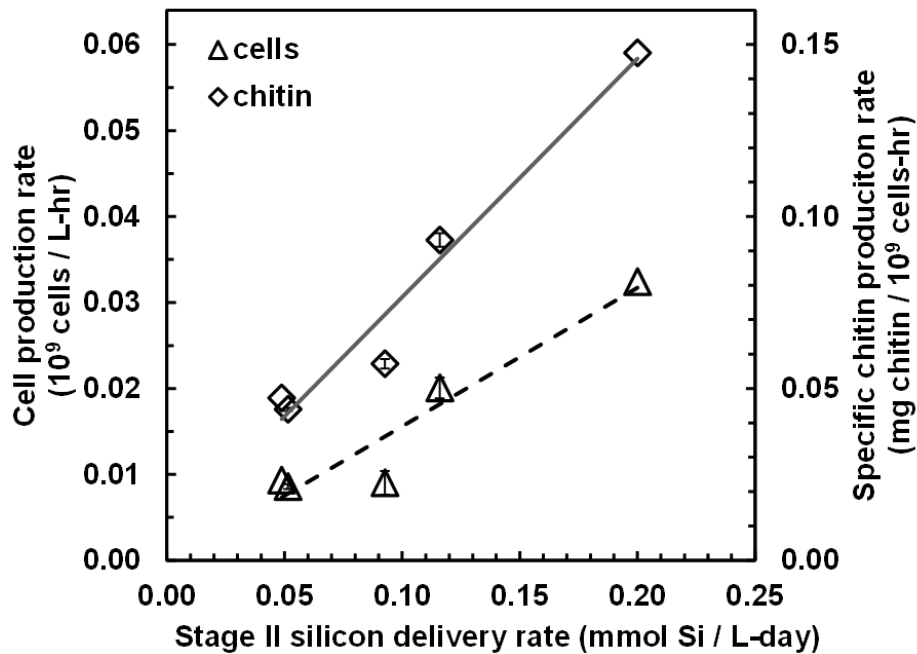


Figure 3.6. Final yields of lipid and chitin (mg / 10^9 cells) vs. Stage II nutrient delivery time at fixed total nutrient loading. The cumulative yields averaged over the three conditions were 13 ± 1 mg chitin/ 10^9 cells and 33 ± 3 mg lipid/ 10^9 cells. All errors were determined from propagated 1.0 S.E. errors.

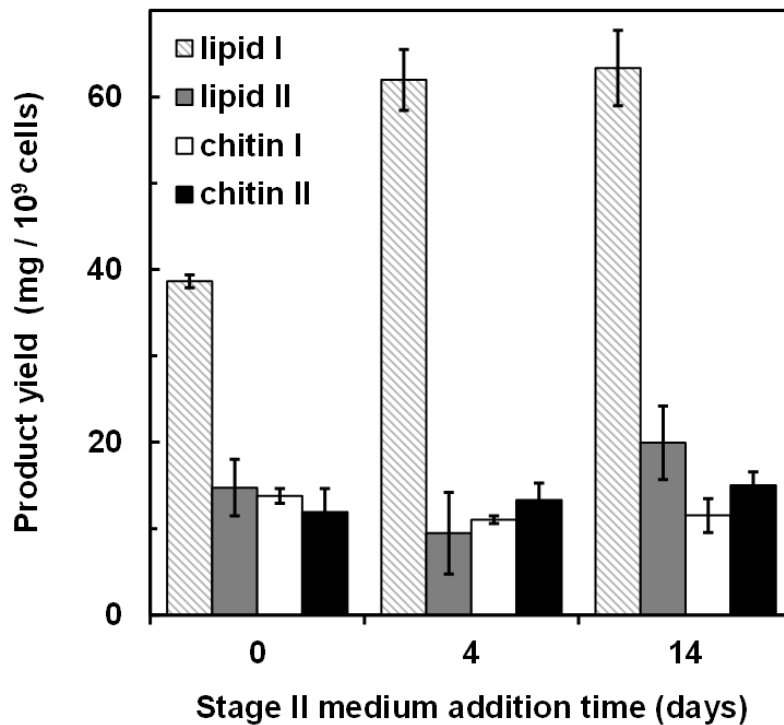


Figure 3.7. Comparison of chlorophyll a formation during Stage II nutrient addition times of 0 days (pulse addition), 4 days continuous fed-batch operation, (96 hr) and 14 days continuous fed-batch operation (336 hr).

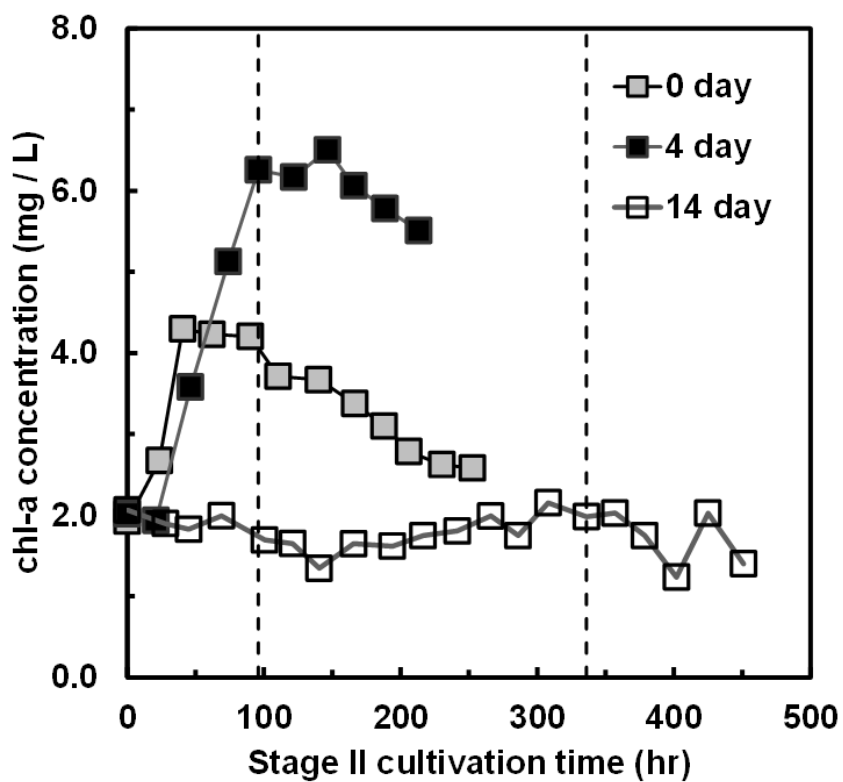


Figure 3.8. SEM image of whole *Cyclotella* diatom cell after critical point drying. (a) Typical diatom cell at beginning of cultivation, Stage I; (b) typical diatom cell at end of cultivation, Stage II. Chitin fibers are shown emanating from pores lining frustule valve rim.

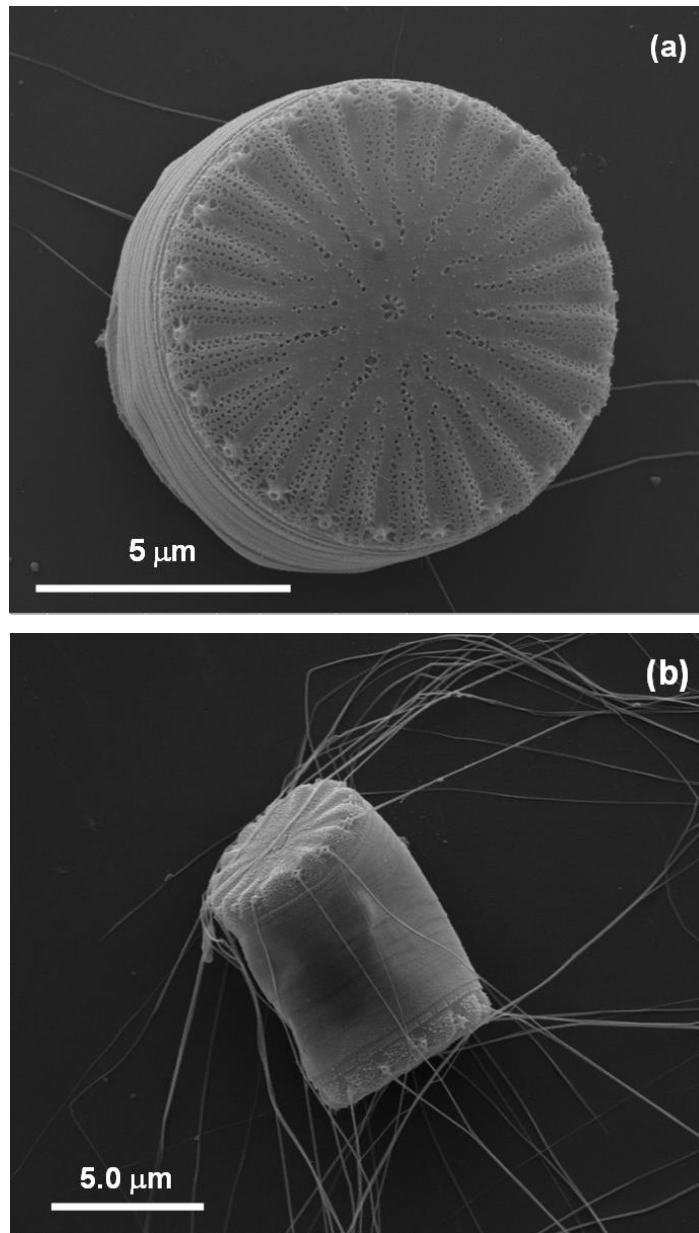
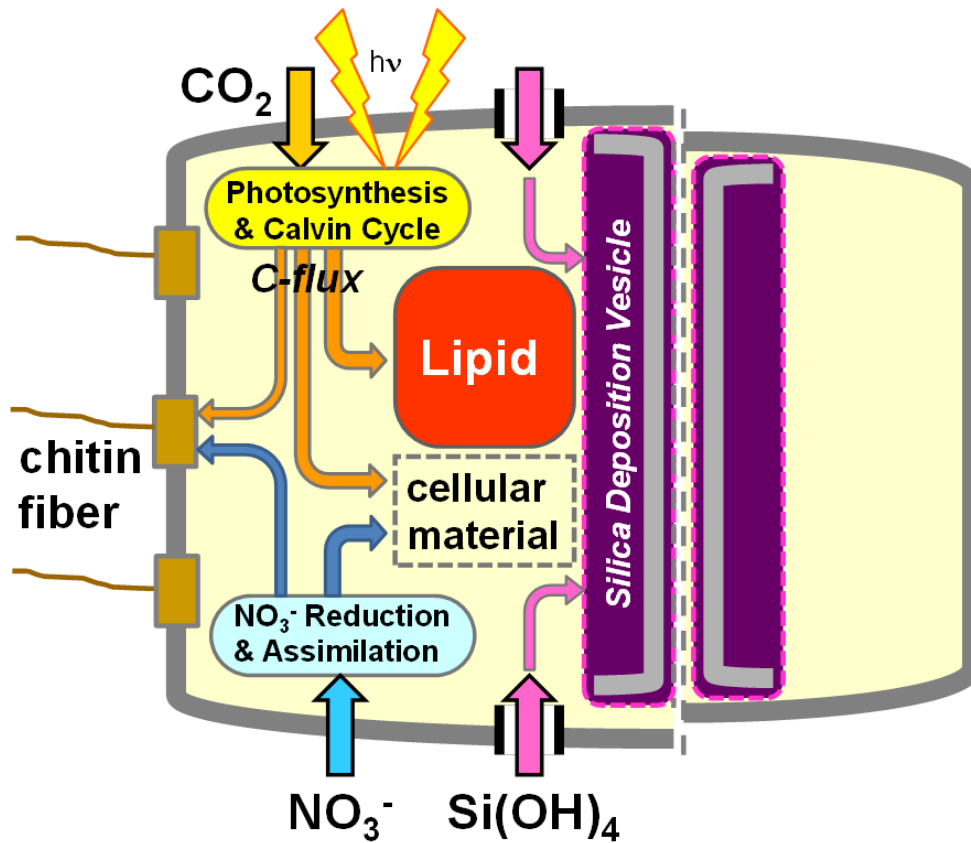


Figure 3.9. A simplified depiction of dissolved silicon, nitrate, and CO₂ uptake into the diatom cell, and the direction of these inputs to cellular products.



Chapter 4: Effects of nitrogen delivery on chitin nanofiber production during batch cultivation of the diatom *Cyclotella* sp. in a bubble-column photobioreactor

Omar G. Chiriboga N., Gregory L. Rorrer

Journal of Applied Phycology (2018). <https://doi.org/10.1007/s10811-017-1368-z>

Abstract

The photosynthetic diatom *Cyclotella* sp. extrudes unique chitin nanofibers following cell division. This diatom requires silicon for cell wall biosynthesis and division, as well as nitrogen for biosynthesis of intracellular material and extracellular chitin, an N-acetyl glucosamine biopolymer. The initial nitrogen/silicon molar ratio was the critical parameter for assessing the limits of nitrogen delivery on cell number and chitin production during batch cultivation of *Cyclotella* in a bubble-column photobioreactor under silicon-limited growth conditions, using nitrate as the nitrogen source. The peak rate of volumetric chitin production increased linearly, from 3.0 to 46 mg chitin L⁻¹ day⁻¹, with increasing N/Si ratio over the range studied (0.82 to 8.6 mol N mol⁻¹ Si). However, the cell number yield and the chitin yield per cell increased asymptotically with increasing N/Si ratio, achieving a final cell number yield of $5.3 \cdot 10^9 \pm 2.6 \cdot 10^8$ cells mol⁻¹ Si, and chitin yield of 28.7 ± 1.2 mg chitin per 10⁹ cells (1.0 S.E.). An N/Si ratio of at least 4.0 mol N mol⁻¹ Si achieved 90% of the asymptotic chitin yield. This study has shown that scalable cultivation systems for maximizing chitin nanofiber production will require delivery of both silicon and optimal nitrogen under silicon-limiting growth conditions to promote cell division and subsequent chitin formation.

Introduction

Diatoms are single-celled algae that make cell walls of biogenic silica called frustules that possess intricate pore arrays patterned at the submicron and nanoscale. Consequently, diatoms require dissolved silicon as a required substrate for cell wall biosynthesis and cell division (1). In addition to silicon metabolism, diatoms possess unique carbon partitioning pathways (2–4), and make a variety of equally unique carbohydrate metabolites, including chitin nanofibers (5). Chitin is a linear biopolymer of N-acetyl glucosamine. Extracellular chitin nanofibers are known to be produced by only two species of diatoms within genera *Cyclotella* and *Thalassiosira* (6–9). In these diatoms, individual chitin nanofibers of approximately 50 nm diameter and up to 100 microns in length are extruded through specialized pores lining the rim of the valve face on the biosilica frustule. Scanning electron

microscopy images show that one fiber is extruded per pore (10). The fibers are of high purity in β -crystalline form (11).

Chitin nanofibers have a variety of emerging advanced material and biomedical applications (12–16). Chitin nanofibers presently used in these emerging applications are typically isolated shellfish waste, which has many contaminants. Furthermore, only small fraction of this raw chitin can be purified, and the chitin nanofibers isolated from this resource are not uniform (17). In this context, pure chitin nanofibers derived from diatoms may have promise as a future biomaterial because of their larger size and aspect ratio, uniformity, and purity.

In previous work, we characterized how light delivery, CO₂ delivery, and fed-batch addition of silicon as a limiting nutrient controlled the relative production of biofuel lipids and chitin nanofibers by our model diatom *Cyclotella* (10,18–21). At silicon-limited cultivation under nitrogen-replete conditions, lipid production paralleled photosynthetic carbon assimilation, and the intracellular carbon pool increased even though cell division ceased to achieve yields of 0.38 g lipid g⁻¹ dry biomass. Chitin yields of up to 0.15 g chitin g⁻¹ dry biomass could also be achieved, but chitin was produced only after cell division and complete consumption of silicon from the medium. Controlled feeding of silicon to the cell suspension at silicon-limiting conditions enabled a sustained linear rate of both cell production and chitin formation, but not lipid production (10). However, the role of nitrogen delivery itself on chitin production was not assessed. This is an important consideration because the nitrogen composition of chitin is 7.3 wt%, which corresponds to 1 mol N per mol of the N-acetyl glucosamine monomer unit. Furthermore, nitrogen is incorporated into intracellular materials, including proteins, nucleic acids, and photosynthetic pigments.

The goal of this study was to assess how nitrogen availability affects chitin production during batch cultivation of the diatom *Cyclotella* sp. The cultivation process was designed so that the final cell number density was limited by the initial silicon concentration. The diatom cells were cultivated in a bubble-column bioreactor to provide CO₂ delivery-replete conditions at a fixed light intensity in a well-mixed cell suspension using sodium nitrate as the nitrogen source. We report that the initial nitrate/silicon ratio was the key parameter for assessing sensitivity of chitin

production to nitrogen delivery, and so the chitin yield per cell was optimized through this parameter.

Materials & methods

Photobioreactor cultivation. The centric diatom *Cyclotella* sp. (UTEX 1269) was maintained in flask culture on Harrison's artificial seawater medium (ASM) as described previously (10). Flask cultures served as the inoculation source for the photobioreactor cultivation experiments. *Cyclotella* diatom cells were phototrophically cultivated in a bubble-column photobioreactor described previously (21,22) at the following conditions: incident light intensity of $94 \mu\text{mol photons m}^{-2}\text{s}^{-1}$, photoperiod of 14 h light/10 h dark, temperature of 22 °C, and aeration rate of 0.5 L air L⁻¹ culture min⁻¹ (sparger plate with 4 x 1.0 mm holes). For *Cyclotella* sp. diatom cells, the light intensity at 63.8% of saturation on the photosynthesis irradiance curve is nominally $60 \mu\text{E m}^{-2}\text{sec}^{-1}$ (18). The total culture volume was 4500 mL, and vessel inner diameter was 10.1 cm. Cells were cultivated in Harrison's ASM. The initial phosphate concentration was fixed at 0.2 mM (as sodium phosphate monobasic, NaH₂PO₄·H₂O). Silicon was added as sodium silicate (Na₂SiO₃) which, speciated to Si(OH)₄ (silicic acid). The initial silicon concentration was targeted to be 0.6 mM, but when measured in the medium at the beginning of the cultivation experiment ranged from 0.55 to 0.75 mM. This initial Si concentration was below the solubility limit of dissolved Si in seawater, which is 1.5-1.7 mM (Kamatani and Riley, 1979; Kato and Kitano, 1968; Krauskopf, 1956). The nitrogen source was sodium nitrate (NaNO₃), and the initial concentration ranged from 0.54 to 5.2 mM. For a given cultivation experiment, the measured initial dissolved silicon concentration ($C_{Si,o}$) and measured initial nitrate concentration ($C_{N,o}$) were used to specify the initial nitrogen (N) to silicon (Si) ratio, which varied from 0.82 to 8.6 mol N/mol Si. The initial pH was typically 8.5.

The initial cell number density ($X_{n,o}$) in the bioreactor was set to $1.3 \cdot 10^5$ cells mL⁻¹. The cell suspension culture was sampled once per day at 4 h into light phase of the photoperiod. Cell number density, dissolved silicon concentration in the medium,

dissolved nitrate concentration in the medium, chlorophyll *a*, and chitin concentration in the whole culture suspension were assayed as described previously (10,20).

Statistical analysis of data. All assays were repeated in duplicate or triplicate, with error bars reported as 1.0 S.D. Analysis errors within 5% of the average value were generally within the size of the data symbol. Cell number density (X_n) and chitin concentration (C_p) vs. time data for the batch cultivation experiments were estimated by the logistic model of the forms

$$X_N = \frac{X_{N,o} e^{k_p(t-t_0)}}{1 + \frac{X_{N,o}}{X_{N,f}} (e^{k_p(t-t_0)} - 1)} \quad \text{Equation 4.1}$$

$$C_P = \frac{C_{P,o} e^{k_p(t-t_0)}}{1 + \frac{C_{P,o}}{C_{P,f}} (e^{k_p(t-t_0)} - 1)} \quad \text{Equation 4.2}$$

where logistic model rate constant k (h^{-1}) and final cell number density ($X_{n,f}$) are the fitted parameters for Eq. 1, and logistic model rate constant k_p (h^{-1}) and final chitin concentration ($C_{p,f}$) are the fitted parameters for Eq. 2. Parameters posed by a given model were fitted to data by nonlinear, least-squares regression (NLS) using the Marquardt method on Statgraphics Centurion XVII software, with errors of fitted parameters reported as 1.0 S.E. Standard errors were propagated by the appropriate propagation rules. The specific growth rate (μ , h^{-1}) was estimated from the least-squares slope of the cell number vs. time data on a semi-log plot during the first 96 h of cultivation.

Results

Cultivation profiles for nutrient consumption, cell number production, and chitin production. Batch cultivation of the diatom *Cyclotella* sp. at representative initial N/Si molar ratios of 1.8 and 3.0 are presented in Figure 4.1. At an initial N/Si molar ratio of 1.8, dissolved silicon and nitrate concentration went to zero at the same time, whereas at an N/Si ratio of 3.0, silicon was consumed occurred first, followed by

nitrate consumption. After silicon consumption was nearly complete, chitin production began, and the cell number production leveled off. Chitin production leveled off after all the nitrate was consumed from the medium, and cell division was complete. The cell number and chitin concentration vs. time profiles were sigmoidal and fit to the logistic model given by Eqns. 1 and 2. Chlorophyll *a* concentration in the cell suspension increased with increasing N/Si ratio, showing incorporation of nitrogen into photosynthetic pigments. Generally, as the initial nitrate/silicon ratio at fixed initial silicon concentration increased, both the final cell number density ($X_{n,f}$) and final chitin concentration ($C_{p,f}$) increased. In order to provide a more fundamental description of productivity from the batch cultivation process, yield parameters for cell number and chitin production were estimated from this data, as detailed below.

Effect of N/Si ratio on cell yield and specific growth rate. The dependence of cell number yield based on silicon consumption ($Y_{X/Si}$, cells produced mmol^{-1} Si consumed) on the initial N/Si molar ratio is presented in Figure 4.2. The $Y_{X/Si}$ values were estimated by

$$Y_{X/Si} = \frac{X_{n,f} - X_{n,o}}{C_{Si,o} - C_{Si,f}} \quad \text{Equation 4.3}$$

where $X_{n,o}$ and $X_{n,f}$ are the initial and final cell number densities, and $C_{Si,o}$ and $C_{Si,f}$ are the initial and final dissolved silicon concentrations. The cell number yield increased and then leveled off with increasing N/Si molar ratio, was fit to a decaying exponential model of the form

$$Y_{X/Si} = Y_{X/Si,f} \left(1 - e^{-\frac{C/N}{K_x}} \right) \quad \text{Equation 4.4}$$

where $Y_{X/Si,f}$ is the asymptotic cell number yield, and K_x is the molar N/Si ratio at 63.8% of saturation. Parameters estimated by NLS regression are provided in Table 1. Although silicon was the required and limiting substrate for cell number

production, additional nitrogen availability extended $Y_{X/Si}$ to higher, but ultimately limiting, values. Therefore, at fixed silicon availability, additional nitrogen availability increased the cell number and decreased the silica content per cell. Also presented in Figure 4.2 is the effect of initial molar N/Si ratio on the on specific growth rate. The specific growth rate was not affected by increasing nitrate concentration, because silicon delivery controlled the cell division process.

Effect of N/Si ratio on chitin yield and production rate. The chitin yield per cell ($Y_{p/X}$, mg chitin per 10^9 cells), defined as

$$Y_{p/X} = \frac{C_{p,f}}{X_{n,f}} \quad \text{Equation 4.5}$$

is a more fundamental measure of chitin productivity than the final chitin concentration ($C_{p,f}$). The dependence of $Y_{p/X}$ on molar N/Si ratios ranging from 0.82 to 8.6 is presented in Figure 4.3. The chitin yield coefficient increased and then leveled off with increasing N/Si molar ratio, and so this parameter was fit to a decaying exponential model of the form

$$Y_{p/X} = Y_{p/X,f} \left(1 - e^{-\frac{C/N}{K_p}} \right) \quad \text{Equation 4.6}$$

where $Y_{p/X,f}$ is the asymptotic chitin yield per cell, and K_p is the molar N/Si ratio at 63.8% of saturation. These parameters were estimated NLS regression (Table 1). Estimates of K_p for chitin, and K_X for cell number, were each near 2.0 mol N/mol Si, which provides further support that chitin production was controlled by cell number production. The asymptotic chitin yield of 28.7 ± 1.2 mg chitin per 10^9 cells (1.0 S.E.) was consistent with our earlier studies at a similar light intensity which optimized chitin production with respect to CO_2 delivery at an initial N/Si ratio of 4.7 (19). Figure 4.3 also presents the effect of molar N/Si ratio on the fraction of nitrogen in the chitin product relative to the nitrate consumed. The fraction of nitrate nitrogen fed that was incorporated into chitin had a maximum of 0.18 mol chitin-N mol⁻¹ N at

an initial N/Si molar ratio of 2.0, and then decreased to approximately 0.09 mol chitin-N mol⁻¹ N consumed.

The peak rate of volumetric chitin formation (R_p , mg chitin L⁻¹ day⁻¹) was estimated from chitin concentration vs. time data. The logistic model for chitin production (Equation. 4.2) was differentiated with respect to time, and then evaluated at inflection point to yield

$$R_p = \left. \frac{dC_P}{dt} \right|_{\max} = \frac{k_P C_{P,f}}{4} \quad \text{Equation 4.7}$$

The effect of initial N/Si molar ratio on the peak rate of chitin production is presented in Figure 4.4. Within the range of initial molar N/Si ratios studied (0.82 to 8.6), the peak rate of chitin production rate increased linearly with increasing initial nitrate concentration, suggesting a first-order process. In contrast, the final chitin yield per cell asymptotically increased with respect increasing N/Si ratio due to the constraint of silicon as the limiting substrate for cell number production.

Discussion

The initial N/Si molar ratio was the critical parameter for assessing the limits of nitrogen delivery on chitin nanofiber production by the diatom cell under silicon-limiting cultivation conditions. In earlier studies, we showed that the production of chitin nanofibers occurred after cell division and complete consumption of silicon from the medium. Specifically, during fed-batch cultivation, the rate of chitin production was determined by the rate of silicon delivery at a fixed N/Si molar ratio, under conditions where the cell division rate was externally controlled by silicon delivery rate (10). In this study, both the cell number yield based on silicon ($Y_{X/Si}$), and the chitin yield per cell ($Y_{p/X}$) increased asymptotically with increasing N/Si molar ratio (Figures. 4.2 and 4.3). Both of these yield parameters worked synergistically to boost the concentration of chitin in the culture broth (Figure. 4.1). An initial N/Si ratio of at least 4.0 mol N mol⁻¹ Si was needed to achieve 90% of the asymptotic chitin yield.

We infer from these results that the diatom cell first responds to increased nitrogen availability by increasing the production of cells with lower silica content. But each cell also contains higher amounts of nitrogen-bearing intracellular materials, and ultimately extracellular chitin, as conceptually illustrated in Figure 4.5. The continued addition of nitrogen under carbon-replete conditions did not allow for the indefinite production of extracellular chitin nanofibers at silicon limitation, where cell division has ceased but the cell was still photosynthetically active.

Chitin biosynthesis in diatoms is presumed to possess biochemical pathways common to other organisms that make chitin (26). Chitin biosynthesis consists of four main steps. First, fructose-6-phosphate in the intracellular pool is converted to glucosamine via aminotransferase using glutamine. Second, glucosamine is converted to N-acetyl glucosamine-6-phosphate via N-acetyl transferase using Acetyl co-A. Third, N-acetyl glucosamine-6-P is converted to UDP-N-acetyl glucosamine via pyrophosphorylase using uridine triphosphate (UTP). Finally, chitin synthase catalyzes β -1,4 glycosidic bond formation between two UDP-N-acetyl glucosamine molecules, releasing UDP. Genes encoding for all of the key enzymes associated with chitin biosynthesis have been identified in *Cyclotella* (2).

In fungi and insects, chitin biosynthesis is tightly regulated at the transcriptional level during growth and development (26). Furthermore, the available form of nitrogen for chitin biosynthesis is glutamine, which is produced through the nitrate reduction and assimilation pathway. Glutamine synthase activity in the diatom *Skeletonema costatum* is enhanced by nitrate, but not ammonium, as the nitrogen source (27). Given these constraints on intracellular nitrogen allocation, we presume that the diatom cell sets a limit on how much chitin can be made based on feeding with nitrate. Since the diatom cell has a maximum chitin yield and cannot indefinitely bio-transform CO₂ and nitrate into chitin, scalable cultivation systems for chitin nanofiber production will require delivery of both silicon and nitrogen under silicon-limiting conditions to promote cell division and subsequent chitin formation.

In summary, the diatom *Cyclotella* sp. extrudes chitin nanofibers following cell division. This diatom requires silicon for cell wall biosynthesis, and nitrogen for biosynthesis of chitin, an N-acetyl glucosamine biopolymer. The nitrate/silicon

molar ratio was the critical parameter for assessing the limits of cell number and chitin production during batch cultivation of *Cyclotella*. The chitin yield per cell increased asymptotically with increasing N/Si ratio, achieving 90% of its final value of 28.7 mg chitin per 10^9 cells at an N/Si ratio of 4.0 mol N mol⁻¹ Si. Scalable systems for maximum chitin nanofiber production will require cultivation of *Cyclotella* cells with optimal nitrogen delivery under silicon-limited growth.

Acknowledgements

This work was supported by the US National Science Foundation (NSF), Emerging Frontiers for Research and Innovation program (EFRI), under award number 1240488.

References

1. Martin-Jézéquel V, Hildebrand M, Brzezinski MA. Silicon metabolism in diatoms: Implications for growth. *J Phycol.* 2000;36(5):821–40.
2. Traller JC, Cokus SJ, Lopez DA, Gaidarenko O, Smith SR, McCrow JP, et al. Genome and methylome of the oleaginous diatom *Cyclotella cryptica* reveal genetic flexibility toward a high lipid phenotype. *Biotechnol Biofuels.* 2016;9(1):258.
3. Smith SR, Abbriano RM, Hildebrand M. Comparative analysis of diatom genomes reveals substantial differences in the organization of carbon partitioning pathways. *Algal Res.* 2012;1(1):2–16.
4. Obata T, Fernie AR, Nunes-Nesi A. The central carbon and energy metabolism of marine diatoms. *Metabolites* [Internet]. 2013 May 7 [cited 2016 Oct 25];3(2):325–46. Available from: <http://www.ncbi.nlm.nih.gov/pubmed/24957995>
5. Gügi B, Costaouec T Le, Burel C, Lerouge P, Helbert W, Bardor M. Diatom-specific oligosaccharide and polysaccharide structures help to unravel biosynthetic capabilities in diatoms. *Mar Drugs.* 2015;13(9):5993–6018.
6. Herth W. The site of β -chitin fibril formation in centric diatoms II. The chitin-forming cytoplasmic structures. *J Ultrastructural Res.* 1979;68:16–27.
7. Herth W, Barthlott W. The site of β -chitin fibril formation in centric diatoms I. Pores and fibril formation. *J Ultrastructural Res.* 1979;68:6–15.
8. Herth W, Zugenmaier P. Ultrastructure of the chitin fibrils of the centric diatom *Cyclotella cryptica*. *J Ultrastructural Res.* 1977;61:230–9.
9. McLachlan J, McInnes G, Falk M. Studies on the chitin (chitin: poly-N-acetylglucosamine) fibers of the diatom *Thalassiosira fluviatilis* Hustedt. I. Production and isolation of chitin fibers. 1965;43:707–13.
10. Chiriboga N. OG, Rorrer GL. Control of chitin nanofiber production by the

- lipid-producing diatom *Cyclotella* Sp. through fed-batch addition of dissolved silicon and nitrate in a bubble-column photobioreactor. *Biotechnol Prog.* 2017;33(2):407–15.
11. Ogawa Y, Kimura S, Wada M. Electron diffraction and high-resolution imaging on highly-crystalline ??-chitin microfibril. *J Struct Biol.* 2011;176(1):83–90.
 12. Azuma K, Ifuku S, Osaki T, Okamoto Y, Minami S. Preparation and biomedical applications of chitin and chitosan nanofibers. *J Biomed Nanotechnol.* 2014;10(10):2891–920.
 13. Habibi Y, Lucia LA. Chitin Nanofibers as Building Blocks for Advanced Materials. In: Habibi Y, Lucia LA, editors. *Polysaccharide Building Blocks: A Sustainable Approach to the Development of Renewable Biomaterials.* John Wiley & Sons, Inc.; 2012. p. 227–45.
 14. Jayakumar R, Prabakaran M, Nair S V., Tamura H. Novel chitin and chitosan nanofibers in biomedical applications. *Biotechnol Adv.* 2010;28(1):142–50.
 15. Ding F, Deng H, Du Y, Shi X, Wang Q. Emerging chitin and chitosan nanofibrous materials for biomedical applications. *Nanoscale.* 2014;6:9477–93.
 16. Rolandi M, Rolandi R. Self-assembled chitin nanofibers and applications. *Adv Colloid Interface Sci.* 2014;207(1):216–22.
 17. Ifuku S, Saimoto H. Chitin nanofibers: preparations, modifications, and applications. *Nanoscale.* 2012;4:3308–18.
 18. Ozkan A, Rorrer GL. Effects of light intensity on the selectivity of lipid and chitin nanofiber production during photobioreactor cultivation of the marine diatom *Cyclotella* sp. *Algal Res.* 2017;25(December 2016):216–27.
 19. Ozkan A, Rorrer GL. Lipid and chitin nanofiber production during cultivation of the marine diatom *Cyclotella* sp. to high cell density with multistage addition of silicon and nitrate. *J Appl Phycol* [Internet]. 2017 Mar 21 [cited

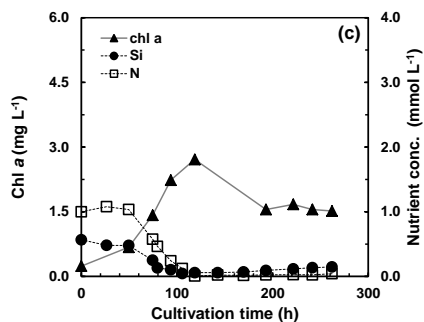
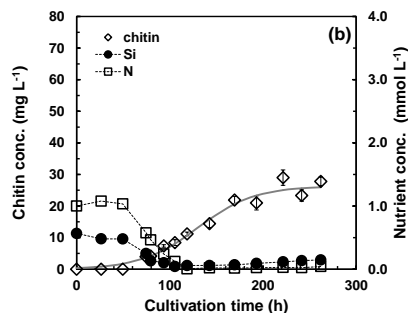
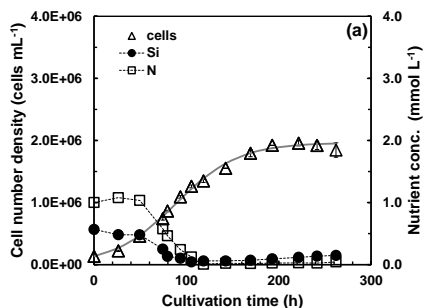
- 2017 May 24];1–8. Available from: <http://link.springer.com/10.1007/s10811-017-1113-7>
20. Ozkan A, Rorrer GL. Effects of CO₂ delivery on fatty acid and chitin nanofiber production during photobioreactor cultivation of the marine diatom *Cyclotella* sp. *Algal Res.* 2017;
 21. Rorrer GL, Antonio J, Durst R, Kelly C, Gale D, Maddux B, et al. The Potential of a Diatom-Based Photosynthetic Biorefinery for Biofuels and Valued Co-Products chitin. *Curr Biotechnol.* 2016;5:237–48.
 22. Jeffryes C, Gutu T, Jiao J, Rorrer GL. Two-stage photobioreactor process for the metabolic insertion of nanostructured germanium into the silica microstructure of the diatom *Pinnularia* sp. *Mater Sci Eng C [Internet]*. 2008 Jan [cited 2016 Jul 26];28(1):107–18. Available from: <http://linkinghub.elsevier.com/retrieve/pii/S0928493107000045>
 23. Krauskopf KB. Dissolution and precipitation of silica at low temperatures. *Geochim Cosmochim Acta.* 1956;10:1–26.
 24. Kamatani A, Riley JP. Rate of dissolution of diatom silica walls in seawater. *Mar Biol.* 1979;55(1):29–35.
 25. Kato, K., Kitano Y. Solubility and Dissolution Rate of Amorphous Silica in Distilled and Sea Water at 20 C. *J Oceanogr Soc Japan.* 1968;24(4):147–52.
 26. Merzendorfer H. The cellular basis of chitin synthesis in fungi and insects: Common principles and differences. *Eur J Cell Biol.* 2011;90(9):759–69.
 27. Takabayashi M, Wilkerson FP, Robertson D. Response of glutamine synthetase gene transcription and enzyme activity to external nitrogen sources in the diatom *Skeletonema costatum* (Bacillariophyceae). *J Phycol.* 2005;41(1):84–94.

Table 4.1Yield parameters for the diatom *Cyclotella* sp.

Yield Parameter	Units	Value (± 1.0 S.E.)
$Y_{X/Si,f}$	cells	#cells mmol ⁻¹ Si
		$5.34 \cdot 10^9 \pm 2.61 \cdot 10^8$
K_X		mol N mol ⁻¹ Si
		2.0 ± 0.3
$Y_{p/X,f}$	chitin	mg chitin per 10^9 cells
		28.7 ± 1.2
K_P		mol N mol ⁻¹ Si
		1.6 ± 0.2
$Y_{p/N,f}$	chitin-N	mol chitin-N mol ⁻¹ N
		0.086 ± 0.012

Figure 4.1. Comparison of the batch cultivation of the diatom *Cyclotella* sp. in a bubble-column photobioreactor at two initial N/Si molar ratios. (a) Cell number density, medium silicon concentration, and medium nitrate concentration vs. time; (b) chitin concentration in cell suspension vs. time; (c) chlorophyll *a* concentration in cell suspension vs. time. The smooth solid lines are the fit of the data to the logistic model for cell number density (Equation. 4.1) and chitin concentration (Equation. 4.2).

Initial mol N / mol Si = 1.8



Initial mol N / mol Si = 3.0

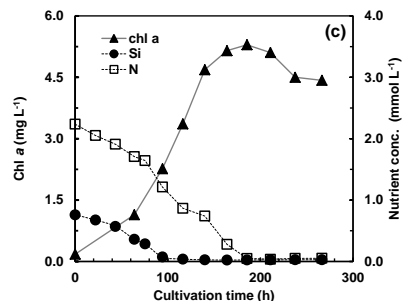
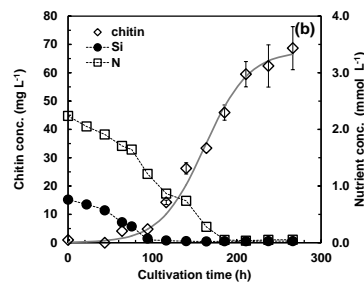
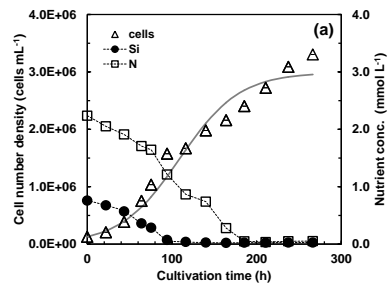


Figure 4.2. Effects of initial N/Si molar ratio on cell number yield based on silicon consumption ($Y_{X/Si}$) and specific growth rate (μ). Solid line is the fit of $Y_{X/Si}$ to Equation. 4.4.

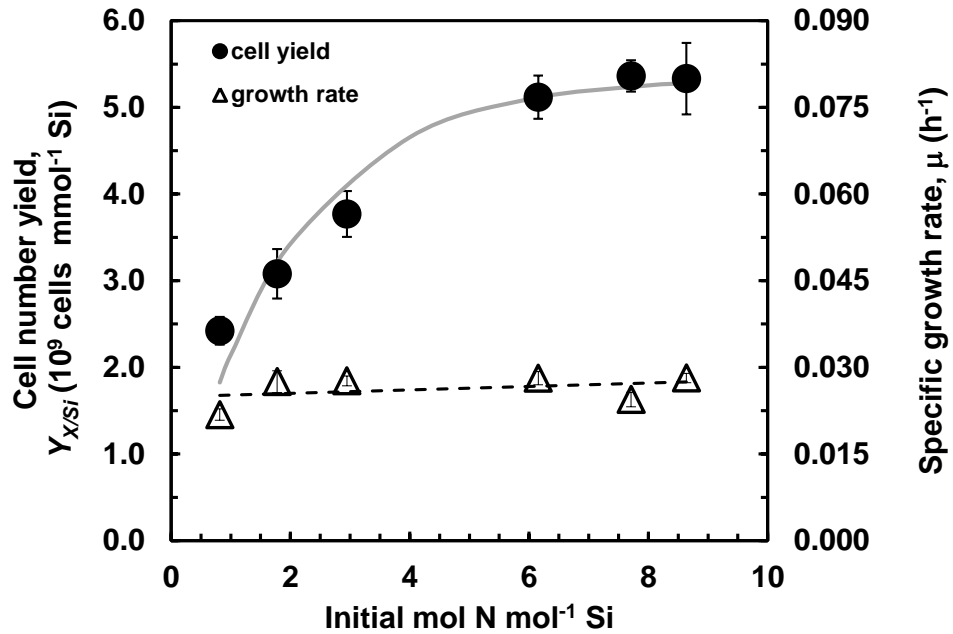


Figure 4.3. Effects of initial N/Si molar ratio on chitin yield per cell ($Y_{X/p}$) and the fraction of nitrate delivered incorporated into the chitin product (mol chitin-N mol⁻¹ N consumed). Solid line is the fit of $Y_{X/Si}$ to Equation. 4.6.

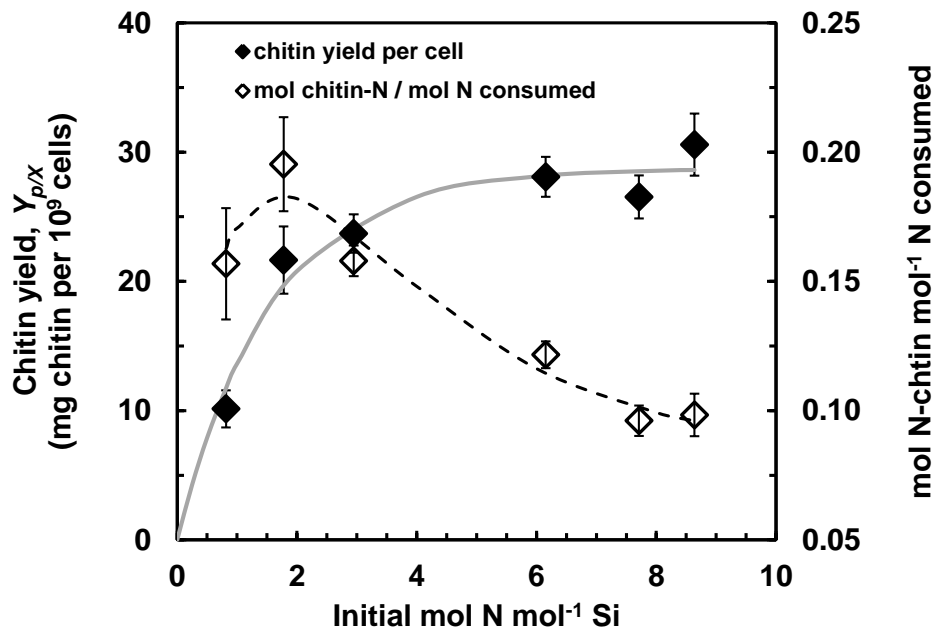


Figure 4.4. Effect of initial N/Si molar ratio on peak rate of chitin production (R_p). Dotted line is best fit from linear regression ($r^2 = 0.89$).

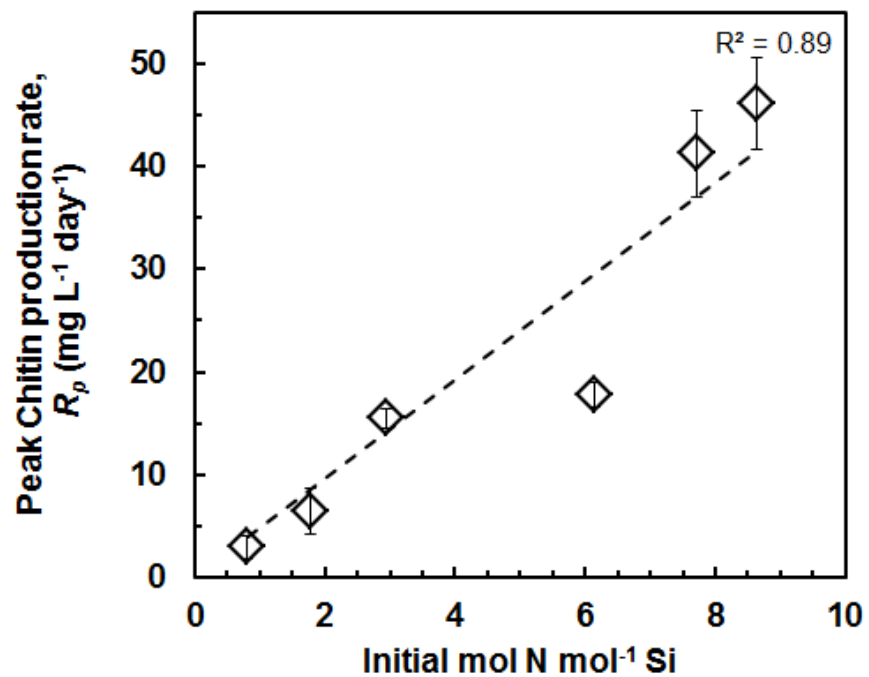
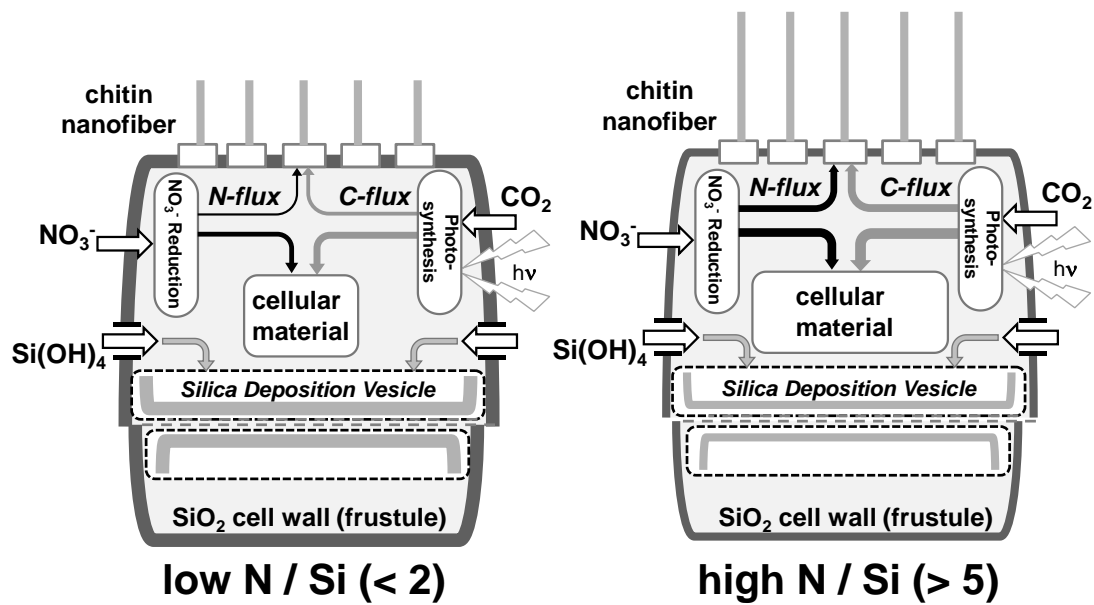


Figure 4.5. Conceptual model of substrate flows into cellular materials at low and high molar N/Si ratios. Not drawn to scale.



Chapter 5: Effects of phosphate concentration on lipid class and chitin nanofiber production during a two stage cultivation of the diatom *Cyclotella* sp. in a bubble-column photobioreactor

Abstract

The model diatom *Cyclotella* sp that has radial symmetry and extrudes chitin nanofibers through the specialized portulaes located in the rims of the valves, requires biogenic silica to create its intricate nano-patterned frustule. Dissolved silicon and its depletion from the media has shown to be a trigger to various cellular processes that induce cell division, *N*-acetylglucosamine biopolymer formation, and intracellular lipid accumulation. Phosphorus depletion and strategic delivery during cultivation, paired with silicon and nitrate co-addition, has shown to induce cellular processes that are of interest. This manuscript determined that phosphate concentration has an effect for lipid class induction in the photobioreactor cultivation of *Cyclotella*. Two approaches were used to capture the lipid class production, one was to cultivate the cells to induce intracellular phosphorus starvation, and the second one was to cultivate the cells in a phosphorus available system. The phosphorus concentration range that was studied varied between (0.01 – 0.37 mmol L⁻¹). Final cell number density varied between (1.5×10⁶ - 9.5×10⁶ cells mL⁻¹), average chitin yield of 9 ± 1 wt% (S.E.) and average lipid yield of 36 ± 6 wt% (S.E.). The minimum phosphorus requirements for *Cyclotella* was determined to be 6.89 ± 0.19 μmol P per 10⁹ cells (S.E.). The phosphate concentration had no emajor effects in chitin or cell, when cells cultivated below the phosphorus threshold, they will be induced to accumulate neutral lipids, whereas in a phosphorus available system, cells accumulate phospholipids over neutral lipids.

Introduction

Diatoms are single celled microalgae that are well known for their intricately patterned cell wall (frustules) made of biosilica that has pore arrays symmetrically patterned in the submicron and nanoscale level. Diatoms require dissolved silicon in the form of Si(OH)₄ as substrate to form their cell walls, characteristic which makes it unique among other microorganisms and facilitates the control of cell division. The current understanding of diatoms has made them re-emerge as important candidates to produce high-value bioproducts in novel biorefineries systems that are gaining traction in science and industry (1)(2)(3) (4). The model diatom *Cyclotella* has proven

to be of great value towards this potential use, and great advances has been made over the past years to consolidate a fundamental understanding of the metabolic capacities of this particular model microorganism in a scalable system. In previous work we characterized how CO₂ delivery, light delivery, silicon (Si) and nitrogen (N) nutrient delivery ratios in batch and fed-batch addition of a nutrient rich mixture (Si,N) with silicon as limiting nutrient controlled bioproduct formation of lipid and chitin nanofibers in the model diatom *Cyclotella* (5)(6)(7) (8) (9). The molar ratio of N/Si of 1.6 is at 63.8% saturation, and anything above the molar ratio of N/Si of 6 has no further effects on the cell and metabolite productivity, however, chitin yield per cell can be maximized at a molar ratio of N/Si of 2. We also determined the maximum chitin yield of 15 wt% in dry biomass, and this yield is related to the cell number density, which can be controlled by the addition of silicon, however, lipids can vary on nutrient conditions, and is always biosynthesized on top of the low energy requirements of the chitin nanofibers carbohydrate production.

These are important parameters to be used in the bioprocessing design of the diatom *Cyclotella*, however we didn't touch upon the important macronutrient phosphorus (P) and how it affects *Cyclotella* in cell, lipid and chitin formation. Phosphorus is a non-renewable macronutrient that is needed by all biomass for growth, and as such, is not used effectively, which complicates the long term sustainable availability (10)(11)(12).

The goal of this study was to assess how phosphate concentration affects cell, lipid, and chitin formation during a two stage cultivation of the diatom *Cyclotella* sp. The cultivation was designed with two different nutrient additions of phosphate in a two stage cultivation process. The first approach (Type-A) was to load different amounts of phosphate at the beginning of Stage I. The second approach (Type-B) was to deliver different amounts of phosphate during Stage II. Both Type- A and B experiments had a constant loading and delivery rate of silicon (Si) and nitrogen (N) in a way that both Si and N were consumed as soon as they were delivered to create a Si and N starved cell. By using these strategies, at a given point in the experimental time the cell suspension will have experienced a spectrum of intracellular phosphorus

starvation to an excess of phosphorus available that will directly affect the metabolic carbon allocation, we hypothesize that by controlling the phosphorus available to the cells in a silicon and nitrogen starved state we can induce the cells to redirect the metabolic carbon allocation into chitin and specific lipid molecules. The outcomes of this cultivation strategy enabled the co-production of cells, chitin, and lipid specific molecules where the yields of cell biomass was dependent on the overall availability of phosphorus in the system. Chitin formation was dependent on the cell biomass and was held constant, and neutral lipid production was favored over phospholipids in a phosphorus starved cell, whereas phospholipids were favored over neutral lipids in a phosphorus rich system.

Materials & methods

Photobioreactor cultivation. The centric diatom *Cyclotella* sp. (UTEX 1269) was maintained in flask culture on Harrison's artificial seawater medium (ASM) as described previously (13). Flask cultures served as the inoculation source for the photobioreactor cultivation experiments. *Cyclotella* diatom cells were phototrophically cultivated in a bubble-column photobioreactor described previously (2,14) at the following conditions: incident light intensity of $187 \pm 30 \mu\text{mol photons m}^{-2}\text{s}^{-1}$ (S.E.), photoperiod of 14 h light/10 h dark, temperature of 22 °C, and pressurized house air with CO₂ concentration of 2000 ppm (sparger plate with 4 x 1.0 mm holes). For *Cyclotella* sp. diatom cells, the light intensity at 63.8% of saturation on the photosynthesis irradiance curve is nominally $60 \mu\text{E m}^{-2}\text{sec}^{-1}$ (6), so experiments were carried in the saturation level. The total culture volume was 5000 mL, and vessel inner diameter was 10.1 cm. Cells were cultivated in Harrison's ASM in two stages. Stage I which was designed to have an initial batch loading of nutrients, sodium metasilicate, Na₂SiO₃, sodium nitrate NaNO₃ and sodium phosphate monobasic, NaH₂PO₄·H₂O (Si, N, P) and an initial cell number density ($X_{n,o,I}$) of $1.2 \times 10^5 \text{ cells mL}^{-1} \pm 6.5 \times 10^3$ (S.E.), as shown in Table 1. Stage II was designed to be a fed-batch addition of nutrients with an initial cell number density ($X_{n,o,II}$) of $7.6 \times 10^5 \text{ cells mL}^{-1} \pm 1.8 \times 10^4$ (S.E.). The experiments were carried out under two different

types of nutrient additions, named Type- A and B. Both types of experiments had the same initial load of silicon and nitrogen for Stage I and the same addition rate of silicon and nitrate for Stage II. Type A experiment was carried out at varying initial loadings of phosphate, and Type B had varying addition rates of phosphate on Stage II. For Type-A experiment, the volumetric flow rate was fixed at $1.26 \text{ mL}\cdot\text{h}^{-1}$, total addition time of 7 days, which accounted for a total volume addition equivalent to 4.2%. For Type-B experiment, the volumetric flow rate was fixed at $2.52 \text{ mL}\cdot\text{h}^{-1}$, total addition time of 9 days, which accounted for a total volume addition equivalent to 10.8%. The initial pH was typically 8.5. The cell suspension culture was sampled once per day at 4 h into light phase of the photoperiod. Cell number density, dissolved silicon concentration in the medium, dissolved nitrate concentration in the medium, ash-free dry weight (AFDW), total lipid, and chitin concentration in the whole culture suspension were assayed as described previously (13,15). Dissolved phosphate concentration in the medium was measured by colorimetric method utilizing the LaMotte Test Kit No 3114-02 for its reagents and readings done with a Shimadzu UV-VIS MultiSpec 1501.

Quantum yield of photosynthesis. An aliquot was removed from the photobioreactor during Stage II cultivation and the cell sample was corrected (dilution or concentration) to achieve a cell number density of $1 \times 10^6 \text{ cells mL}^{-1}$. The aliquot was set to rest in the dark for 5 minutes. The photosynthetic parameters were measured with a Qubit® Fluorometer Model FL1 equipped with Qubit® cuvette holder accessory, a gain potentiometer, actinic light potentiometer control box, timer to control saturating pulses, LED chlorophyll excitation light, chlorophyll fluorescence detector, filtered 50W actinic halogen lamp. Digital signals were acquired with a Vernier LabPro and recorder with Logger Pro 3.2. A high flash of light of $5000 \mu\text{mol photons m}^{-2}\text{s}^{-1}$ is irradiated to the sample which determined the F_m and F_o , followed by turning on the actinic light potentiometer at a light intensity of $250 \mu\text{mol photons m}^{-2}\text{s}^{-1}$ with an automatic saturating flash of light every 20 seconds. The actinic light with saturating pulses is recorded until steady state is achieved (10 min). The value F_t is determined before the saturation pulse at steady state, and the F'_m is determined in the last saturation pulse.

Ultra-performance LC-TOF-MS/MS lipidomic analyses. A representative sample of experiments Type- A and B respectively were picked at 9 days after the beginning of Stage II, and the lipids were extracted from microalgae by the method described above. The extract was evaporated with N₂ and then reconstituted with 500 μ L [25:65:10 (v/v/v) methylene chloride:methanol:isopropanol with 0.5% butylated hydroxytoluene]. The mixture was vortexed mixed and then centrifuged at 10000 \times g for 5 minutes, and the supernatant was separated in another vial for identification. To identify the lipid metabolites from microalgae, LC was performed using a 1.8 μ m particle 100 \times 2.1 mm id HSS T3 column (Waters, Milford, MA) coupled to a quadrupole TOF mass spectrometer (AB SCIEX, TripleTOF 5600) operated in information-dependent MS/MS acquisition mode. The column was heated to 65°C in the column oven. A gradient system was used consisting of mobile phase A (60:40 acetonitrile:water containing 10 mM ammonium formate and 0.1% formic acid) and mobile phase B [90:10 (v/v/v) isopropanol:acetonitrile:water with 10 mM ammonium formate and 0.1% formic acid] with sample analysis performed over 14 min total run time. The initial starting conditions were 85% A and 15% B for 0.3 min with same gradient. The gradient was ramped to 30% B for 1.7 min, kept for 2 min, increased to 50% B for 0.2 min, increased to 80% B to 9 min. The solvent was increased to 100% B for 0.3 min and held to 11.5 min. Subsequently, the system was switched to the initial ratio for 0.3 min, and equilibrated at the initial ratio for additional 2.2 min. The flow rate was 0.5 mL/min and the injection volume was 5 μ L. TOF-Mass Spectrometry (MS) acquisition time was 0.25 seconds, and MS/MS acquisition time was 0.1 seconds. The scan range was m/z 70–1700 for TOF MS and m/z 50–1700 for MS/MS. Source parameters included nebulizing gases GS1 at 45, GS2 at 50, curtain gas at 35, positive mode ion spray voltage 5500 V, negative mode ion spray voltage at -4500 V, declustering potential at 80 and -80 V for positive and negative ion mode, respectively and at an ESI source operating temperature of 550 °C. Collision energy for MS/MS step was 35 \pm 10 eV. Data was imported into PeakView software for identification and MultiQuant software for relative quantification.

SEM images. Whole diatom cells of representative experiments were settled on a glass slide, fixated with 2.5 wt% glutaraldehyde (in 1 wt% paraform and 0.1 M

sodium cacodylate buffer for 30 min, 20 C), rinsed with 0.1 M sodium cacodylate buffer, ethanol dehydration (sequential washes from 20% to 100% in steps), and critical point dried. Samples were sputtered with gold and then imaged on a FEI Quanta 600 FED SEM.

Statistical Analysis of Data

All assays described above were repeated in duplicate or triplicate. Point standard errors (1.0 S.E.) were within 5% of the average value, and when plotted were generally within the size of the data symbol. For Type-A experiments, in Stage II of the cultivation process, cell number density vs time data was fitted to the logistic model given the *Equation 5.1*, and lipid and chitin concentration vs. time data was fitted to the logistic model given the equation *Equation 5.2*. These data were fitted by nonlinear, least-squares regression using the Marquardt method on Statgraphics Centurion XVII Software, and errors on the fitted parameters are reported as 1.0 S.E. Peak production rates were estimated by *Equation 5.3* using the fitted parameters, with overall error reported as 1.0 S.E. based on error propagation 1.0 S.E. values of the individual fitted parameters.

For Type-B experiments, in Stage II of the cultivation process, cell number density vs time data was fitted to a line and the slope was determined by least-squares. Lipid and chitin concentration vs. time were also fitted to a line and the slope was determined by least-squares. The cell, lipid and chitin production rate used the slopes and scaled to volumetric production with *Equation 5.4*. The final cell number density, lipid, and chitin concentration was determined by averaging the four last data points of the experiment starting at the end of Stage II.

The minimum phosphate requirements per cell was determined with data obtained from experiment Type-A applying *Equation 5.5*. The biomass yield was calculated by averaging the four last data points of the experiment starting at the end of Stage II and applying *Equation 5.6* for experiments Type- A and B. The product yield per cell for lipid and chitin was calculated by using *Equation 5.7* for Type- A and B. The quantum yield of photosynthesis was calculated using Eq. 8.

The lipidomic extracted ion chromatogram area for each molecule was normalized to the total amount of lipid that was extracted and analyzed. The areas of each lipid type were then added together, and then compared to their direct counterpart from each experiment.

$$X_N = \frac{X_{N,0}e^{k_p(t-t_0)}}{1 + \frac{X_{N,0}}{X_{N,f}}(e^{k_p(t-t_0)} - 1)} \quad \text{Equation 5.1}$$

$$P_i = \frac{P_{0,i}e^{k_{p,i}(t-t_0)}}{1 + \frac{P_{0,i}}{P_{f,i}}(e^{k_{p,i}(t-t_0)} - 1)} \quad \text{Equation 5.2}$$

$$\dot{R}_z = \left. \frac{dC_P}{dt} \right|_{max} = \frac{k_P C_{P,f}}{4} \quad \text{Equation 5.3}$$

$$\hat{R}_z = \frac{R_z}{\bar{V}_L} \quad \text{Equation 5.4}$$

$$Y_{Phos/X} = \frac{C_{Phos,o,I} - C_{Phos,f,I}}{X_{n,f,II} - X_{n,o,I}} \quad \text{Equation 5.5}$$

$$Y_{b/X} = \frac{C_{b,f,II}}{X_{n,f,II} - X_{n,o,I}} \quad \text{Equation 5.6}$$

$$Y_{c/X} = \frac{C_{P,f,II}}{X_{n,f,II} - X_{n,o,I}} \quad \text{Equation 5.7}$$

$$\Phi_{PSII} = \frac{F'_m - F_t}{F'_m} \quad \text{Equation 5.8}$$

Results

Cultivation profiles for nutrient consumption, cell number production, and nutrient delivery for Type A and B experiments. Cell number density, soluble nutrient concentration (Si, N, & P) and nutrient delivery time profiles for representative experiment Type A is presented in Figure 5.1. Experiment Type-A was

designed to be have a constant load of Si and N in Stage I, constant Si and N addition in Stage II, and a variable amount of P loading in Stage I as shown in Table 1. From time 0 to 120 h cultivation on Stage I conditions were carried out at an initial Si/N/P molar ratio of 12:15:1, dissolved silicon, nitrate and phosphate concentration went to zero at the same time during Stage I. From time 120 h to 288 h Stage II addition of silicon and nitrogen to the system was carried out (Figure 5.1b). Cell number density increases with the addition of nutrients and at 210 h cell number density starts to level off for the remainder of the experimental time. During the time window of 120 h – 210 h silicon and nitrogen that were being delivered to the cell suspension were consumed, giving nutrient concentrations of zero in the liquid medium. When cell number density starts to plateau at 210 h we observe that silicon and nitrogen concentration in the liquid medium start to increase until the end of the nutrient addition time of 288 h.

Cell number density, soluble nutrient concentration (Si, N, & P) and nutrient delivery time profiles of a representative experiment Type B is presented in Figure 5.2. Experiment Type-B was designed to be have a constant load of Si, N, and P in Stage I, a constant Si, and N addition in Stage II, and a variable P addition in Stage II.

From time 0 to 120 h cultivation on Stage I conditions were carried out at an initial fixed Si/N/P molar ratio of 20:25:1 for all experiments, dissolved silicon, nitrate and phosphate concentration went to zero at the same time during Stage I. From time 120 h to 336 h Stage II addition of silicon, nitrogen, and phosphate to the system was carried out (Figure 5.2b). At all nutrient addition rates, the dissolved silicon, nitrogen, and phosphate concentrations within the cell suspension were zero during the entire duration of Stage II. The total amount of silicon added to Stage II was designed to enable at least three cell doublings, from approximately $7.6 \cdot 10^5$ cells/mL at the end of Stage I to $6.1 \cdot 10^6$ cells /mL at the end of Stage II. Nutrient (Si, N, P) delivered to the system are consumed throughout the whole experimental time of Stage II. When the nutrient delivery ends, cell division stops and it levels off.

Cultivation of *Cyclotella* under Type-A conditions caused the cell to uptake the variable initial concentrations of phosphate in nominally the same time. In Type-B experiment during Stage II cultivation, the increasing amount of phosphate delivered

to the cell suspension also caused the cells to uptake more phosphorus. This suggests that luxury uptake of phosphorus was promoted during these two stages at different modes of addition of nutrients, which is in agreement with previous research (16).

Biomass, lipid and chitin production. Biomass, lipid, and chitin productivity time profiles for experiments Type A and B for Stage II are presented in Figure 5.3. For the 7 day Stage II fed-batch experiment, ash free dry weight (AFDW) biomass increases until the midpoint of the 7 day perfusion, biomass accumulation ceases after 220 hours and remains constant until the termination of the experiment. Lipid increases during the whole time of Stage II and chitin follows the same trend of biomass, with an increase since the beginning of the addition of nutrients and ceases by the midpoint of Stage II, and remains constant until the end of the experiment. In Type B experiment (Figure 5.3b) AFDW biomass increases during the 9 day duration of Stage II, and it keeps increasing until the end of the experiment. Lipid increases linearly during Stage II and it levels off by the end of the experiment. Chitin increases linearly over time during Stage II, and it also levels off by the end of the experiment.

Nutrient limitation and photosynthetic activity. Ash free dry weight biomass and photosynthetic parameter of Photosystem II (PSII) F_v'/F_m' time profiles for experiments Type A and B are presented in Figure 5.4. For Type A experiment, the AFDW biomass increases during the fed-batch addition of Si and N, and it plateaus at 210 h as explained above (Figure 5.4a). The photosynthetic parameter F_v'/F_m' decreases over time with a drastic slope change at 210 h, and it continues to decrease until the end of the experiment. This occurrence is seen in the four Type-A experiments carried out. For Type B experiment, the AFDW biomass increases linearly during the addition of Si, N, and P on Stage II. The photosynthetic parameter F_v'/F_m' decreases over time, maintaining an average of 0.68.

Effect of phosphate concentration on AFDW biomass, lipid, and chitin yield per cell. The dependence on AFDW biomass, lipid, and chitin per 10^9 cells based on cumulative phosphate concentration consumed for experiments Type A and B are

presented in Figure 5.5. Perhaps, a better way to assess the differences between the two type of experiments is to look at them from the cumulative amount of phosphate delivered to the system and normalized to the working volume of the beginning of Stage II, which gives a phosphate concentration. The dependence of $Y_{b/X}$ on consumed phosphate concentration ranging from 0 to 0.05 mM phosphate in experiment Type A (P-starved) and from 0 to 0.5 mM phosphate in experiment Type B (P-available) is presented in Figure 5.5a-b and Figure 5.5c-d, respectively.

The biomass yield per cell remains constant as consumed phosphate concentration increases in the low phosphate concentration window (Figure 5.5a). The biomass yield per cell a small decrease as the consumed phosphate concentration increases in the high phosphate concentration window (Figure 5.5c). The dependence of chitin yield per cell, $Y_{c/X}$, on cumulative phosphate concentration for experiments Type A and B remains constant at levels of 10% of the biomass content.

The dependence of lipid yield per cell, $Y_{l/X}$, on cumulative phosphate concentration for experiments Type A and B are presented in Figure 5.5c, and 5.5d respectively. We can observe the at low phosphate there is a declining amount of lipid at increasing phosphate concentration in the narrow window (Figure 5.5b) with an accumulation of 35% of total biomass, whereas the lipid yield at high phosphate remains constant at levels of about 16% of total biomass (Figure 5.5d). Lipid is produced and accumulated on top of the chitin, which is in good agreement with our previous findings (15).

The dependence on cell, lipid and chitin productivity based on cumulative phosphate concentration for experiments Type A and B are presented in Figure 5.6. The cell, lipid and chitin productivity at P-starved (Figure 5.6a,b) were estimated as peak rate of formation from the cell, lipid, and chitin concentration vs. time data on Stage II. The effect seen by increasing cumulative phosphate concentration in the P-starved regime is that cell productivity increases, while chitin productivity follows the cell productivity. Lipid productivity is the same at the different cumulative phosphate concentrations in the P starved regime (Figure 5.6b) The cell, lipid and chitin productivity at high phosphate (Figure 5.6c,d) were estimated by least-square slope of

cell, lipid, and chitin concentration vs. time data on Stage II. Cell and chitin productivity have no major change in response to increasing cumulative phosphate concentration at the P-available regime. Lipid productivity has no major change as the cumulative phosphate concentration increases.

To have a better understanding of what is happening intracellularly, a representative lipidomic analysis was performed for an experiment of Type- A and B respectively and the lipid class molecules are shown in Table 2, and worked data is presented in Figure 5.7. The sample used for comparison was selected at 9 days after the beginning of Stage II to ensure that all nutrients were delivered to the system. There is a relative higher abundance area count per milligram of lipid of free fatty acids (FFA) and triacylglycerides (TAG) for experiments carried out at Type-A conditions, whereas, there is a higher relative abundance area count per milligram of lipid lysophosphatidylcholine (LPC) and phosphatidylcholine (PC) in experiment Type-B.

A representative SEM image of *Cyclotella* at the end of Stage II cultivation with chitin nanofibers surrounding the cell is presented in figure 5.8. The chitin nanofibers are extruded from the portulaes located in the rims of the valves (Figure 5.8a), and not all fibers seem to be attached to a cell (Figure 5.8b).

Discussion

This study utilized a two-stage (Stage- I and II) cultivation process with two different type of experiments (Type- A and B) where the Si and N loadings and addition rates were held constant for both types of experiments in Stages I and II. The addition of Si and N was designed for the cells to consume Si and N upon the immediate delivery, creating a Si and N starved cell. Experiment Type-A had a varying initial amount of P delivered on Stage I, and experiment Type-B had a varying addition rate of P on Stage II. The overall phosphate concentration reported was calculated by adding the total amount of P consumed by the cell suspension on Stages I and II and normalized to the total working volume of the cell suspension at the beginning of Stage II. This was done because it is the best way to express how

the phosphate concentration affects the cells, chitin, and lipid specific molecule formation.

Cumulative phosphate concentration has no significant effect in biomass yield per cell in each experiment type, however, there is a significant change between biomass yields per cell for experiments Type- A and B. The overall biomass yield is 40% higher at experiments carried out under Type-A conditions. The cell productivity for Type-A experiments increase with increasing phosphate concentration, and it remains almost the same for Type-B experiments. This is due to the cultivation process design that was adding an excess of silicon for Type-A with respect to P, whereas for Type-B, the addition of silicon was the limiting substrate. This is a key difference between these type of experiments, where P was a limiting nutrient in once case (Type-A), and was in excess in the other (Type-B). Silicon drives cell division in *Cyclotella*, however, there has to be other accompanying nutrients in enough quantities for the cell to divide. Since there is more P available per cell in type-A, cells are able to divide, therefore, their rate increases in this particular concentration window. In Type-B, the cell production rate is constant, and it is driven by the constant rate of addition of silicon, therefore, it marginally increases.

The effect of increasing cumulative phosphate concentration in chitin yield per cell in experiment Type-A is a marginal increase, whereas in Type-B, it remains constant. The effects of phosphate concentration in chitin productivity is an increases in Type-A experiments, while it has no significant effect in Type-B experiments. Chitin production is controlled by cell division, and cell division is controlled by silicon addition. As previously explained, we are controlling the cell production through the addition of silicon, and that silicon addition is indirectly controlling chitin production, through cell division. In Type-A experiments, phosphorus was not available in enough quantities to sustain production with all the silicon provided, therefore, as we increased the silicon available, there was more production of cells, more cell division, therefore, more chitin production. In type B experiments, the

silicon added was constant, and the phosphate concentration had no significant effect in the overall yield or productivity in Type B.

The overall effect of cumulative phosphate concentration on lipid yield per cell is not significant in each experiment type, however there is a 3-fold difference in the overall yield of lipids per cell for Type-A experiments compared to Type-B. This shows that the key difference here is not phosphorus concentration itself, but the cellular state which in this case is P-starved for Type-A experiments, and P-available for Type-B experiments. We are looking at different cellular responses in these two experiments, while in experiment Type-A cells reach intracellular P-starvation, the photosynthetic response declines quickly (Figure 5.3), suggesting that the cell halts photosynthesis. The drastic change in the slope of the photosynthetic activity parameter of Type A experiments suggest that there is a P-nutrient stress that is causing the cells to stop the photosynthetic activity (17). This effect is caused by the design of the experiments, were it was intended for the cells to use all of the intracellularly available phosphorus and partition them from mother to daughter cells until division get inhibited by intracellular P-availability. The minimum phosphorus requirements per cell for the marine diatom *Cyclotella* is $6.89 \pm 0.19 \mu\text{mol P per } 10^9$ cells (S.E.) There is a minimum amount of P required per cell, and when the cell reaches that minimum threshold, it inhibits division despite the abundance of all other nutrients available. In experiment Type-B we are observing lipid production in a photosynthetically active and dividing cell (Figure 5.3b) which suggests that the lipids are being produced from an extracellular carbon source

Intracellular P-starvation stops the uptake of nutrients, cell division stops, and as previously explained, photosynthesis is shut down as well. The cell is forced to scavenge for available intracellular P, which is explained by (), and source of P is phospholipids. This intracellular scavenging of P promotes an accumulation of neutral lipids, in the detriment of phospholipids.

This causes the cell to accumulate Triacylglycerides, (TAG), diglycerides (DG) and free fatty acids (FFA) over phospholipids. On the other side of the spectrum,

experiment Type-B is being cultivated in a P available mode. Cells division and photosynthesis are active, suggesting that extracellular carbon is being actively incorporated to the cells. In this active dividing state, lipid production rates are high, higher than in Type-A experiments. Cells are producing lipids at a faster rate, so that they can divide, and not only that, the P available in the system is boosting the lipid class production as well. In this state, phospholipids are highly promoted in a way that they act as a P sink.

From a bioprocessing engineering perspective, the use of phosphorus has always shown its particular difficulties due to the many effects that it can have in the cell. P is critical to sustain cell, lipid and chitin production. P may be used to fine tune the carbon allocation by redirecting the lipid biosynthesis to a lipid class, such as natural lipids and phospholipids. The lipid production rate is higher at the lower side of phosphate concentration (Figure 5.6d) suggesting that a phosphorus limited culture is more desirable than a phosphorus replete condition if production rate is to be optimized, however, the end goal of the cultivation needs to be assessed to select the P addition mode. In a similar manner, chitin biosynthesis can be downregulated by using a P-starved condition, however, in the P available regime there is no control by the addition of extra P to the system.

Conclusions

The co-production of biomass, chitin nanofibers, and lipid class from the marine diatom *Cyclotella* was studied over a range of cumulative phosphate concentrations in a 5-liter bubble column photobioreactor by varying the method of addition of phosphorus in two different type of additions coupled to a co-limited addition of silicon and nitrate. The silicon and nitrate addition was held constant in both types of experiments, so that we could better assess the effect of varying the amount of phosphorus delivered in Stage I (Type-A), and varying the P-addition rate in Stage II (Type-B). In this context, the cumulative phosphate concentration was either the limiting nutrient (Type-A), or the excess nutrient (Type-B). Forcing P to be the limiting nutrient creates a P-starved cell (Type-A) that has a different response than a cell that has P-available (Type-B). In a P-starved cell, cell division stops and

photosynthesis declines rapidly in the onset of P-starvation, and nutrients in the media are no longer uptaken by the cell. The cell accumulates neutral lipids in detriment of phospholipids due to the metabolic mechanisms of intracellular P scavenging. In a P-available cell, cell division is active, the uptake of nutrients is active, and photosynthesis is also active. Under this regime, the cell has a higher lipid production rate, and phospholipids are promoted in a higher level than neutral lipids when compared to a P-starved cell. Chitin was not directly affected by phosphate concentration, however, it was controlled by cell division. This study has showed that it is possible to selectively control the lipid class production by modifying the phosphate concentration, and this strategy coupled to silicon and nitrogen co-addition can be used as a tool for scale up production.

Acknowledgements

This work was supported by the US National Science Foundation (NSF), Emerging Frontiers for Research and Innovation program (EFRI), under award number 1240488.

References

1. Jeffryes C, Campbell J, Li H, Jiao J, Rorrer G. The potential of diatom nanobiotechnology for applications in solar cells, batteries, and electroluminescent devices. *Energy Environ Sci* [Internet]. 2011 Sep 27 [cited 2018 Apr 25];4(10):3930. Available from: <http://xlink.rsc.org/?DOI=c0ee00306a>
2. Rorrer GL, Antonio J, Durst R, Kelly C, Gale D, Maddux B, et al. The Potential of a Diatom-Based Photosynthetic Biorefinery for Biofuels and Valued Co-Products chitin. *Curr Biotechnol*. 2016;5:237–48.
3. Jeffryes C, Agathos SN, Rorrer G. Biogenic nanomaterials from photosynthetic microorganisms. Vol. 33, *Current Opinion in Biotechnology*. 2015. p. 23–31.
4. Hildebrand M, Davis AK, Smith SR, Traller JC, Abbriano R. The place of diatoms in the biofuels industry. *Biofuels*. 2012;3(2):221–40.
5. Ozkan A, Rorrer GL. Lipid and chitin nanofiber production during cultivation of the marine diatom *Cyclotella* sp. to high cell density with multistage addition of silicon and nitrate. *J Appl Phycol* [Internet]. 2017 Mar 21 [cited 2017 May 24];1–8. Available from: <http://link.springer.com/10.1007/s10811-017-1113-7>
6. Ozkan A, Rorrer GL. Effects of light intensity on the selectivity of lipid and chitin nanofiber production during photobioreactor cultivation of the marine diatom *Cyclotella* sp. 2017 [cited 2018 Apr 3]; Available from: https://ac.els-cdn.com/S2211926416308323/1-s2.0-S2211926416308323-main.pdf?_tid=ce575a8b-de75-4eb5-a81b-2b463ab59b36&acdnat=1522790521_514587b28e7d46d7682ac65eec7d007c
7. Ozkan A, Rorrer GL. Effects of CO₂ delivery on fatty acid and chitin nanofiber production during photobioreactor cultivation of the marine diatom *Cyclotella* sp. 2017 [cited 2018 Mar 12]; Available from: www.elsevier.com/locate/algal

8. Chiriboga O, Rorrer GL. Control of Chitin Nanofiber Production by the Lipid-Producing Diatom *Cyclotella* sp. through Fed-Batch Addition of Dissolved Silicon and Nitrate in a Bubble-Column Photobioreactor. *Biotechnol Prog* [Internet]. 2017 Feb 11 [cited 2017 Feb 28];33(2):407–15. Available from: <http://www.ncbi.nlm.nih.gov/pubmed/28188702>
9. Chiriboga O, Rorrer GL. Effects of nitrogen delivery on chitin nanofiber production during batch cultivation of the diatom *Cyclotella* sp. in a bubble column photobioreactor. *J Appl Phycol* [Internet]. 2018 [cited 2018 Feb 2]; Available from: <https://link.springer.com/content/pdf/10.1007%2Fs10811-017-1368-z.pdf>
10. Cordell D, Drangert J-O, White S. The story of phosphorus: Global food security and food for thought. [cited 2018 Apr 25]; Available from: <https://pdfs.semanticscholar.org/f674/49e965d9e23b2c2fb777d1c3d05133fcc3e8.pdf>
11. Cordell D, Rosemarin A, Schröder JJ, Smit AL. Towards global phosphorus security: A systems framework for phosphorus recovery and reuse options. *Chemosphere* [Internet]. 2011 Aug 1 [cited 2018 Apr 25];84(6):747–58. Available from: <https://www.sciencedirect.com/science/article/pii/S0045653511001652#f0015>
12. Rittmann BE, Mayer B, Westerhoff P, Edwards M. Capturing the lost phosphorus. *Chemosphere* [Internet]. 2011 Aug 1 [cited 2018 Apr 25];84(6):846–53. Available from: <https://www.sciencedirect.com/science/article/pii/S0045653511001196>
13. Chiriboga N. OG, Rorrer GL. Control of chitin nanofiber production by the lipid-producing diatom *Cyclotella* Sp. through fed-batch addition of dissolved silicon and nitrate in a bubble-column photobioreactor. *Biotechnol Prog*. 2017;33(2):407–15.
14. Jeffryes C, Gutu T, Jiao J, Rorrer GL. Two-stage photobioreactor process for the metabolic insertion of nanostructured germanium into the silica

- microstructure of the diatom *Pinnularia* sp. *Mater Sci Eng C* [Internet]. 2008 Jan [cited 2016 Jul 26];28(1):107–18. Available from:
<http://linkinghub.elsevier.com/retrieve/pii/S0928493107000045>
15. Ozkan A, Rorrer GL. Effects of CO₂ delivery on fatty acid and chitin nanofiber production during photobioreactor cultivation of the marine diatom *Cyclotella* sp. *Algal Res.* 2017;
 16. Fuhs GW. Phosphorus content and rate of growth in the diatoms *Cyclotella nana* and *Thalassiosira fluviatilis*. *Phycology.* 1969;5:312–921.
 17. Napoléon C, Raimbault V, Clauquin P. Influence of Nutrient Stress on the Relationships between PAM Measurements and Carbon Incorporation in Four Phytoplankton Species. *PLoS One* [Internet]. 2013 [cited 2016 Oct 4];8(6):e66423. Available from:
<http://www.ncbi.nlm.nih.gov/pubmed/23805221>

Table 5.1Nutrient process parameters for the cultivation of the diatom *Cyclotella* sp.

Cultivation Process Parameters	Phosphorus Starved	
	Type A (Batch-P)	Phosphorus Available Type B (Fed-Batch-P)
<i>Stage I</i>		
Initial silicon (mmol Si/L)	0.30	0.30
Initial nitrate (mmol N/L)	0.38	0.38
Initial phosphate (mmol P/L)	0.008 – 0.034	0.015
<i>Stage II</i>		
Si delivery (mmol Si/L-day)	0.32	0.32
N delivery (mmol N/L-day)	0.61	0.61
P delivery (mmol P/L-day)	0	0.005 – 0.061
Delivery time (days)	7	9

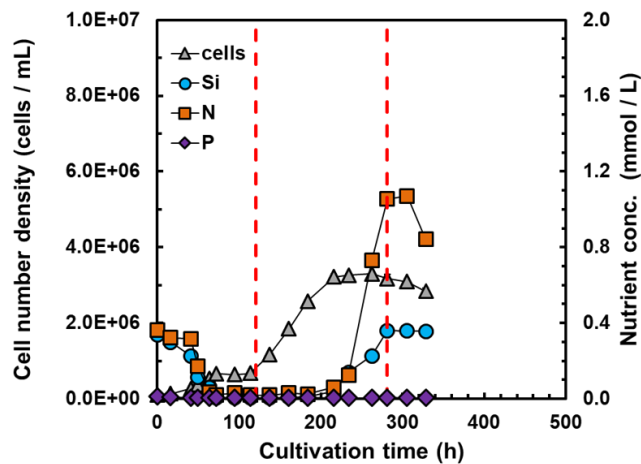
Table 5.2

Lipid class molecules found in samples, categorized as neutral lipids and phospholipids. Symbol represents the area response range of the extracted ion chromatogram. (- : no response; + : $1 \leq x < 5 \times 10^4$; ++ : $5 \times 10^4 \leq x < 5 \times 10^5$; +++ : $5 \times 10^5 \leq x < 5 \times 10^6$; ++++ : $5 \times 10^6 \geq x$).

Neutral Lipids	Type – A	Type – B	Phospholipids	Type – A	Type – B
FFA 14:0	+	+	PG 36:3	++	++
FFA 16:0	+	+	PG 36:2	++	++
FFA 18:0	++	++	PG 36:1	+	+
FFA 18:1	+	+	PG 38:5	+	+
FFA 20:1	+	+	PG 38:6	++	+++
FFA 22:5	+	+	PG 30:0	+	+
FFA 22:6	+	+	LPG 16:0	+	++
FFA 24:0	+	+	LPG 18:1	+	+
DG 32:0	++	++	LPC 14:0	+	+++
DG 32:1	+++	++	LPC 16:0	+	+++
DG 34:0	+	+	LPC 16:1	+	++
DG 34:1	+	+	LPC 18:0	+	+
TAG 46:2	++++	+++	LPC 18:1	+	++
TAG 48:2	++++	++++	LPC 18:2	-	+
TAG 48:1	++++	++++	LPC 20:5	-	++
TAG 50:2	+++	++	LPC 22:6	-	+
TAG 50:1	+++	++	PC 32:1	+	++
TAG 52:4	+	+	PC 34:1	+	+
TAG 52:3	+	++	PC 34:2	+	++
TAG 52:2	++	++	PC 36:5	+	+
TAG 54:5	+	++	PC 36:6	+	++
TAG 54:3	++	++	PC 38:6	+	+
TAG 54:2	++	++	PG 32:1	+	++
TAG 40:0	+	++	PG 32:0	+	+
TAG 44:0	++	++	PG 34:2	+	+
TAG 46:1	++++	+++	PG 36:4	+	+
TAG 48:0	+++	+++			
TAG 52:1	++	++			
TAG 54:1	++	++			
TAG 54:4	+	++			
TAG 56:2	+	++			
TAG 56:3	+	+			
TAG 44:1	+++	++			
TAG 46:0	++	+++			

Figure 5.1: Two stage photobioreactor cultivation of *Cyclotella* diatom cells under Type-A nutrient conditions, with variable phosphorus concentration at the beginning of Stage I. (a) Cell number density, dissolved silicon concentration, nitrate concentration, and phosphate concentration vs. cultivation time; (b) Silicon, nitrate and phosphate concentration delivered to the cell suspension vs. cultivation time.

a



b

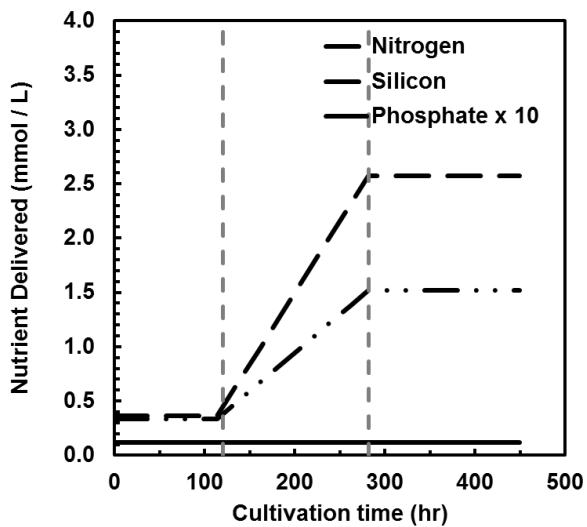
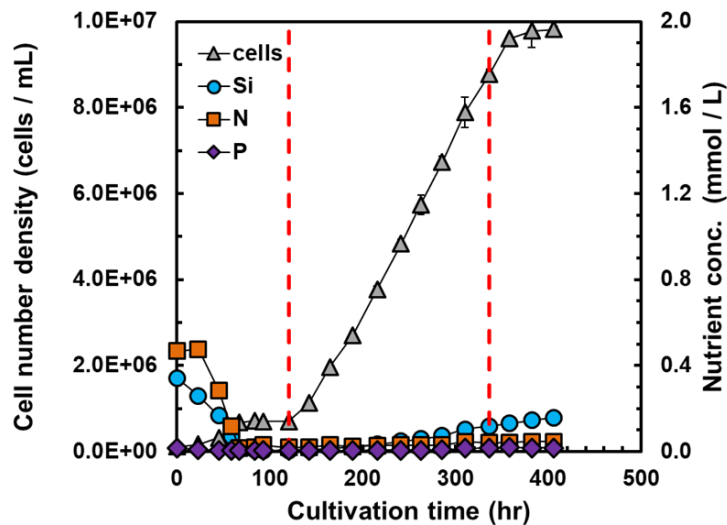


Figure 5.2: Two stage photobioreactor cultivation of *Cyclotella* diatom cells under Type-B nutrient conditions, with fixed phosphorus concentration on Stage I and variable phosphorus addition on Stage II. (a) Cell number density, dissolved silicon concentration, nitrate concentration, and phosphate concentration vs. cultivation time; (b) Silicon, nitrate and phosphate concentration delivered to the cell suspension vs. cultivation time.

a



b

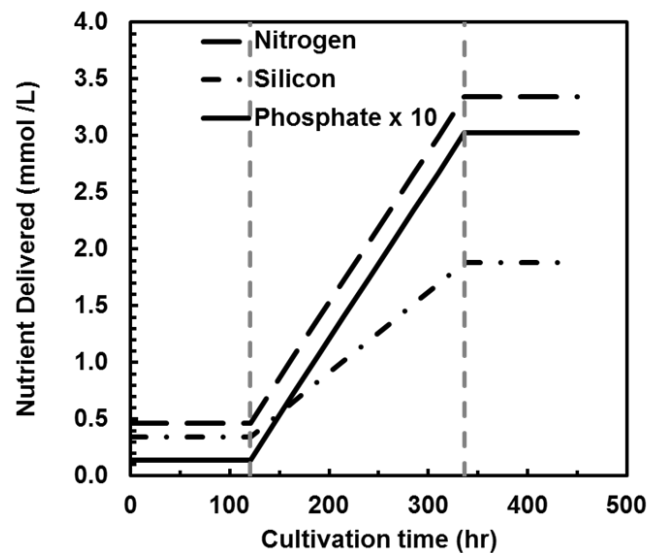
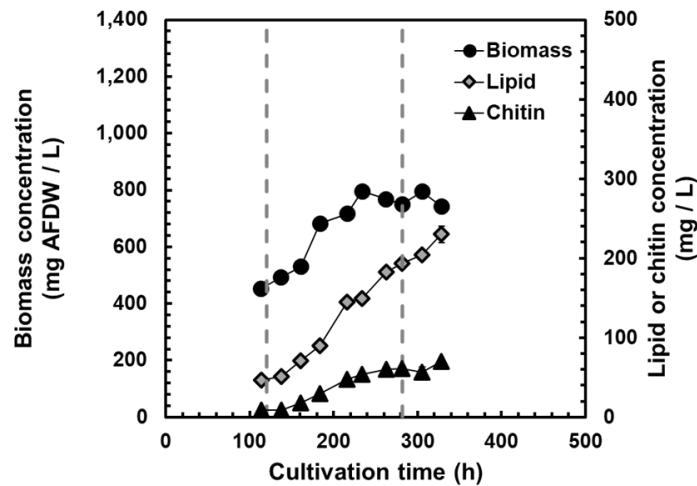


Figure 5.3: Comparison of the biomass, total lipid, and chitin concentration vs. cultivation time profiles at two different type of experiments corresponding to a different phosphate concentration (a) Type-A experiment with phosphate concentration 0.03 mM; (b) Type-A experiment with phosphate concentration 0.37 mM.

a



b

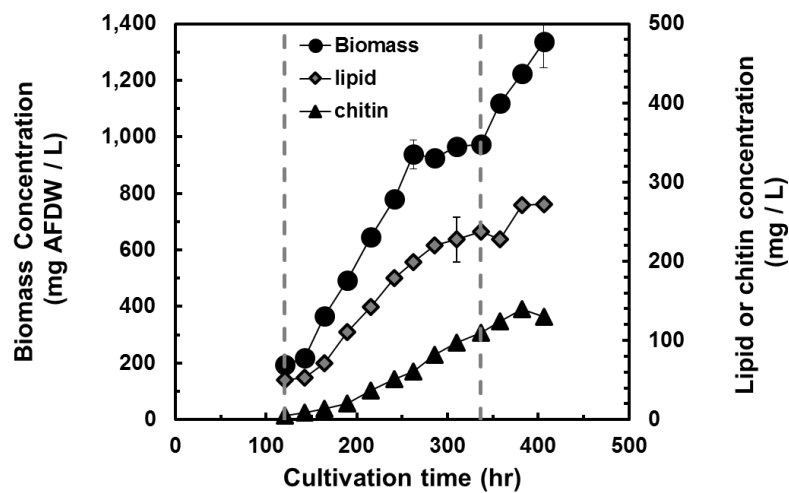
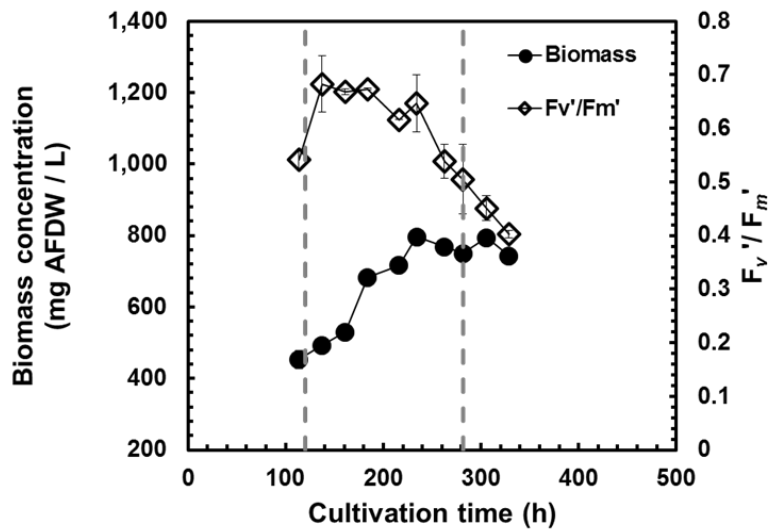


Figure 5.4: Comparison of the biomass concentration, F_v'/F_m' vs. cultivation time profiles at two different type of experiments corresponding to a different phosphate concentration (a) Type-A experiment with phosphate concentration 0.03 mM; (b) Type-A experiment with phosphate concentration 0.37 mM.

a



b

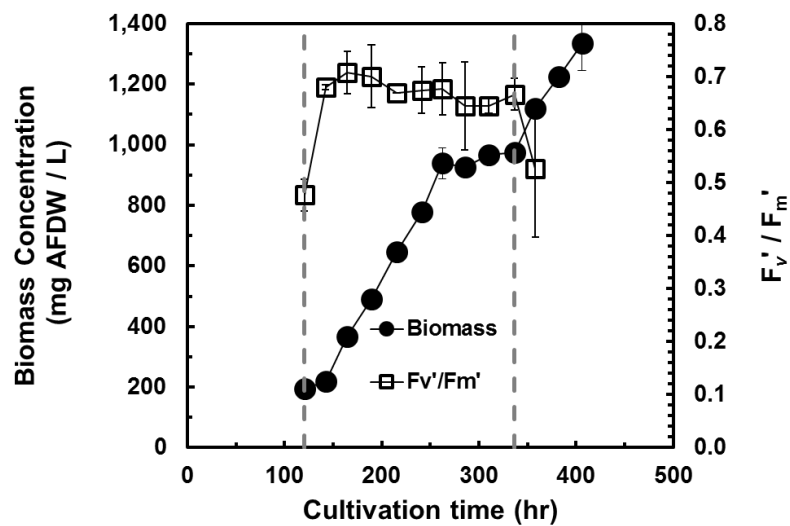


Figure 5.5: Comparison of biomass, lipid, and chitin yield per 10^9 cells vs. overall phosphate concentration (mM) in the cell suspension, (a-b) Type-A experiment with phosphate concentration window between 0 – 0.05 mM; (c-d) Type-B experiment with phosphate concentration window between 0 – 0.5 mM.

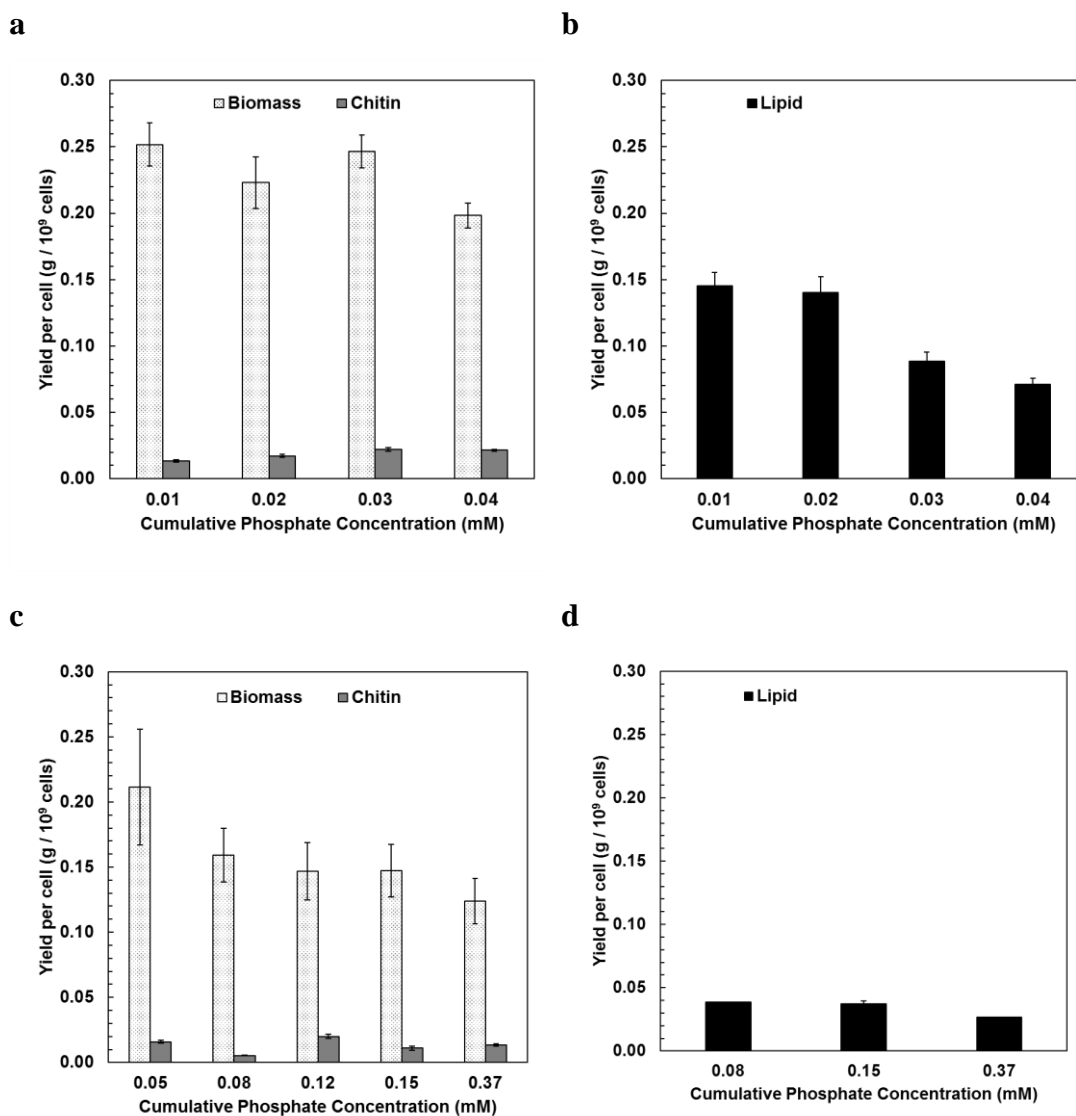


Figure 5.6: Comparison of biomass, lipid, and chitin yield per 10^9 cells vs. overall phosphate concentration (mM) in the cell suspension, (a-b) Type-A experiment with phosphate concentration window between 0 – 0.05 mM; (c-d) Type-B experiment with phosphate concentration window between 0 – 0.5 mM.

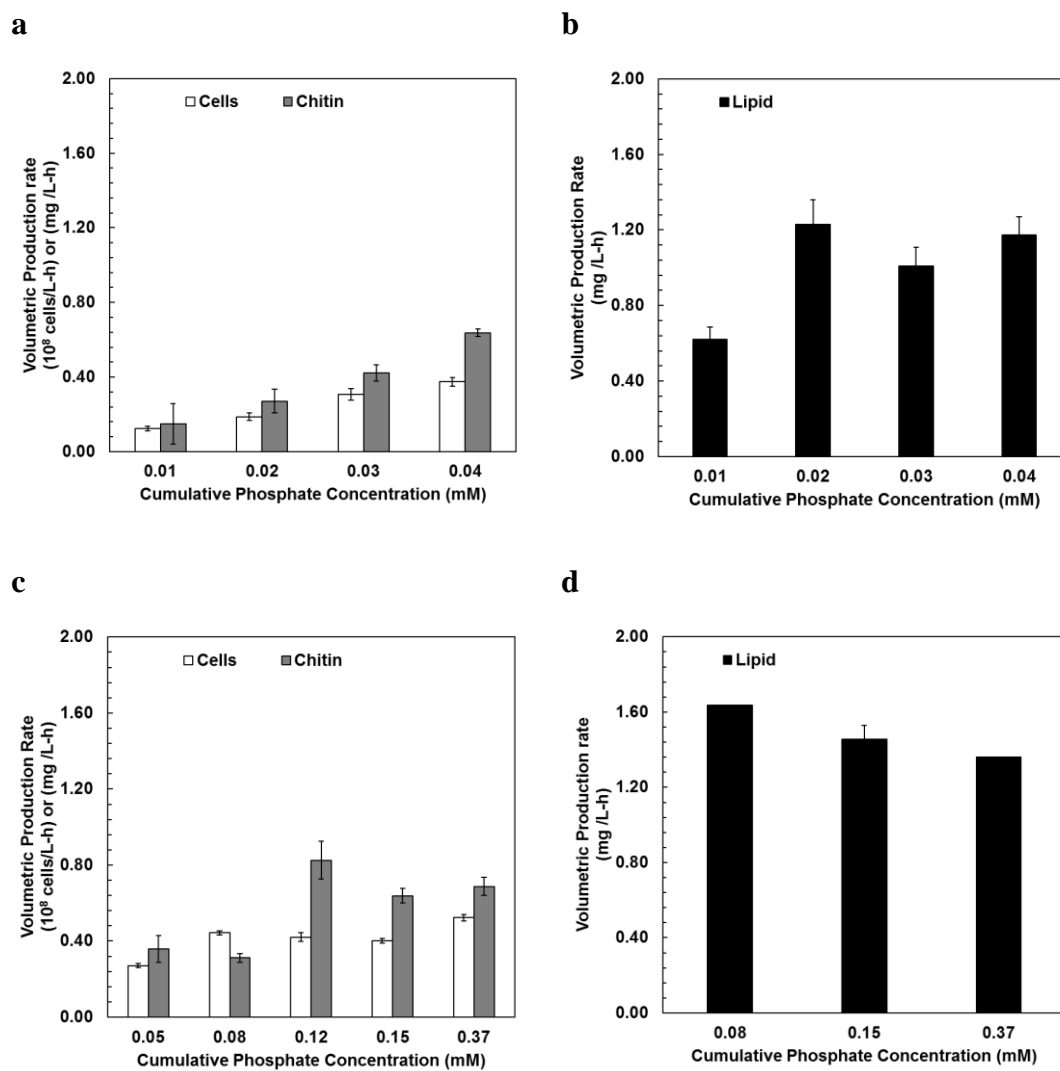
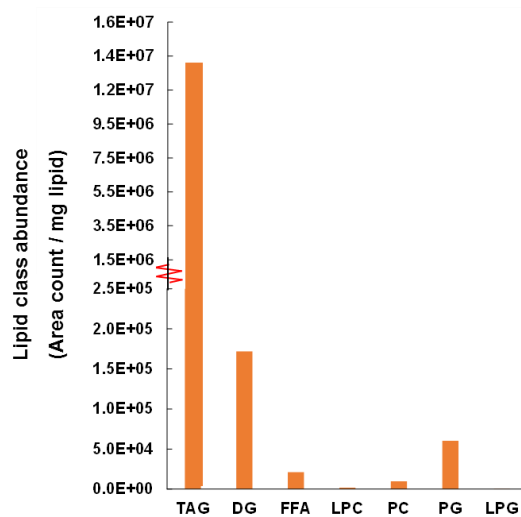


Figure 5.7: Comparison of lipid class abundance compared by area count divided by lipid amount in milligrams of lipidomic data at time point of 9 days after the beginning of Stage II for a representative sample of Type-A (a) and Type-B (b) experiments (0.03 and 0.37 mM phosphate respectively). Triacylglycerides (TAG), diacylglycerides (DG), free fatty acids (FFA), lysophosphatidylcholine (LPC), phosphatidylcholine (PC), phosphatidylglycerol (PG), and lysophosphatidylglycerol (LPG).

a



b

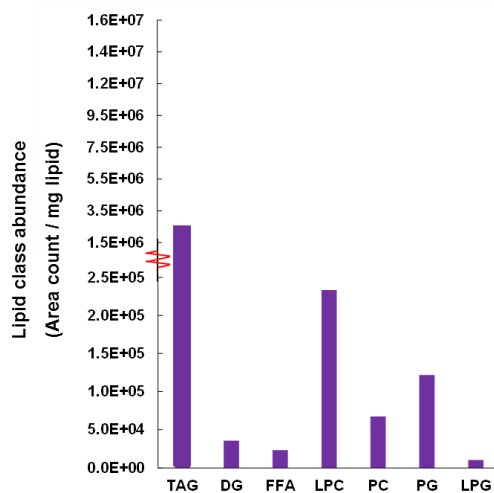
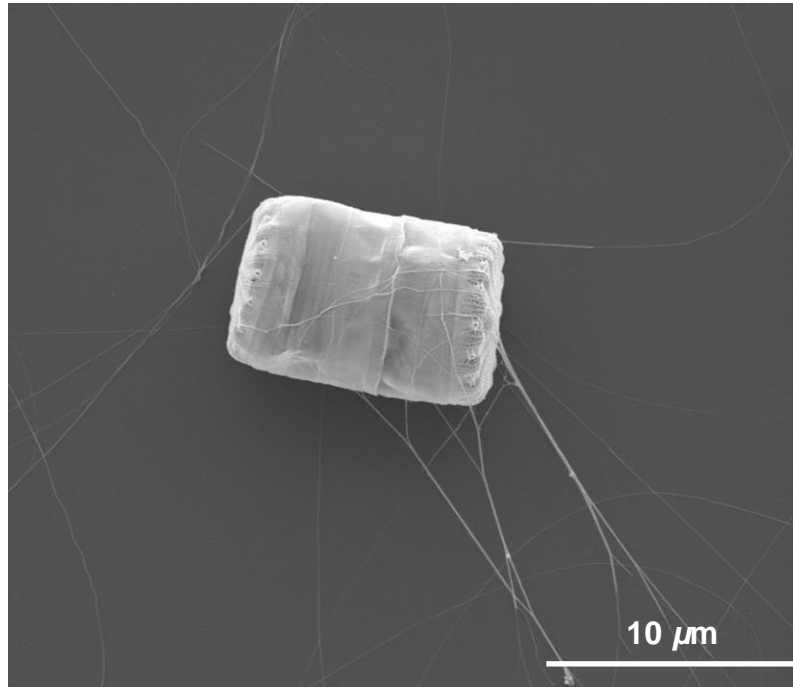
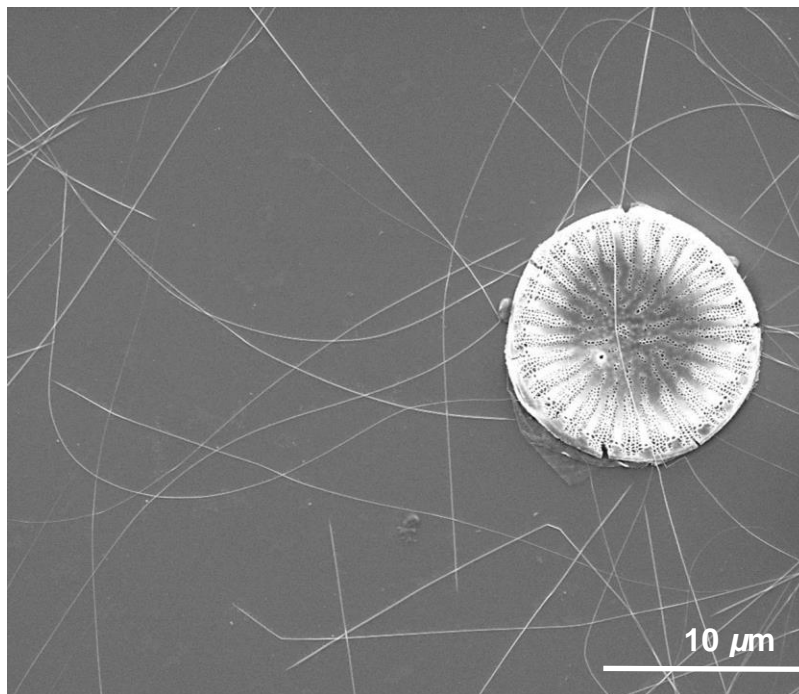


Figure 5.8: SEM image of *Cyclotella* sp. diatom cell showing native chitin nanofibers surrounding the cell (a) girdle band view, (b) valve view.

a



b



Chapter 6: Conclusions

The model marine diatom *Cyclotella* has shown to be a promising candidate to be used in a photosynthetic biorefinery, where multiple bio-products such as lipids and valuable chitin nanofibers can be harvested by utilizing bioprocess engineering techniques that have been discussed previously.

Cyclotella has specialized ports located in the rim of the valves where chitin nanofibers are produced. The nanofibers extruded from centric marine diatom *Cyclotella* sp. are pure and paracrystalline, and are not attached to proteins or other structural polysaccharide material. The mechanism of production is a cascade of biochemical reactions that occur intracellularly that lead to the production of UDP-*N*-Acetyl-Glucosamine. The polymerization of chitin nanofibers is a transmembrane process where the *N*-Acetylglucosamine chains are formed and expelled to the chitin pocket with the aid of chitin synthase. Chitin synthase catalyzes β -1,4 glycosidic bond formation between two UDP-*N*-acetyl glucosamine molecules, releasing UDP. Once the chitin chains are in the chitin pocket, crystallization occurs which connects the chitin chains into a nanofiber through hydrogen bonding, and finally the nanofibers are extruded to the through the fultoportulae. The chitin nanofibers have a β configuration, which means that the chains are parallel to each other, causing less hydrogen bonds than the α -polymorph. This makes the fiber easier to dissolve and better for chemical modification and functionalization.

To advance the applications of β -chitin nanofibers, a reliable, consistent, and sustainable production of β -chitin nanofibers can be achieved by cultivating the marine diatom *Cyclotella*. Controlled production of β -chitin nanofibers in a bioprocessing environment through diatom cultivation enables traceability of materials and recovery of the bio-product.

The marine diatom *Cyclotella* has nutrient requirements that are specific for different functions. *Cyclotella* needs dissolved silicon as required substrate for cell wall biosynthesis and cell division, and produces intracellular lipids, and also extrudes chitin nanofibers from its biosilica cell wall. Cultivation of this microorganism can be achieved in a bubble column photobioreactor, and a two-stage process was developed to carry out the cultivation.

In a two stage cultivation process, when dissolved silicon was continuously fed to the cell suspension at rate which limited cell division, both cell division and chitin production were linear with time. Increasing the rate of silicon delivery linearly increased the rate of cell number division and chitin production. Therefore, silicon delivery controls chitin production through control of the cell division rate.

The amount of nitrogen coupled with silicon is an important parameter to consider when cultivating *Cyclotella*. Cell number yield based on silicon, and the chitin yield per cell increases asymptotically with increasing N/Si molar ratio. Both of these yield parameters worked synergistically to boost the concentration of chitin in the culture broth. An initial N/Si ratio of at least 4.0 mol N mol⁻¹ Si is needed to achieve 90% of the asymptotic chitin yield. *Cyclotella* sets a limit on how much chitin can be made based on feeding with nitrate. Since the cell has a maximum chitin yield and cannot indefinitely bio-transform CO₂ and nitrate into chitin, scalable cultivation systems for chitin nanofiber production will require delivery of both silicon and nitrogen under silicon-limiting conditions to promote cell division and subsequent chitin formation.

The effect of cumulative phosphate concentration coupled with the co-addition of silicon and nitrate is another parameter that was studied and that should be considered in a scalable system. Phosphate concentration has no effect on chitin production, whereas it has an effect in lipid production. When *Cyclotella* is intracellularly starved with phosphorus, neutral lipid production is triggered. When the cells are fed with plenty of phosphorus, phospholipid production is enhanced over neutral lipids. By controlling the amount of phosphorus that is delivered to the cell, and is maintained above $6.89 \pm 0.19 \mu\text{mol P per } 10^9 \text{ cells}$, there will be phospholipid production. If cells reach this threshold, cell division will be stopped, nutrient uptake will be arrested, and neutral lipid production will be induced.

Scalable cultivation of *Cyclotella* and its bio-product formation can be achieved by controlling the nutrient addition parameters of silicon, nitrogen, and phosphorus, in a light and CO₂ controlled system. Future work should look into other nutrients that are of interest, and where out of the scope of this project, such as iron,

and ammonium. There are currently many applications for marine diatoms in industry and science, and their photosynthetic machinery is still a promising platform for novel production of biomolecules.

Appendices

Stage II Perfusion Planning

Omar Chiriboga

Materials

- TI-89 titanium Texas Instruments Calculator
- Pencil
- Engineering paper
- 60 mL Luer lock syringes
- Sterilized 1 L Kimax bottles
- 1 L volumetric flask
- Analytical balance
- Reagents as needed
- Plastic weighing boats

Procedure

The following explanation is in context of a 2-stage photobioreactor cultivation

Definitions:

$X_{N,f,I}$	cells/mL	Final cell number density Stage I
d	--	Doublings
$X_{N,f,II}$	cells/mL	Final cell number density Stage II (<i>Target cell number density</i>)
$C_{Si,o}$	mmol Si/L	Silicon concentration in the liquid feed (<i>Syringe</i>)
F	mL/h	Flow rate of feed to photobioreactor
V_L	mL	Working volume of photobioreactor at beginning of Stage II
μ_s	1/hr	specific growth rate of <i>Cyclotella</i> at specific conditions
$Y_{\frac{X}{Si}}$	cells/mmol Si	Cell yield per silicon substrate
t	hr	Perfusion time
$m_{Si,P}$	mmol Si	Total silicon amount needed to achieve $X_{N,f,II}$

With the following relationship:

$$X_{N,f,II} = \frac{X_{N,f,I} + 2^d * X_{N,f,I}}{2} \quad \text{Equation 1}$$

$$C_{Si,o} * F = \frac{V_L * X_{N,f,II} * \mu_s}{Y_{X/Si}} \quad \text{Equation 2}$$

$$C_{Si,o} * F * t = \frac{(2^d * X_{N,f,I} - X_{N,f,I}) * V_L}{Y_{X/Si}} \quad \text{Equation 3}$$

$$m_{Si,P} = C_{Si,o} * F * t \quad \text{Equation 4}$$

1. Determine the $X_{N,f,II}$ of your experiment using Equation 1
2. Solve for $(C_{Si,o} * F)$ using Equation 2
3. Solve for t using Equation 3 and the value obtained from Equation 2
4. Use the values obtained from Equation 2 and 3 and solve for Equation 4
5. Congratulations! This is the amount needed to achieve your target cell number density
6. Determine the syringe volume that you will use for your perfusion experiment. Account for the total duration for your experiment, the syringe volume, add the total volume that you will add to the system, and finally, once you have figured out all of the above
7. Weight the right amount of silicon needed and create the solution needed
8. If you are adding Nitrogen, and/or phosphate, make the solutions as a ratio of your silicon amount
9. Filter sterilize your feed solutions in the proper sterilized glassware, utilizing the right aseptic techniques in the sterilized laminar flow hood
10. Load your syringes in the pump
11. Set to the desired flow rate
12. Press Start and run your experiment.

13. (I used 60 mL Luer-lock syringes, and flow rate of 1.24 mL/hr, so that I could change the syringes every two days. Plus, you will be diluting your cell suspension, so you really want to think about the implications of diluting your cell suspension while you run your experiment)

Chitin Extraction and Purification from Algal Suspension

Omar Chiriboga

Extraction:

1. Measure 40 mL of cell suspension and transfer them to a 50 mL falcon tube
2. Homogenize the sample volume with the tissue homogenizer at medium speed for 20 seconds.
3. Load the falcon tube in the centrifuge
4. Centrifuge the homogenized algal suspension at $1500 \times g$ for 10 minutes.
5. Collect the supernatant in an adequate container. Discard the pellet (mainly cell biomass, frustules).
6. Transfer 2 mL of the recovered supernatant to a 2 mL Eppendorf centrifuge tube. (Use as many centrifuge tubes as needed to recover chitin from the supernatant).
7. Centrifuge at $16000 \times g$ for 30 minutes. Collect the pellet in a 10 mL borosilicate glass vial. Discard the supernatant. Collect all the chitin-rich pellets in the same vial for further purification

Purification:

1. Transfer the chitin-rich pellet to a 125 mL Erlenmeyer flask
2. Add 30 mL of 1M Hydrochloric acid
3. Put the Erlenmeyer flask in a magnetic stirrer – heater
4. Set the temperature at 70 °C and turn
5. Stir the mix at mild mixing conditions for 30 minutes.
6. After 30 minutes, stop the mixing and heat from the plate. Let it cool.
7. Once cooled, filter the suspension with a bottle top filtration funnel (Polystyrene 0.2 μ m PES)
8. Carefully collect the fibers from the filter and transfer them to a clean 125 mL Erlenmeyer flask
9. Add 50 mL of 0.5% SDS, and let it stir for 12 hours.

10. Filter the suspension with a bottle top filtration funnel (Polystyrene 0.2 μ m PES)
11. Carefully collect the fibers from the filter and transfer them to a clean 125 mL Erlenmeyer flask
12. Add 50 mL of 95% ethanol
13. Stir the suspension for 30 minutes
14. Transfer the chitin-ethanol suspension to a 2 mL Eppendorf centrifuge tubes (use as many as needed to process all the volume)
15. Centrifuge the suspension at 16000 $\times g$ for 30 minutes.
16. Collect the pellet, discard the supernatant. Let the remaining ethanol in the chitin pellet evaporate under N₂ flow.
17. Store the purified chitin fibers in an airtight container for further use.

Chitin Hydrolysis

Omar Chiriboga

Specialized Equipment:

- Vortex mixer (Mo Bio, Vortex Genie 2)
- Mechanical homogenizer (Cole Parmer, LabGEN 125)
- Dry block heater (IKA, Dry Block Heater 4)
- Microcentrifuge (Eppendorf, 5475 R)
- 100 - 1000 μ L Eppendorf Research Pippette
- 1-5 mL Eppendorf Research Pippette

Reagents

- 12 M HCl (Use directly from bottle)
- 6 M NaOH (239.982g NaOH/L) (use HPLC grade water)
- Nitrate and silicon free ASM (ASM0)
- Deionized water HPLC grade
- Purified algal chitin
- Ice

Procedure:

To wash the cells with silicon and nitrate free media:

1. Thaw algal samples for 6 hours at room temperature.
2. Mix algal samples using the vortex mixer for one minute and when visible flocs are present homogenize using the mechanical homogenizer at 35,000 rpm for 30 seconds.
3. In a 2 mL epi-tube, add 2 mL from the thawed/homogenized algal sample. Do this four times. You should have 4 epi-tubes for each sample. *(Use the green screen scale to control the mass that you added into the 5 epi-tubes, RECORD

THE MASS, this will be helpful later, when reconstituting the original volume).

4. Centrifuge the epi-tubes at 16,100 g for 15 minutes
5. Collect the supernatant by pipetting it out of the epi-tubes (about 1.8 ml from each vial) (* Leave 0.1 mL in the tube, so that chitin is not carried out) and combine them in one 15 mL centrifuge tube. Label the tube.
6. Collect the algal pellets into a clean 15 mL centrifuge tube.
 - a. Add 0.5 mL of ASM₀ in each epi-tube that contains the pellet.
 - b. Vortex-mix the epi-tubes.
 - c. Transfer the mixed suspension to a single 15 mL centrifuge tube.
 - d. Add another 0.5 mL of ASM₀ in each epi-tube. Vortex mix it, and transfer it to the 15 mL centrifuge tube.
 - e. Repeat step (d) again. This ensures that all the pellet was removed from the epi-tube.
7. Adjust the volume of the washed algal suspension to the original value of 8 mL with ASM₀. *(You can add ASM₀ to the reconstituted pellet, to match the original mass used).

To test the reconstituted algal suspension for chitin:

1. In a 6 mL glass vial, add 0.5 ml of the reconstituted algal sample, 0.5 ml of DI water (HPLC grade), and 2 mL of 12 M HCl. Do this in duplicates. * (Use plastic pipette tips).
2. Seal the vials using a PTFE lined cap.
3. Label the vials accordingly.
4. Mix all the samples using the vortex mixer for 1 minute.

To test the collected supernatant for chitin:

1. In a 6 mL glass vial, add 0.5 mL supernatant, 0.5 mL DI water and 2 mL 12 M HCl.
2. Seal the vials using a PTFE lined cap

3. Label the vials accordingly.
4. Mix all the samples using the vortex mixer for 1 minute.

Acid Hydrolysis Procedure:

1. Turn ON the Dry Block heater. (Make sure you do this well in advance of time. It takes like an hour to reach 91 inside the vials °C.)
2. Set Temperature of Dry Block at **99 °C**.
3. Select the mode “Timer On”
4. Place the samples in the dry block heater for 3 hours.
5. After three hours of hydrolysis, remove the vial from the heating block.
6. Place the vials in a water bath at room temperature for 5 minutes.
7. After the 5 minutes transfer the vials to an ice bath, let them sit there for 10 minutes.

Sample Preparation for HPLC measurement:

1. In a 2mL epi-tube, add 0.45 mL of the hydrolysate into 0.6 mL 6 M NaOH (previously cooled in freezer for 3 hours).
2. Centrifuge the samples at 16,100 g for 10 minutes.
3. Pipette 500 µL of the solutions into a PTFE lined HPLC vial.
4. Keep the vials in refrigerator until HPLC analysis.

Lipid Content Determination of Freeze-Dried Diatoms

Omar Chiriboga

Specialized Equipment

- Spectrophotometer
- Vortex mixer
- IKA heating block

Reagents:

- Potassium dichromate solution in concentrated H_2SO_4 (2.5 g/L), prepared by dissolving 2.5 g $\text{K}_2\text{Cr}_2\text{O}_7$ in 50 mL DI water, and then slowly transferring it to a 1L volumetric flask that has the acid in it. Stir the mix at a low speed. (Prepare this solution at least one day before lipid analysis and perform a calibration curve for every new batch made)

Procedure:

1. Get an aliquot of 0.2 mL of lipid extract into an 8 mL glass vial with PTFE-lined cap.
2. Evaporate to dryness with N_2 .
3. Add 2 mL of potassium dichromate solution with a 5 mL Eppendorf Research Plus pipette.
4. Close the vial with the PTFE lined cap and place it in a hot plate for 45 min.
Temperature set of hot plate: 105 °C
5. During the heating procedure, around minute 25, shake each vial to ensure that the sample is homogenized. Used forceps to hold the hot vials.
6. After 45 mins, take the samples out of the bath and cool them to room temperature.

7. Take 0.5 mL and dilute with 4.5 mL DI water. Caution, this is an exothermic rxn.
8. Let samples cool and then measure the absorbance at 350 nm against water as the blank solution.

Note: All steps should be repeated with a control from the lipid extraction process, which contains solvents but no lipids. After heating the samples in the boiling water bath the lipid samples should turn from a golden yellow color to a greenish color. The control should remain a golden yellow color.

Sample Preparation, Extraction, and Determination of Lipids From Any Cell Suspension Containing Diatoms.

Omar Chiriboga

Specialized Equipment

- Centrifuge
- Vortex mixer
- Orbital Shaker
- IKA Heating Block
- Spectrophotometer

Reagents

- Chloroform:Methanol (2:1, v:v)
- Methanol:H₂O (1:1, v:v)
- 0.88 wt% KCl in water (0.88 g KCl in 100 mL DI water)
- Potassium dichromate solution in concentrated H₂SO₄ (2.5 g/L), prepared by dissolving 2.5 g K₂Cr₂O₇ in 50 mL DI water, and then slowly transferring it to a 1L volumetric flask that has the H₂SO₄ in it. Stir the mix at a low speed. (Prepare this solution at least one day before lipid analysis and perform a calibration curve for every new batch made)

Assumptions

- There is 60% biomass in a sample of Total Solids (TS). AFDCW ≈ 30 wt%.
- There is 40% Lipid content in biomass.
- Calibration curve range for lipids is 0.1 to 1.0 mg Lipid /mL.

Sample Preparation

1. Measure 25 mL of cell suspension with the 5 mL Eppendorf Research Plus pipette into a 50 mL centrifuge tube (“Falcon tube”) (Cell suspension has cell number density between 6.0×10^5 to 3.0×10^6 cells/mL) (If using higher cell number densities in the suspension, volume can be lowered to 20 mL or even 15 mL).
2. Centrifuge at 1000g for 10 minutes
3. Carefully remove the supernatant from the pellet
4. Add 2 mL of deionized water to the pellet
5. Resuspend the pellet, and transfer it to a 8 mL borosilicate glass (make sure you weigh the vial and record the mass of the vial before adding the resuspended pellet).
6. Put the vial in the oven for 24-36 hours at 60 °C until all water has evaporated
7. Take the vial out of the oven, let it cool, and measure the mass of the vial with the dry pellet. The difference between the mass of the vial and the mass of the vial with the pellet is the weight of your dry pellet. (Dry solids)
8. Carefully remove the dry solids from the walls of the vial, and pulverize the dry solids into the smallest particle size that you can. (use caution to not break the glass vial) (this will help with the extraction procedure).
9. Once dry biomass is pulverized, cap the vial with a PTFE lined cap and freeze dry it until analysis.

Procedure:

10. Take the samples containing the pulverized dry solids in the borosilicate vials from the freezer.
11. Add 3 mL 2:1 Chloroform:Methanol.
12. Vortex the mixture for 60 seconds and then put it in the orbital shaker for 12 hours.
13. Recover the organic extract and place it in a 8 mL glass vial with a PTFE-lined cap. Set the organic extract aside.

14. Add 1 mL 2:1 Chloroform:MeOH to the solids, vortex for 60 seconds then let the solids settle.
15. Recover the organic extract and combine with the previous extract in the 8 mL glass vial.
16. Add 1 mL 2:1 Chloroform:MeOH to the solids, vortex for 60 seconds then let the solids settle.
17. Recover the organic extract and combine with the previous extracts in the 8 mL glass vial. Dispose the remaining solids as waste.
18. To the combined extracts add 1 mL 0.88 wt% KCl in H₂O.
19. Vortex for 60 seconds, then centrifuge at 1000 rpm for 10 min.
20. Remove the lower extract layer by pipette (Pasteur pipette) and dispose of the upper layer and any precipitates at the interface. Transfer the extract layer to a clean 8 mL vial.
21. Add 1 mL 1:1 Methanol:H₂O to the extract layer.
22. Vortex for 60 seconds then centrifuge at 1000 rpm for 10 min.
23. Remove and dispose of the upper layer and any precipitates at the interface, keeping only the lower extract layer.
24. Recover the extract volume, transfer to a glass vial with a PTFE lined cap and store at 0°C or less until needed for analysis. If performing analysis, go to step 16.
25. Get an aliquot of 0.2 mL of lipid extract into an 8 mL glass vial with PTFE-lined cap.
26. Evaporate to dryness with N₂.
27. Add 2 mL of potassium dichromate solution with a pipette
28. Close the vial with the PTFE lined cap and place it in the IKA DRY HEATING BLOCK at Temperature set 105 °C.
29. After 45 mins, take the samples out of the heating and cool them to room temperature.
30. Take 0.5 mL of the derivatized sample and dilute it with 4.5 mL DI water. Caution, this addition is exothermic.

31. Let cool and then measure the absorbance at 350 nm against water as the blank solution.

Note: All steps should be repeated with a control which contains no lipids, only solvents.

Chlorophyll Assay for Microalgae (*Cyclotella* sp.) from live Culture Samples from Photobioreactors

Omar Chiriboga

Equipment

- Centrifuge
- Micro - Centrifuge
- 2 mL epi-tubes
- 15 mL centrifuge tubes
- 5 mL pipette
- Shimadzu spectrophotometer

Solutions

- 100% ethanol (ChemStores refillable bottle)

Procedure

1. Get a 10 mL sample from a photobioreactor
2. Transfer a 5 mL aliquot into a 15 mL centrifuge tube. (measure volume with a 5 mL Eppendorf pipette) (do this in duplicates)
3. Centrifuge the vials for 10 minutes at 2000G
4. Remove the supernatant from the each sample. Leave 1 mL of supernatant to facilitate pellet transfer.
5. Transfer the pellet into a 2 mL epi-tube. Label each epi-tube.
6. Centrifuge the epi-tubes at 15000rpm for 8 minutes.
7. With a 1000 uL pipette, remove the supernatant from the pellet. The pellet should have no supernatant.
8. In the same epi-tube, add 1 mL of 100% ethanol to each vial.
9. Vortex mix the vial for 30 seconds. Ensure that the pellet is homogenized in ethanol. There shouldn't be any clumps of biomass.

10. Centrifuge the epi-tubes at 15000 rpm for 8 minutes.
11. Transfer the extracted chlorophyll (supernatant) into a new 2 mL epi-tube.
Make sure you label the new vials accordingly.
12. In the vials which have the whitish pellet, add 0.5 mL of 100% ethanol.
13. Vortex mix the vials for 30 seconds until homogenized. You should see a pale green color.
14. Centrifuge the epi-tubes at 15000 rpm for 8 minutes.
15. Remove the supernatant from the epi-tubes and mix them with the previous extracted chlorophyll. You should have a chlorophyll extract of 1.5 mL per sample.
16. Immediately run a spec-reading of the samples, to avoid chlorophyll degradation.
17. Blank the spec with 100% ethanol. You may use plastic micro cuvettes, and you only need 1 mL of sample to run the spec reading.
18. Save the spec readings for further analysis.

Transesterification of Fatty Acids from Lipid Extracts

Omar Chiriboga

Equipment:

- Reacti-Therm Heating Module
- Vortex mixer
- Centrifuge
- Dry block heater (IKA, Dry Block Heater 4)

Reagents:

- 1% (v/v) H₂SO₄/MeOH
- Hexane

Procedure:

1. Add 1.0 mL of Lipid extract into a 1.8 mL crimp glass vial
2. Evaporate the 1.0 mL of lipid extract to dryness with nitrogen.
3. Add 1.0 mL of a 0.25 mg/mL Nonadecanoic Acid to be used as an Internal Standard (IS)
4. Evaporate the **0.5 mL** IS to dryness with nitrogen
5. Add 0.5 mL 1% (v/v) H₂SO₄/MeOH.
6. Heat at 100°C for 60 minutes then cool to room temperature.
7. Once cooled, transfer the 0.5 mL derivatized solution to a 8 mL glass vial
8. Add 1.0 mL H₂O followed by 1.0 mL hexane.
9. Vortex for 60 seconds.
10. Separated the aqueous from solvent layers by centrifugation at 2000 rpm for 3 minutes.
11. Remove the upper solvent phase with a pasteur pipette, transfer to another 8 mL glass vial
12. Add anhydrous Na₂SO₄ (powder form) to dry the derivatized.
13. Once dried, remove the derivatized solution to another 8 mL glass vial, label and run it in the GC.

Standard Preparation for Transesterification of Fatty Acids Lipid Extracts

Omar Chiriboga

Reagents:

- Nonadecanoic acid (C19:0) MW: 298.50 g/mol
- Palmitic Acid (C16:0) MW: 256.42 g/mol
- Chloroform (100%) as organic solvent

Procedure:

For Palmitic Acid

1. Weigh 10.5 mg of Palmitic Acid (PA)
2. Add the weighed Palmitic acid into a 25 mL Volumetric flask
3. Add 20 mL of 100% Chloroform and dissolve the PA
4. Add 5 mL of 100% Chloroform to complete the required volume in the flask
5. Make a serial of dilution (75%, 50%, 25%, 12.5 %) from the prepared stock solution in 10 mL volumetric Flasks.

For Nonadecanoic Acid

1. Weigh 12.7 mg of Nonadecanoic Acid (NA)
2. Add the weighed NA into a 25 mL Volumetric flask
3. Add 20 mL of 100% Chloroform and dissolve the NA
4. Add 5 mL of 100% Chloroform to complete the required volume in the flask
5. Make a serial of dilution (75%, 50%, 25%, 12.5 %) from the prepared stock solution in 10 mL volumetric Flasks.

Standard Preparation for Transesterification

1. Add 1.0 mL of PA into a 1.8 mL crimp glass vial
2. Evaporate the 1.0 mL of the PA to dryness with nitrogen.
3. In the same vial add 1.0 mL of NA

4. Evaporate the 1.0 mL of the PA to dryness with nitrogen
5. Repeat steps 1 through 4 for all the dilutions prepared (75%, 50%, 25%, 12.5%)
6. Tranesterify the standards utilizing the procedure described above

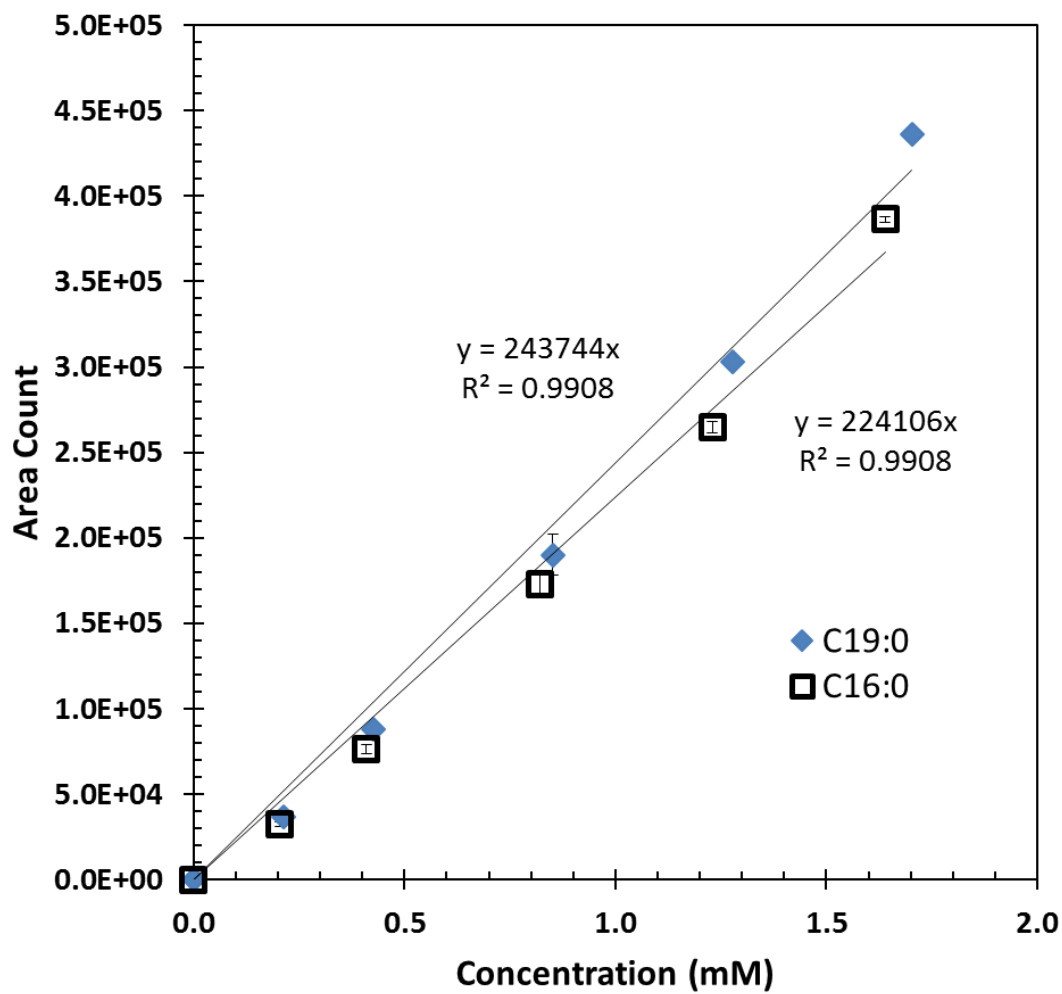


Figure 1: Standard Calibration in GC-FID HP5890 from the method described above, by Altan Ozkan, 07/11/2016

Separation of Microalgal Phospholipid Fatty Acids From Lipid Extracts

Omar Chiriboga

Adapted from: Quideau, S et al. Extraction and Analysis of Microbial Phospholipids in Soils. J. Vis. Exp., August 26, 2016

Equipment:

- Thermo Scientific Hypersep-SI 500 mg, 10 mL column
- Vacuum system with eluent recovery inserts (Picture below)
- Use glassware only. Pasteur pipettes

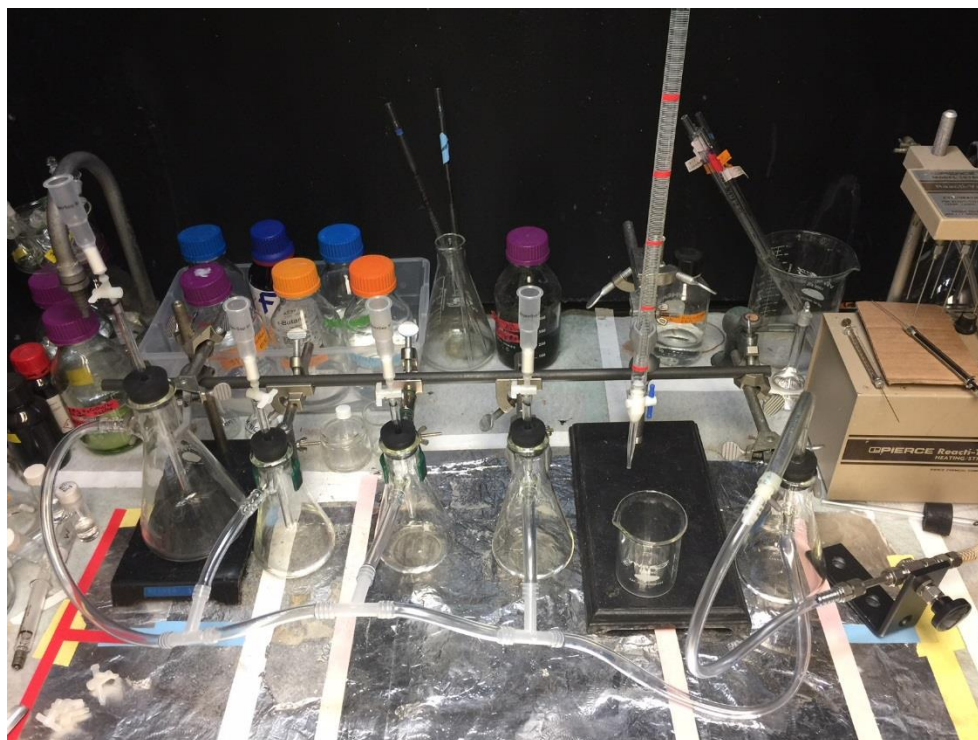
Reagents:

- Chloroform
- Acetone
- Methanol

Procedure:

1. Prepare the vacuum extraction set in a functional hood as shown in the picture below
2. Set the column in place
3. Condition the column with 5 mL acetone
4. Continue conditioning the column with 5 mL chloroform
5. Close the valve
6. Load the total lipid sample with the desired volume and amount as needed
7. Load the column with 5 mL chloroform
8. Open the valve and collect the eluent in a glass vial (this fraction has neutral lipids). Close the valve.
9. Change the collector vial
10. Load 5 mL of acetone in the column
11. Open the valve and collect the eluent (this fraction has Glycolipids). Close the valve

12. Change the collector vial
13. Load 5 mL of methanol in the column
14. Open the valve and collect the eluent (this fraction contains the phospholipids that you were looking for)
15. Carefully remove the collection vial from the system and transfer the methanol eluent to a clean 8 mL borosilicate vial
16. Dry the methanol in a nitrogen stream
17. Once the methanol has been dried, use a PTFE lined cap, close the vial tightly and store the vial in a dark cold place (-5 °C) until you get all your samples ready for analysis
18. Be cautious about storing phospholipid samples for too long, oxidation occurs and it may damage your sample.
19. Transesterify your phospholipids with the method of your choice and the internal standard that best suits your needs.



PAM Fluorometry of Photosynthetic Active Cell Suspensions from Photobioreactors

Omar Chiriboga

Equipment:

- Qubit® Fluorometer Model FL1

Procedure:

1. Remove an aliquot from the photobioreactor
2. Measure the cell number density of your cell suspension
3. Correct the concentration of your cell suspension to 1×10^6 cell/mL. Anything lower will be harder to read, anything higher should be fine, however, always keep track of your cell number density because there are effects to consider when comparing numbers from different concentrations.
4. Set the cell suspension in the dark for 5 minutes
5. Immediately transfer 2 mL of your cell suspension to the plastic cuvette.
6. Measure the photosynthetic parameters following the procedures for the instrument found in the Rorrer Lab – Qubit system binder.
7. This measurement has to be done immediately while the cells are still active. (do not attempt to get a sample and leave it in the countertop for too long).
8. Always perform a calibration curve of your light source, and the fluorescence response to different light intensities and different cell number densities. Check periodically for proper functioning and responses of your system.